THE TRANSPORT MECHANISM OF A GLUTAMATE TRANSPORTER HOMOLOG

By

Erika A. Riederer

A DISSERTATION

Presented to the Department of Physiology & Pharmacology
and the Oregon Health & Science University
School of Medicine in partial fulfillment of
the requirements for the degree of

Doctor of Philosophy

April 2021

School of Medicine

Oregon Health & Science University

CERTIFICATE OF APPROVAL

This is to certify that the PhD dissertation [or] Master's thesis of

Erika A. Riederer

has been approved

Francis I. Valiyaveetil, Ph.D. (Mentor)

Michael Cohen, Ph.D. (Committee Chair)

Show-Ling Shyng, Ph.D. (Member)

Eric Gouaux, Ph.D. (Member)

David Farrens, Ph.D. (Member)

Table of Contents

Acknowledgements

Graduate school has been a lesson in constantly striving for self-improvement or in other words, leveling up. This has disseminated throughout my life both in and out of the lab. I have learned how to approach science and empirically determined how to do scientific research, all part of the journey necessary to becoming a productive member of the scientific community. All the lessons and know-how derived during this experience were enabled by the environment at OHSU. The exposure to different types of science and the highly collaborative and stimulating environment fostered an open-mindedness to new information, diverse techniques, and a general love of science. With the help of the department and institution, I have been afforded many opportunities. Some of these include traveling to conferences, presenting my work, and being actively involved in hosting conferences, all of which have played important roles in my development as a scientist.

I especially thank the members of my lab, both past and present as well as my mentor, Francis Valiyaveetil. By being a member of the Valiyaveetil lab, I have been taught how to do research, how to take a mutli-pronged approach to answer a question of interest, how to set up experiments to reveal a truth no matter the outcome, and how to have an active scientific dialog to enrich and enhance my research. Through graduate school, the value of quality lab mates has become apparent, so I want to especially thank both Ravikumar Reddi and Kim Matulef for accompanying me in my scientific journey and aiding in my metamorphosis into a scientist. I also want to thank my fellow graduate students for their commiseration and willingness to discuss different aspects of science.

I also want to specifically thank my DAC committee members for their help in guiding my thesis research and proving to be invaluable resources in this process. On a similar note, I want to thank my additional funding from an America Heart Association

predoctoral fellowship. The fellowship enabled me to continue my research without concern from the various highs and lows of science funding.

Last, but not least, I want to thank my family and friends. Without their continual support, encouragement, as well as skills, I would not have made it to graduate school, let alone complete it. No matter the scale of an issue, they are always willing to help in whatever way possible and always champion me. There was never any doubt that I could finish this journey and their faith in me was instrumental in getting through various rough patches that are inherent to graduate school. Overall, they helped make me who I am, especially in becoming a competent scientist.

It truly takes a village to accomplish anything, so I want to say a final thanks to my family and OHSU community for everything which allowed me to complete this journey and become a contributing member of the scientific community.

List of Figures and Tables

Figures

Tables

Abstract

Harnessing pre-existing sodium gradients to transport solute across membranes is a common theme across all branches of life. Glutamate transporters exploit ionic gradients for the concentrative uptake of glutamate. Normal function of glutamate transporters is required for rapid removal of glutamate from the synaptic space, which is required for efficient neurotransmission and preventing excitotoxicity. A key question in glutamate transporters is the mechanism by which the ionic gradient is coupled to glutamate uptake. Specifically, the allosteric mechanism necessary to accomplish coupled binding of substrate and ions for successful translocation of substrate into the cell. The general sequence of binding events was proposed to involve two Na^+ ions binding first to cause conformational changes necessary for substrate to bind, including the extracellular gate opening. One molecule of substrate can then bind and close the extracellular gate, followed by a subsequent third Na^+ ion.

In order to study the molecular coupling mechanism, various fluorescence-based functional assays were developed to assess discrete steps along the process in an archaeal homolog, Glt_{Ph}. These novel functional assays monitored Na^+ binding and conformational changes downstream from Na^+ binding. One downstream assay monitors the conformational switch in a highly conserved unwound region identified to participate in Na^+ coordination and another monitors the movement of the extracellular gate, HP2. Using these novel functional assays with structural analysis and mutagenesis experiments, insights into the coupling process were uncovered. Key molecular events which must occur in the binding site to accomplish extracellular gate opening as well as the roles of each of the Na^+ sites that bind before substrate were determined. In addition, protein interactions with the backbone of the substrate were found to be essential for extracellular gate closure. Through implementation of the *in vitro* heteromeric transporter assembly methodology, it was established that there is no crosstalk between protomers

during the coupled binding process. These studies together with previous data led to the herein proposed molecular mechanism for the coupling of ion and solute needed for substrate translocation.

The assays developed in this thesis research also offer a path to address some remaining gaps in our knowledge such as substrate assisted gate closure and the substrate release mechanism. The mechanism elucidated in this thesis should also be applicable to human glutamate transporters since the residues identified as important in Glt_{Ph} are conserved in humans and in their placement in the protein's quaternary structure.

Chapter 1: Introduction

Na^+ symport in SLC1 family

Harnessing pre-existing sodium gradients to transport solute across membranes is a common theme across all branches of life. The inherent coupling between the electrochemical gradient and substrate is poorly understood despite being a fundamental mechanism for a variety of proteins. Sodium symporters are one class of transporters responsible for a wide variety of vital functions such as Na^+ coupled transport of sugars(1), nucleosides(2), vitamins(3), amino acids(4, 5), and neurotransmitters(6, 7). One family responsible for amino acid transport are the Solute Carrier 1 or SLC1 family. This family is comprised of acidic amino acid transporters and neutral amino acid transporters with prokaryotic to eukaryotic members. Mammalian members of this family (SLC1A) include excitatory amino acid transporters, EAATs, responsible for the rapid uptake of glutamate in synapses and alanine serine cysteine transporters, ASCTs. These proteins can transport a wide variety of amino acids in an isoform dependent manner. There are 5 isoforms of EAATs (EAAT1-5)(8-10) and two isoforms of ASCTs (ASCT1-2)(4, 11) in humans. EAAT1 and EAAT2 both have rodent equivalents GLAST1(5) and GLT-1(12) respectively while EAAT3 has an equivalent cloned from rabbit, EAAC1(13), all of which have been extensively studied. The respective designations are EAAT1 as SLC1A3, EAAT2 as SLC1A2, EAAT3 as SLC1A1, EAAT4 as SLC1A6, EAAT5 as SLC1A7, ASCT1 as SLC1A4, and ASCT2 as SLC1A5.

Localization and physiological roles

The main substrate of EAATs is glutamate, the major excitatory neurotransmitter in the central nervous system (CNS)(14). EAATs are an integral part of maintaining glutamatergic neurotransmission since they are responsible for the rapid clearance of glutamate in synapses(15). This function allows for a new signal to be relayed across a

synapse as well as preventing excitotoxicity and scavenging glutamate for further use in the cell (Figure 1.1). The five different EAAT isoforms are differentially expressed throughout the CNS and peripheral organs with varying in aspects of their transport function. EAAT1 is predominately expressed by astrocytes in the cerebellum(16), the inner ear(17), retina(18); and peripherally(19) in the placenta(20), mammary glands(21), heart(22, 23), and bone osteocytes(24, 25). EAAT2 is predominately expressed by astrocytes throughout the rest of the CNS such as the spinal cord and hippocampus and by some presynaptic neurons(16, 26-29). EAAT2 is responsible for roughly 90% of glutamate reuptake(30). There is peripheral expression of EAAT2 in the liver(31, 32), mammary glands(21), and placenta(20, 33). The EAAT1 and EAAT2 isoforms are the most abundant and exist as homotrimers(34).

EAAT3 is predominately expressed in post-synaptic terminals of neurons in the cerebellum, cortex, hippocampus, and basal ganglia, but at a lower concentration than EAAT2(35-38). Interestingly, EAAT3 is mostly in the cytosol and relocates to the plasma membrane when needed. It is the only isoform to have this type of expression regulation and suggests a different role in cell metabolism as opposed to direct regulation of synaptic transmission (39). EAAT3 is also the most abundant isoform outside of the CNS with expression in the kidney(31, 40), heart(22), intestines(31), placenta(20), and liver(41). EAAT3 is responsible for the vital function of reabsorption of dicarboxylate amino acids in the kidneys(42, 43). In the CNS, EAAT4 and EAAT5 are neuronal isoforms with more specific localization: EAAT4 is found in mainly in Purkinje cells in the cerebellum(44) while EAAT5 is exclusively in the retina in the CNS(8, 45, 46). However, EAAT5 can be found outside the CNS in the liver, intestine, skeletal muscle, heart, and kidney although its role in the physiology of these regions is unresolved (47). EAAT3, EAAT4, and EAAT5 also predominately exist as homodimers, although there is some evidence that EAAT3 and EAAT4 can form mixed heterotrimers(48).

ASCTs are responsible for the transport of neutral amino acids and are one of the four major neutral amino acid transporters systems in the human body (11, 49). These proteins, just like their excitatory transporter counterparts, are found both in the CNS and periphery. In the brain, ASCTs deliver amino acids across the blood brain barrier(50) and have a variety of expression patterns in different cell types depending on the developmental stage and study(51-54). One of the proposed roles of ASCTs in the CNS involves serine flux from astrocytes to neurons in order to produce D-serine, a neuromodulator, since L- and D-serine are substrates (55-58). In the periphery, ASCTs can be found in the intestine, kidney, lung, and skeletal muscle (11, 49, 59). ASCT1 is broadly expressed in the digestive system as well as the heart and ovaries while ASCT2 can also be found in adipose tissue and the testes(60).

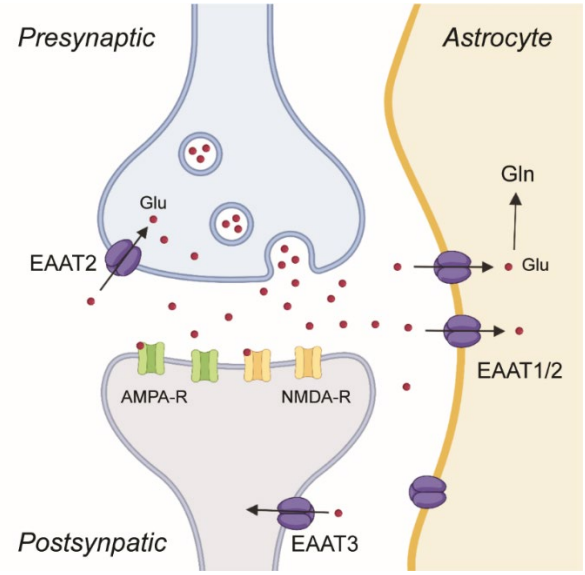

Figure 1.1. Example of EAATs localization and role in native physiology regulating glutamatergic synapses through rapid reuptake in CNS. Adapted from (61).

SLC1A family in pathological states

As described above both EAATs and ASCTs have vital roles in normal physiology and therefore have been implicated in various pathological states. Since EAATs are essential for glutamatergic synapses, the altered properties of these

transporters contribute to a wide variety of neurological conditions (62). In ischemia, the lack of blood supply causes a chain of events where there is less adenosine triphosphate (ATP) produced to fuel K^+/ Na^+ gradients across neuronal and glial membranes (63). The lack of the appropriate gradients decreases the concentrative uptake of glutamate through EAATs and elevates extracellular glutamate levels leading to excitotoxicity. Ischemia can also lead to a decrease in the expression of EAAT2 to further contribute to increased extracellular glutamate levels(64-66). Other neurological diseases such as Amyotrophic Lateral Sclerosis (ALS) and Alzheimer's Disease also have altered glutamate transport(67, 68). Through different mechanism, these disease states have a reduction in EAAT2 expression or function which therefore decreases glutamate transport and contributes to the disease state(69-72). Mutations in EAATs have also been shown to contribute to Dicarboxylic Amino Aciduria, a metabolic disorder where glutamate and aspartate are not properly reabsorbed in the kidneys(42, 73), and Episodic Ataxia, a rare neurological condition(74, 75).

Since EAATs and ASCTs are responsible for the uptake and regulation of several vital amino acids, they have also been implicated in several cancers. EAAT1 and 2 expression is suppressed in gliomas and suppression increases as the glioma progresses(76-80). In other cancers of the periphery, EAAT expression is increased to aid in tumor growth and resistance to stress(81-83). The role of EAATs in cancer is still emerging, while the role of ASCT2 in cancer has been extensively studied(84-86). ASCT2 has been shown to be upregulated across many cancer types such as breast(87), gastric(88), esophageal(89), prostate(90), and more. The upregulation of this transporter in cancer stems from a metabolic switch to rely on glutamine and glycolysis for energy known as the Warburg Effect(91, 92). Therefore, ASCT2 has been identified as an important therapeutic target due to its role in cancer cell nutrient acquisition.

EAATs are also potential therapeutic targets for neurological diseases with altered glutamate regulation.

Transport stoichiometry and chloride conductance

To accomplish the vital function of amino acid transport, both EAATs and ASCTs rely on the pre-existing Na^+ electrochemical gradient. Both members couple one molecule of substrate(49, 61, 93-95) with three Na^+ ions to translocate substrate across the plasma membrane from the extracellular space into the cell. However, ASCTs are amino acid exchangers where a molecule of substrate coupled to three Na^+ ions can be moved across the plasma membrane in either direction (extracellular to intracellular or intracellular to extracellular) (96-98)(Figure 1.2A). EAATs only transport in one direction along with three Na^+ ions and a proton (H^+). To resume the extracellular facing state and complete the transport cycle, a potassium ion (K^+) is required for countertransport(99-101) (Figure 1.2A/B). The transport cycle can be functionally tested through electrophysiology since there is a thermodynamically uncoupled chloride flux (Cl^-) through the transporter upon ligand addition(9, 97, 102-105). EAAT4 and EAAT5 essentially function as glutamate activated Cl^- channels while in EAAT1-3, the chloride flux is one component of the ion fluxes associated with transport(106, 107). The chloride conductance is proposed to help offset the net positive 2 charge transfer across the membrane with substrate translocation and maintain transport rates(108-110). The different isoforms of EAATs all have different kinetic properties for turn over as well as varied affinities for glutamate (Figure 1.2C).

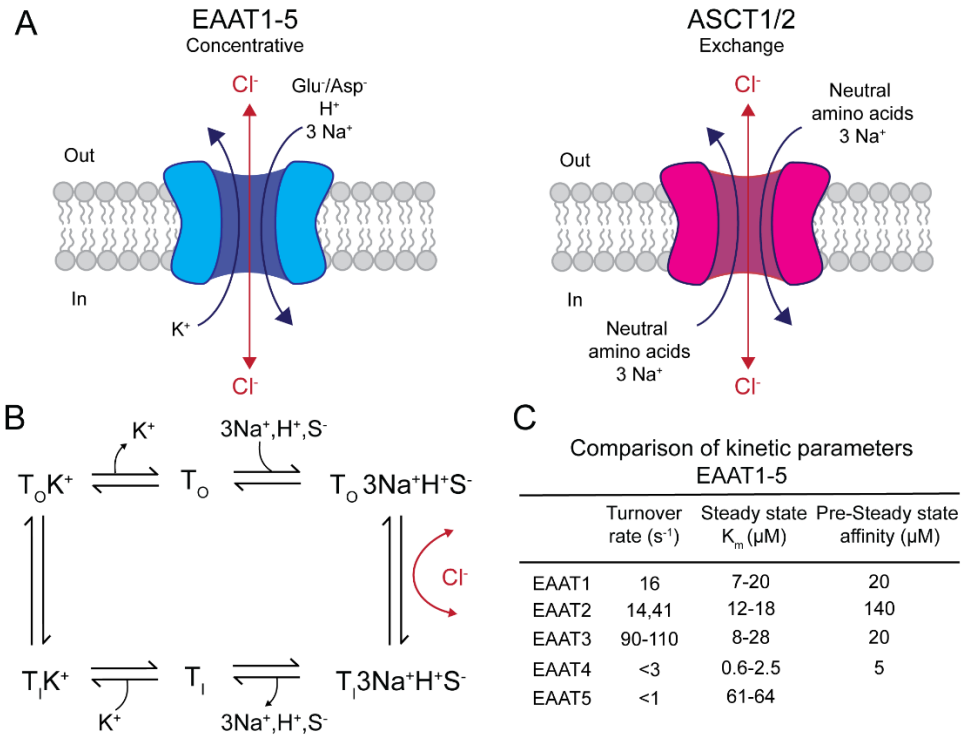

C

Comparison of kinetic parameters
EAAT1-5

	Turnover rate (s^{-1})	Steady state K_m (μM)	Pre-Steady state affinity (μM)
EAAT1	16	7-20	20
EAAT2	14,41	12-18	140
EAAT3	90-110	8-28	20
EAAT4	<3	0.6-2.5	5
EAAT5	<1	61-64	

Figure 1.2. Stoichiometry of transport cycle and differences in transport properties across EAAT isoforms. A) Depicts the overall transport stoichiometry for EAATs concentrative uptake in which $3Na^+$:$1H^+$:1Substrate are coupled to accomplish forward transport from extracellular facing to intracellular state resulting in a chloride conductance (Cl^-) and a K^+ ion is required for counter transport to resume extracellular facing state. Neutral amino acid exchangers, ASCTs, require $3Na^+$:1substrate to accomplish translocation in either direction and also have a chloride conductance **B)** Outline of EAAT transport cycle and order of events starting at T_o which is the Apo transporter in the extracellular facing state or outward facing state (subscript O). The I subscript stands for intracellular or inward facing state and S^- is the substrate **C)** Comparison of kinetic parameters of transport across EAAT isoforms. K_m is a term describing the affinity of glutamate. Adapted from (61) and original data from (9, 10, 109-113).

Structural features of EAATs and residues implicated in ligand binding

Various studies have identified basic structural components of EAATs and how they change according to ligand state. EAATs are trimers which form a central cavity that restricts ligand diffusion(114, 115). Through hydropathy analysis and cysteine scanning, eight transmembrane helices with two reentrant loops were described for each protomer (Figure 1.3) (116-119). Each subunit can also transport independently(120-122). Initial experiments showed different ligands alter the accessibility of the various reentrant loops as well as the fact that in the quaternary structure the two loops are

close to each other(123-129). The fact that accessibility changes depending on the presence of various ligands gave the first clues to some of the necessary conformational changes which must take place during the transport cycle. Experiments on EAATs have not only described the stoichiometry of transport, but also the order of binding and evidence for the ligand binding sites. Through kinetics studies on EAATs, it was proposed that at least one Na^+ ion, most likely two, bind before the substrate. The final third Na^+ ion binds after the substrate(130-132). The molecular underpinnings necessary to accomplish this coupled binding were unresolved.

A variety of mutagenesis studies have identified key residues involved with ligand binding necessary for transport (Ligands: Na^+, K^+, H^+ and substrate). For Na^+ binding, several residues belonging to a highly conserved moiety have been implicated: D368 in EAAC1 which decreased affinity for Na^+ when mutated (133) and T370 which showed decreased cation dependence for transport (134) and an effect on Na^+ affinity(135). A residue near T370, D440 in EAAC1, also showed a substantial decrease in the rate of Na^+ binding and a decreased affinity for both Na^+ and K^+ when substituted (136, 137). In several studies some of the same residues suggested to form Na^+ binding sites were also suggested to form K^+ binding site like D368(138) and T370. For K^+ binding, additional residues were identified such as N366 in EAAC1 and E404 in GLT-1(138, 139). Substitutions to these residues resulted in a loss of coupled countertransport where the transporter acts in a Na^+ dependent exchanger mode. A Tyr residue, 403 in GLT-1, and a nearby Arg residue, R477 in EAAT1, also have a similar effect when substituted and are implicated in a potential K^+ binding site (140-142)(Figure 1.3). There are also residues on each of the reentrant moieties which influence cation selectivity.

The need for H^+ binding for transport was not fully established until the Kanner 1996 study(100). Initial theories were centered on the possibility of the substrate being protonated to ensure proton coupling(117), but further studies indicated that was not the

case(143, 144). A conserved glutamine, E373 (equivalent E404), was then suggested to be the proton acceptor in EAAT3(145). A substitution at this E373 results in the loss of net flux, but retains Na^+ dependent, pH independent substrate exchange and can be inserted into ASCT2 to introduce pH sensitivity(145). Residues implicated in substrate binding have also been reported (Figure 1.3). These residues partially overlap with residues implicated in Na^+ and K^+ binding: R447 in EAAC1(146) and T370. Other residues which were mutated and greatly decreased transport or affinity for substrate were clustered around R447, including D444(147) and N451(135, 148) which are each one helical turn away from R447.

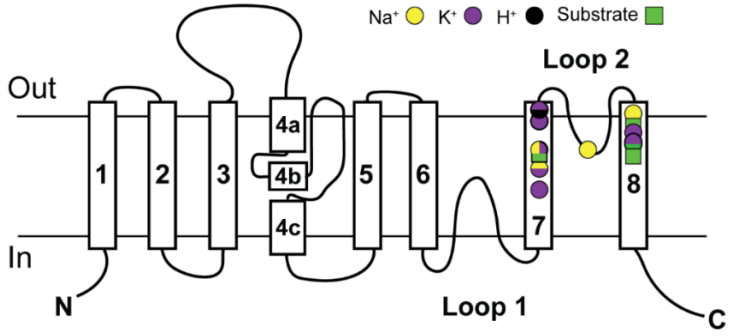

Figure 1.3. Residues implicated in ligand binding mapped to secondary structure of EAATs. EAATs have 8 transmembrane helices (TM) with their respective numbering and two reentrant loops, 1 and 2. Each residue described to be involved in ligand binding has a corresponding symbol to depict the location in the secondary structure and which ligand it affects. As the legend describes, circles are for ions and the green square corresponds to substrate binding. Residues implicated in more than one ligand have corresponding two or three colors in their respective symbols. For example, T370 has been implicated in Na^+, K^+, and substrate binding and therefore shows a circle colored for Na^+ and K^+ merged with a square for substrate binding. N and C are the respective amino and carboxyl termini of the protein.

With the wealth of functional data and characterization of different structural features, key residues involved in ligand binding during the transport cycle were identified. To incorporate these data into an understanding of the molecular basis underlying coupled binding, a molecular resolution of the protein was necessary. The first structure of the SLC1 family paved the way for structure-function studies to inform our understanding of the transport mechanism of the SLC1 family.

Key prokaryotic member of the SLC1 family

The first structure of the SLC1 family was solved using a prokaryotic homolog in 2004(149). The archaeal homolog, Glt_{Ph}, is from *Pyrococcus horikoshii*, and shares 37% amino acid identity with human EAAT2(149). The key regions toward the C-terminus of the protein which are involved in the transport mechanism are highly conserved across SLC1 family members (Figure 1.7). The stoichiometry of transport for Glt_{Ph} differs from EAATs in that substrate translocation does not require a proton and countertransport is also K^+ independent. Glt_{Ph} maintains one molecule of substrate coupled to three Na^+ ions with a similar binding order of two Na^+ ions binding first, followed by substrate binding, and then the final third Na^+ ion(150-152). The substrate for Glt_{Ph} is also highly specific for Asp with a higher affinity when compared Glu and to EAATs (10, 150, 151). All these features of Glt_{Ph} prove it to be a valid model for studying the transport mechanism of glutamate transporters. Not only has Glt_{Ph} been used for structural studies, it also has several features which make it amenable for spectroscopic studies. Glt_{Ph} is stable in detergent micelles and readily recombinantly expressed, has no native Trp, and has a single cysteine that can be substituted to Ser or Ala without effecting function.

From the structure of Glt_{Ph}, the general architecture of these proteins was revealed to be a homotrimer which adopts a bowl shape conformation (Figure 1.4A/B). In the outward or extracellular facing state (OFS) the trimer bowl formation allows for water and ligands to gain access to the protein situated within the plasma membrane. Each protomer has a wedge shape which contains two distinct domains: the transport domain and trimerization domain (Figure 1.4C/D). The transport domain contains the binding sites for the substrate and ions (Figure 1.4C/E). The binding sites are partially formed by two hair pin loops, HP1 and HP2, which were identified as the reentrant loops in EAAT studies. The substrate, Asp, is coordinated by several residues include R397,

T314, D394, and N401 which were implicated to be involved in substrate binding in EAATs. R397 has been mutated to Ala, Cys, and citrulline to show it controls substrate selectivity and is vital for high affinity substrate binding(153-155). The substrate is also coordinated by residues on HP2 and HP1 solidifying the occluded state of the transporter (Figure 1.4E). Using structures and previous EAAT data, HP2 was proposed to serve as the extracellular gate which regulates access to the substrate binding site. The structural breakthrough for the SLC1A family allowed for functional data to be mapped to the actual quaternary structure and paved the way for defining the structure-function relationships required for transport.

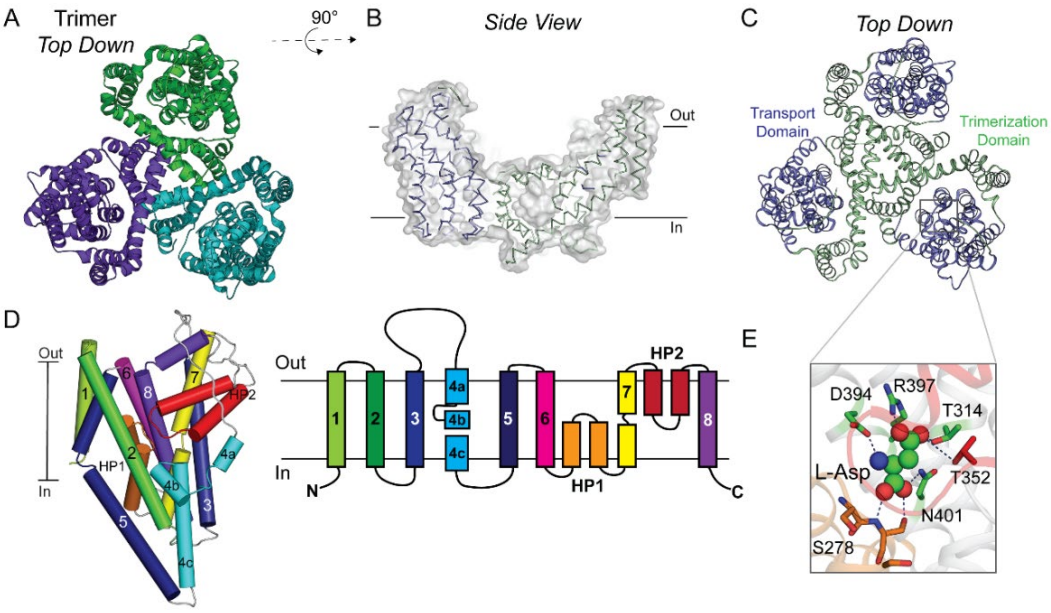

Figure 1.4. Structural features of SLC1 revealed through Glt_{Ph}. A) Trimer of Glt_{Ph} from pdb 2nwx which has both Na^+ and Asp bound. Each protomer is colored differently **B)** Side view of the trimer to highlight bowl shape which creates a way for water and ligands to gain access to the protein situated within the membrane **C)** Trimer with two domains of each protomer highlighted. Trimerization domains (TM1,2,4,5) are shown in green with the transport domain (TM3,6-8) which house the binding sites for ligands shown in blue **D)** A single protomer wedge architecture and corresponding numbering for the TM helices and HP loops **E)** Substrate binding site and coordinating residue. Binding site in the transport domain is partially formed by HP2, shown in red, and HP1, shown in orange. The box shows where the binding site is within the transport domain.

Novel alternating access transport mechanism

The overall transport mechanism for the SLC1 family was proposed to be one of alternating access already in 1966(156). Alternating access mechanism for a transporter essentially describes allowing access to their respective solute binding sites in one direction at a time: either extracellular, OFS, or intracellular, IFS (157). A series of allosteric changes involving ligand binding and release allow for the switch between OFS and IFS states (Figure 1.5A). Classically, there have been two main alternating access transport mechanisms: rocker switch and rocker bundle. In these mechanisms the scaffold domain moves within the membrane in different motions along with other protein domains to accomplish translocation. Through structural studies in Glt_{Ph}, a new alternating access mechanism was proposed(158). In this mode of transport, the scaffold domain is fixed in the membrane while another domain containing ligands moves within the membrane. Due to the nature of domain movements, this mechanism was coined as an elevator mechanism. After being discovered in glutamate transporters, evidence for the elevator mechanism was also found for the sodium-proton exchanger(159) as well as implicated for sodium-dicarboxylate symporter (VcINDY)(160), a citrate transporter(161), and a phosphorylation-coupled saccharide transporter(162).

The first structure of Glt_{Ph} trapped in the inward facing state showed the trimerization domain roughly unmoved when compared to the OFS(158). The main structural difference lies in the transport domain which contains the binding sites for substrate and ions (Figure 1.5B/C). The transport domain reorients in an 'elevator motion' of about 15-18 Å along the membrane and a 30° twist (Figure 1.5B/C). The residues of the trimerization domain, predominately on TM2 and TM5, form the interface between trimerization – transport domains consisting of mainly hydrophobic residues. In

the OFS state these residues interact mainly with residue along HP1 and bottom of TM7 belonging to the transport domain (Figure 1.5D). After the transport domain isomerizes into the IFS, the trimerization domain interface in turn interacts with residues along HP2 and the top of TM8 (Figure 1.5E). The conformation changes along the OFS-IFS isomerization pathway were further expanded upon when Glt_{Ph} was solved in an asymmetric trimer conformation(163). Two protomers were in previously solved OFS and IFS states with the third protomer in an intermediate state. The intermediate protomer is similar to OFS with a slight twist of the transport domain and a lowering into the membrane. The other noticeable difference in the intermediate was an unlocking of the transport domain from the trimerization domain or a loss of interactions with the scaffold. Therefore, to accomplish the transition from OFS to IFS, the transport domain must 'unlock' from the trimerization domain. The asymmetric structure also supports that each protomer can work independently.

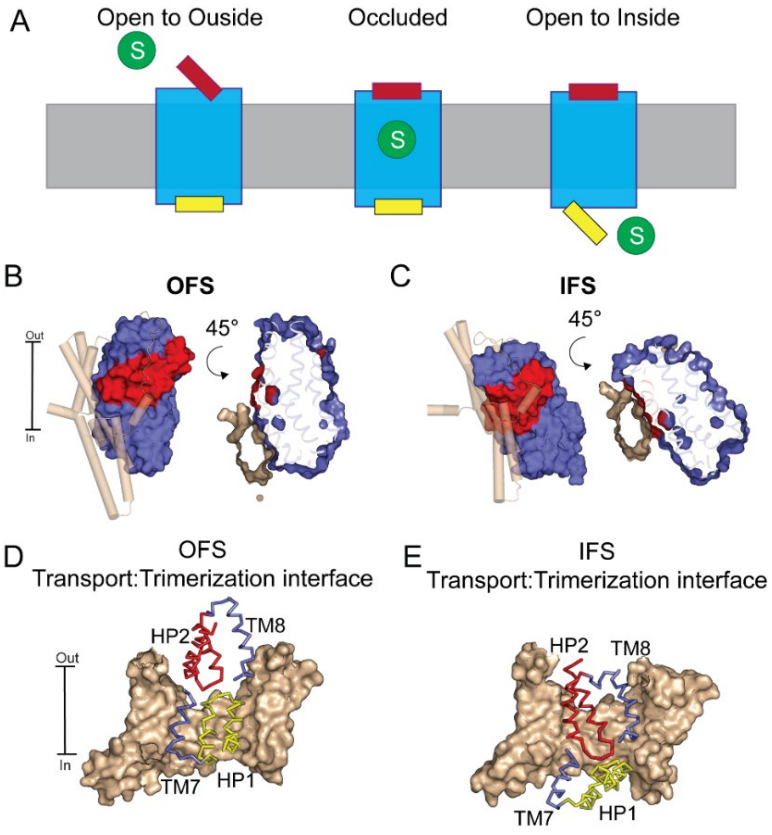

Figure 1.5. Elevator mechanism of glutamate transporters A) Cartoon depicting alternating access mechanism of transporters **B)** OFS state with Na^+ and Asp bound, pdb 2nwx. The transport domain shown as a surface representation in blue, HP2 is colored red as a reference for domain movement, trimerization domain is shown as cylindrical helices in wheat. The second image is slightly rotated to further show trimerization – transport domain localization **C)** IFS state with Na^+ and Asp bound, pdb 6x15. The transport domain shown as a surface representation in blue, HP2 is colored red as a reference for domain movement, trimerization domain is shown as cylindrical helices in wheat. The second image is slightly rotated to further show trimerization – transport domain localization **D-E)** Trimerization – transport domain interface differing between the OFS and IFS.

Insight into ion binding sites

Several structures of Glt_{Ph} and another closely related homolog Glt_{Tk}, have been solved at high resolution to reveal the three Na^+ binding sites that are required for substrate translocation(150, 164, 165). Initially Na1 and Na2 were first visualized through thallium binding(150). These sites were confirmed by competitive binding of Na^+ to drive off thallium resulting in diminished anomalous Tl^+ signal.

The site designated Na1 is situated within the transport domain and is partially occluded by HP2 (Figure 1.6A). Na1 is coordinated by the single side chain of D405 and several backbone carbonyls belonging to N310, N401, G306 with N310 being part of the highly conserved NMDGT moiety (N310-T314). A D405N mutation in Glt_{Ph} was able to diminish Tl^+ binding to the Na1 site and showed corresponding functional consequences indicative of perturbed Na^+ binding. The D405N mutant had a reduced dependence on Na^+ for substrate binding, suggesting a coupling of substrate binding with one Na^+ ion instead of two Na^+ ions proposed to bind before substrate(150). The analogous residue and substitution in EAATs show a variety of effects with either no loss of Na^+ dependency on glutamate binding and no transport(133), a shift in cation selectivity and a shift to an exchange mode(166), or an effect predominately on the K^+ translocation step(167). Therefore, D405 has been suggested to be part of the K^+ binding site in EAATs or participating in overlapping Na^+ and K^+ sites(166).

The site designated Na2 is mainly formed from backbone carbonyls on HP2 (T352, S349, I350) along with carbonyls of TM7 residues below the NMDGT motif and potential side chain coordination with T308 (Figure 1.6A). The position of the Na2 site suggests that this is the final Na^+ ion which binds post substrate. The site location agrees with experiments in EAATs where HP2 residues affected cation selectivity(168).

The third Na^+ binding site, Na3, was not identified through structural means until 2016 when Glt_{Tk} was solved to 2.8 Å with Na^+ and substrate bound(164). Previously, studies using molecular dynamics (MD) simulations, mutagenesis studies, and electrostatic calculations were implemented to suggest various potential Na3 sites. One of these sites partially overlaps with the substrate binding site including T314 and N401 (135) which showed reduced Na^+ affinity and impaired substrate translocation when substituted in EAATs. Other proposed sites involved the side chain residues in the NMDGT: N310 and D312 with varying other participating residues, whether it be TM3 residues (S93, T92, Y89) or TM8 residues (G404)(169, 170). The Glt_{Tk} structure confirmed that the Na3 site is indeed coordinated by sidechain moieties on TM3 and N310 and D312 of the NMDGT motif (Figure 1.6A). Residues involved in Na3 coordination have been substituted in EAATs to probe the validity of the site and reveal functional consequences from perturbing the site. When either T92, S93, N310, or D312 equivalents are substituted with Ala, there is a loss of Na^+ affinity or lack of transport all together supporting this site in both prokaryotic and eukaryotic members(169).

Glt_{Ph} does not require a proton for substrate translocation or K^+ for countertransport. The residue which has been identified in EAATs to be important for protonation in the transport cycle, E373, is already a Gln in Glt_{Ph}, Q318 (Figure 1.6B). Glt_{Ph} structures of different states have been used to create homology models for EAATs to identify possible K^+ binding sites. Glt_{Ph} also serves to identify difference between EAATs to reveal insights into K^+ coupling. One study identified a conserved Arg on TM8

which is a Met in Glt_{Ph}, M395, and an Arg in HP1 in Glt_{Ph}, R267, which is predominantly a Ser in EAATs. The two residues were substituted to their corresponding counterpart's amino acids in both Glt_{Ph} and EAAT1. Moving the Arg from HP1 to TM8 to mimic EAATs in Glt_{Ph} resulted in reduced substrate affinity while the converse Arg on TM8 moved to Arg on HP1 in EAATs resulted in an increase in substrate affinity for both glutamate and aspartate and K^+ independent transport(141). Various possible K^+ sites have been suggested through MD simulations to be around the substrate binding site and Na1 site. One of the proposed sites involves the equivalent residues for D405 and N401. This site overlaps with the Na1 site which would ensure mutually exclusive transport by different ions in the different arms of the transport cycle (154, 171, 172)(Figure 1.6C). Further experiments in EAATs are needed to confirm the K^+ binding site and its role in coupled transport.

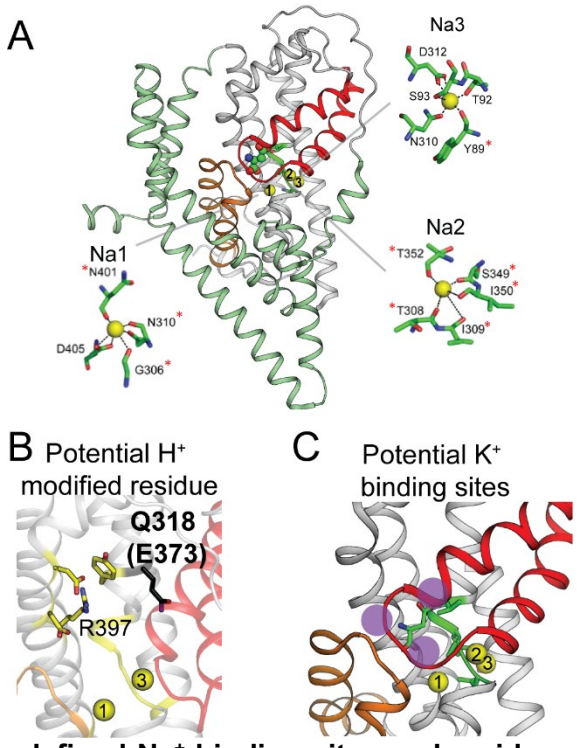

Figure 1.6. Structurally defined Na^+ binding sites and residues involved in H^+ and K^+ binding mapped to structures A) Glt_{Tk} protomer with transport domain in grey, trimerization domain in green, HP2 in red, HP1 in orange, and Na^+ as yellow spheres (pdb 5e9s). Insets are the coordination spheres of each of the three Na^+ binding sites, red asterisk denotes carbonyl oxygen coordination **B)** Residue identified in H^+ coupling in

EAATs is Q318 in Glt_{Ph} (pdb 7ahk) **C)** Purple spheres indicate potential K^+ binding sites through Glt_{Ph} homology modeling and EAAT mutagenesis data (pdb 5e9s).

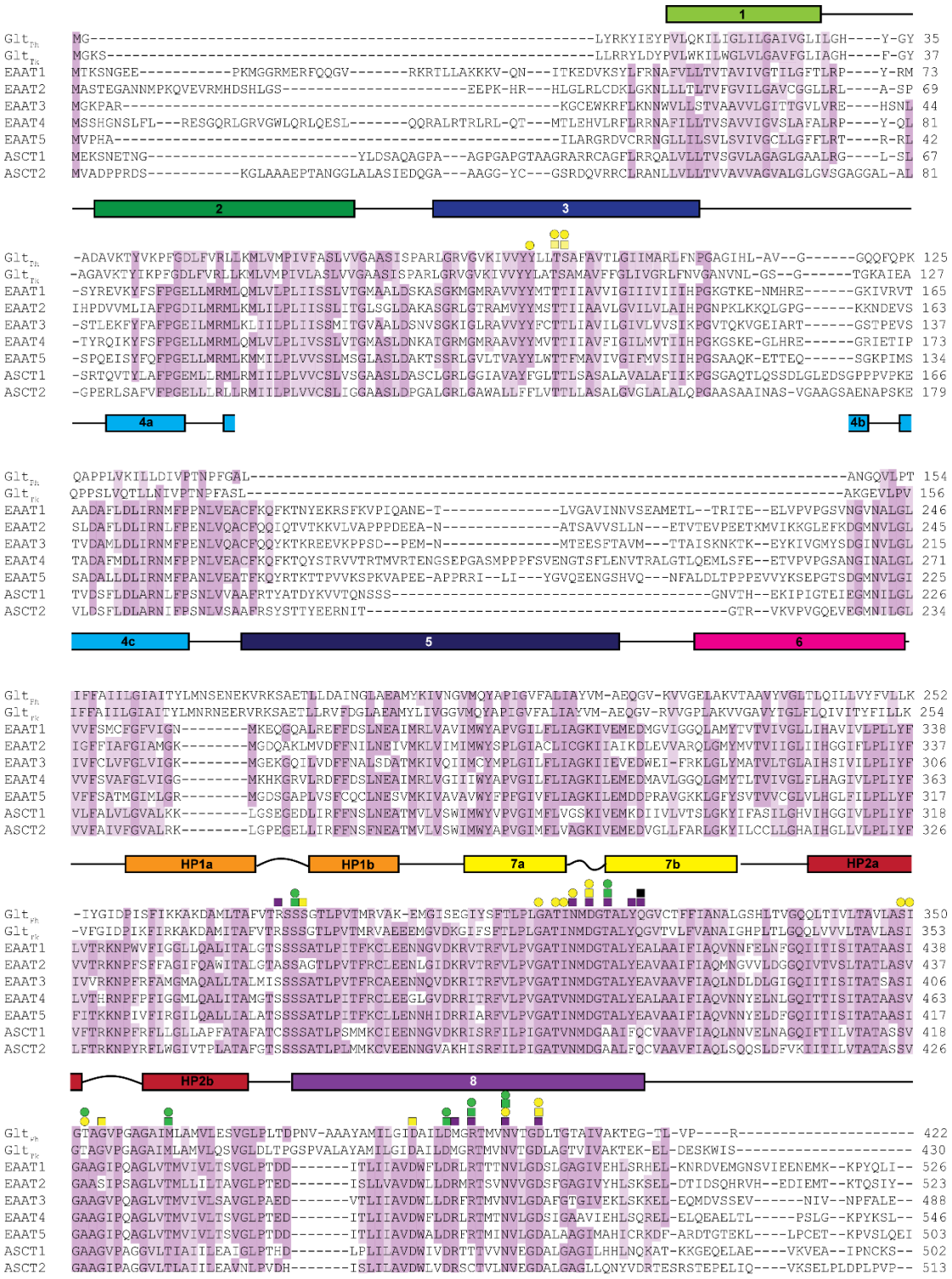

Figure 1.7. Sequence alignment with relevant ligand coordinating residues annotated. Multiple sequence alignment of Glt_{Ph}, Glt_{Tk}, EAAT1-5, and ASCT1/2 (C-

terminus omitted for other SLC1 members after end of Glt_{Ph} sequence. Dark purple indicates conservation of a single amino acid while lighter purple indicates conservation of amino acid property (ex: all hydrophobic). The secondary structure is denoted for Glt_{Ph} above the sequence alignment. Symbols above the sequences denote residues that have been functionally implicated in Na^+ binding (yellow), K^+ binding (purple), H^+ binding (black), and substrate binding (green). Circles represent Glt_{Ph} while squares indicate EAATs. MSA generated through t-coffee server(173).

Insight into chloride conductance with Glt_{Ph}

In EAATs, substrate binding induces a thermodynamically uncoupled chloride flux in addition to coupled ion fluxes. The Cl^- conductance takes less energy for activation than the coupled transport cycle similar to a channel mechanism(110). From Cys scanning experiments on HP2 in EAATs, it was demonstrated that glutamate transport can be blocked without affecting the corresponding glutamate activated chloride conductance, therefore there are separate molecular elements for each process(143, 174).The first indication of the chloride conductance pathway in EAATs involved Cys scanning of TM2 residues. These TM2 Cys substituted residues were aqueous accessible, sensitive to negative Cys modifying reagents, and altered the extent of anion conductance activation as well as anion permeability when modified (175). The loop between TM2 and TM3 also showed no transport related anion conductance when altered(175). Other residues near the potential K^+ binding site (such as R477) were also shown to tune the anion selectivity (176).

Glt_{Ph} also has a substrate induced chloride conductance. When an equivalent TM2 residue substitution in EAATs was made in Glt_{Ph}, S65V, a similar phenotype of impaired anion conductance was observed(177). With MD simulations, electrostatic mapping, functional studies, and resolution of key structures, the Cl^- pathway was identified (Figure 1.8A) as well as the molecular basis for channel activation in the context of the transport cycle (Figure 1.8C)(106, 121, 122, 163, 175, 177-180). Briefly, when the transport domain unlocks from the trimerization domain and is in the process of isomerizing into the inward facing state, a pathway for anion conductance opens

(Figure 1.8). This pathway also allows for water to pass and is gated by two hydrophobic patches involving TM2 and TM5 residues. The pathway was also tested in EAAT1 to confirm that the pathway and mechanism identified in Glt_{Ph} is conserved(178).

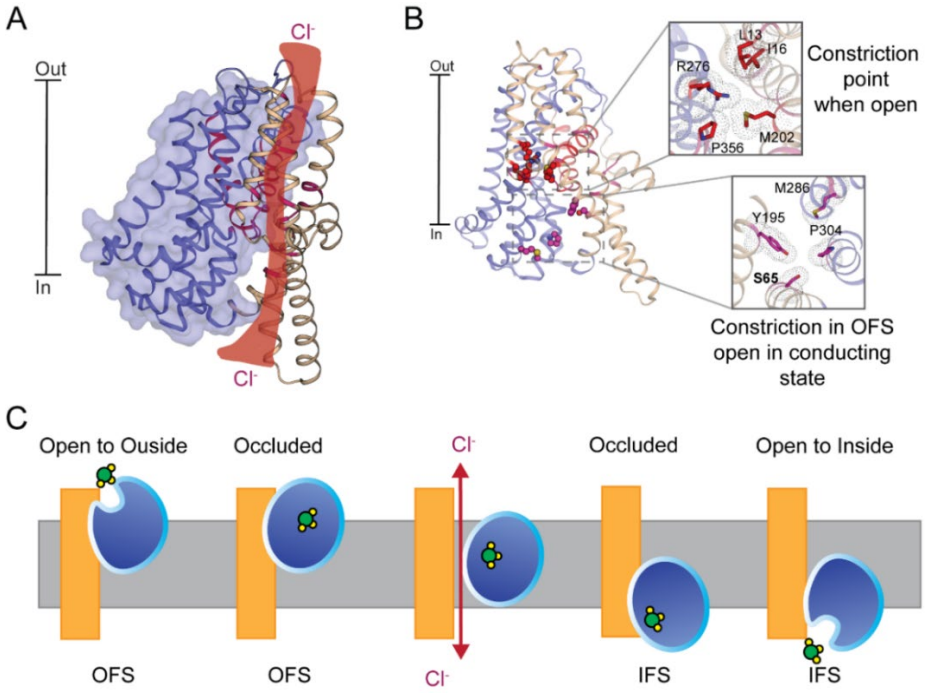

Figure 1.8. Chloride conductance revealed through functional, MD, and structural studies. A) Glt_{Ph} protomer captured in the chloride conducting state through crosslinking (pdb 6wyk). The transport domain is shown in blue with HP2 in red and a surface overlay while the trimerization domain shown as wheat cartoons, pink residues are implicated to interact with chloride from MD simulations. The red swatch indicates the chloride permeation pathway which is accessible when the transport domain unlocks from the trimerization domain **B)** Constriction points in the chloride conducting pathway. Insets are the protein viewed from the intracellular side. Red residues form the pathway constriction site when the channel is open while pink residues form the constriction site when in the OFS **C)** Cartoon depicting how chloride conductance factors into the transport cycle. The orange blocks represent the scaffold/trimerization domain while the blue oval represent the transport domain. The green sphere represents the substrate while yellow spheres are Na^+ ions. Adapted from (178).

Dynamics of transport and conformational states along the cycle

The elevator transition of the transport domain along the membrane with a fixed trimerization domain was functionally supported by studies utilizing single-molecule fluorescence resonance energy transfer, smFRET (181, 182), double electron-electron resonance, DEER (183, 184), and High Speed Atomic Force Microscopy, HS-AFM(185).

The dynamics of transport domain movements were observed in these studies and showed a sampling of multiple conformations in the presence or absence of ligands. Essentially, the protein can transition from OFS and IFS in the Apo or fully bound state. The presence of ligands causes shifts in conformational population distribution, but the transport domain state remains heterogeneous. The dynamics of conformational changes are also stochastic, protomers experience periods of inactivity with bursts of rapid activity. Only in the Na^+ alone condition was stalling observed which indicated Na^+ based conformational changes are a slow step in the transport cycle(185). The spectroscopic data also agreed with what the asymmetric trimer suggested: each protomer of Glt_{Ph} isomerizes independently. Another study following single molecule transport kinetics uncovered another feature of transport: distinct kinetic populations of protomers(186). The different populations of protomers experience persistent fast, intermediate, and slow transport. These distinct kinetic behaviors persist on a promoter basis over multiple turn over events and suggest these proteins experience a 'molecular memory'.

Time resolved smFRET data also alluded to the isomerization of the fully loaded OFS protomer to the IFS as the rate limiting arm of the transport cycle. The event proposed to be responsible for the slow step is the unlocking of the transport domain from the scaffold prior to isomerization. When investigating the potential high energy transition state which limits the rate of substrate translocation, it was found the transition state most resembles the IFS, further supporting OFS to IFS transition as the main energy barrier in the cycle(187). Disrupting the domain interface with point mutations led to faster transport rates indicating that transport domain unlocking is a key component of the slow substrate translocation. One set of the gain of function mutants includes the Arg swap from HP1 to TM8 previously discussed (R267S on HP1 and M395R on TM8). There is a correlation between increased substrate translocation with disruption of the

trimerization-transport domain interface and a decrease in substrate affinity(182, 187). These data support substrate translocation and the prerequisite conformation changes (ligand binding and domain unlocking) as the slow step in the cycle. Dwell times of different states in the transport cycle were also resolved with high-speed AFM linear-scanning in both the Apo and fully bound states(188) (Figure 1.9). The data corroborates the ability to make the OFS to IFS transitions in the Apo or Fully bound states and suggests an intermediate state is possible in both pathways to the IFS. The intermediate state is in between the OFS and IFS and most resembles the trapped intermediate recently found to conduct anions and water. The protomer can also attempt unsuccessful excursions into the intermediate state.

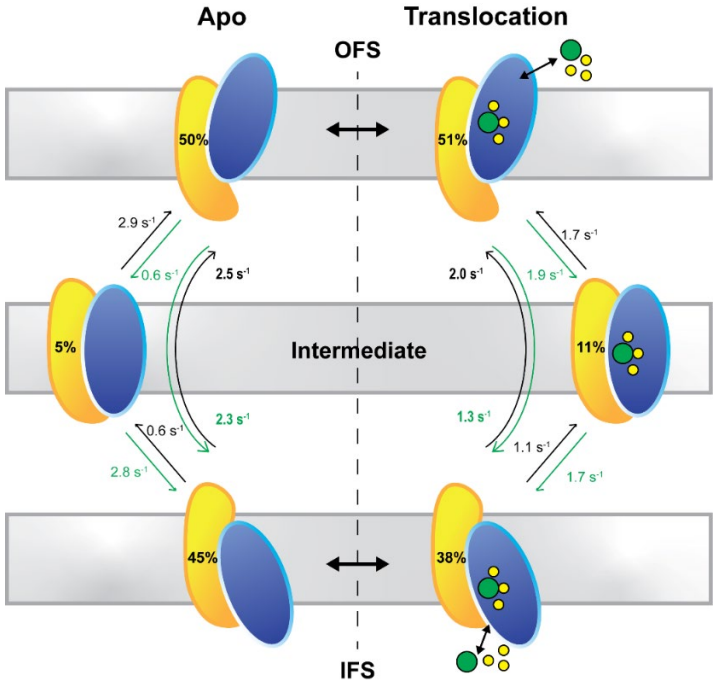

Figure 1.9. Conformational dwell times in different ligand conditions. Two sets of conditions are Apo and Na^+/Asp bound. The yellow oval represents the trimerization domain while the transport domain is the blue oval, Na^+ ions are depicted as yellow spheres while substrate is the green circle. The percent change next to each "protomer" is the occupancy of each state in the pathway. Each arrow indicates the transport domain pathway and the numbers next to the arrows are weighted rate constants taken from (188). Adapted from (188).

Another factor to consider in understanding the dynamics of the transport cycle is the role of lipids and the lipid membrane. In the inward facing state, there is a sizeable deformation of the membrane which needs to be energetically offset somewhere within the protein or in the environment (189-191). This energetic cost could contribute to the rate limited substrate translocation and the ability for protomers to work independently. With more single particle cryo-electron microscopy (Cryo-EM) structures solved in nanodiscs, there are emerging body of lipid-protein interactions. Lipids can be observed in the pockets between the transport domain and trimerization including a 'lipid window' when the transport domain unlocks (OFS to IFS). Lipids have been suggested to help ease the transition between OFS and IFS and therefore play a role in transport. Lipids can also be observed inserted in between the elevator gate and the rest of the transport domain as well as in between the transport domain core and the loop between TM3 and TM4, 3L4. The functional importance of these specific lipids remains unresolved. It has been demonstrated that lipids do affect the transport of Glt_{Ph}, specifically the substrate translocation arm of the cycle(192). In the study, it was suggested that lipid head group interaction with the trimerization domain through Y33 on TM1 influences conformational flexibility and therefore the rate of transport(192). Essentially, the more cation-π interactions between the top of TM1 and lipid headgroups, the less likely the OFS to IFS transition.

Coupled binding necessary for substrate translocation

As mentioned above, there have been many structures of Glt_{Ph} solved in states along the transport cycle as well as human members of the SLC1 family (EAAT1, EAAT3, and ASCT2)(193-197). These structures provide insight into the conformational changes necessary to accomplish transport in an elevator mechanism including the structural basis for large transport domain transitions and the elevator gate. Key arrangements have already been discussed in preceding sections including the

unlocking of the transport domain from the trimerization and the isomerization from the occluded OFS to occluded IFS. The structural changes required for the transport have been expanded upon with a variety of Cryo-EM studies in nanodiscs(191). The ensemble of structures available now follows from Apo OFS to Apo IFS and shows a transport domain swinging and twisting motion accompanying the previous identified transport unlocking (Figure 1.10). The swinging motion of the transport domain away from the trimerization domain is observed in the inward facing state structures and highlights the necessity to allow for the intracellular gate, HP2, to open and release ligands. These data along with other structures, implicate HP2 as both the extracellular and intracellular elevator door supporting a one gate mechanism.

HP2 was proposed to be the extracellular gate in the alternating access mechanism based on the original structure of Glt_{Ph} and functional EAAT data. Cysteine scanning studies in EAATs established that HP2 forms an aqueous pore which is blocked by glutamate and certain modifications can block flux of substrate(124, 125, 128, 129, 198). All suggest HP2 is involved in coupling flux of Na^+ and substrate(199). Crosslinking studies also provided evidence HP2 adopts different conformations along the transport cycle depending on the ligand state, specifically substrate causing distinct conformations of HP2. In conclusion, HP2 is indeed the extracellular gate in EAATs and Glt_{Ph} (198). Structural data from Glt_{Ph} also supports HP2 as the extracellular gate which adopts different conformations based on the presence of different ligands (Figure 1.10)(150, 164). The initial structure of Glt_{Ph} was solved in the presence of Na^+ and substrate with HP2 closed. The next structure of Glt_{Ph} was determined with Na^+ and an aspartate analogue, DL-*threo*-β-Benzyloxyaspartic acid (TBOA)(150). TBOA has the backbone of Asp with an additional bulky moiety and the structure shows TBOA in the substrate binding site propping HP2 open. These initial structures indirectly confirm HP2 as the extracellular gate and give information on which Na^+ sites are occupied before

substate binding. In the presence of TBOA and Na^+, only electron density is observed at the Na1 site with none at the Na2 site. The Na2 site is predominately formed by HP2 so if HP2 is open, the Na2 site does not exist and suggests Na2 binds following substrate. TBOA is also a transport inhibitor and proves coupled HP2 conformational changes are essential for transport since the transport domain cannot isomerize into the inward facing state when HP2 is open.

As the alternating access model suggests there is a gate in both the extracellular and intracellular facing states to regulate substrate binding and release. Initially, it was proposed that HP1 is the intracellular gate due to inverted repeat structural moieties and cysteine scanning of HP1 in EAAT (200). One MD study looking at substrate release and the inward facing state suggested it is in fact HP2 that acts as the intracellular gate (201). This was further supported by the influx of structures from both prokaryotic and eukaryotic members which showed HP2 opening in the inward facing state and HP1 remaining mostly rigid within the transport domain(194, 197). Even with the new revelation of a one gate elevator mechanism, the molecular mechanism for substrate release is still poorly understood. Theoretically, the molecular mechanism for substrate release should mirror the mechanism for substrate association. Na^+ affinities are also similar for both the OFS and the IFS(202).

Structures have resolved the conformation states of HP2 with different ligands as well as interactions HP2 makes within the protein throughout the cycle. For forward transport starting at the Apo-OFS state, HP2 is closed forming interactions with fellow components of the transport domain. With only Na^+ present in the OFS, HP2 is open to a similar extent as the TBOA bound form(203). When HP2 is open it does not interact with the core transport domain, but with the loop between TM3 and TM4 (3L4). The two Na^+ sites that are bound in the HP2 open structure are Na3 and Na1, confirming that these sites are occupied before substrate binding. In the fully bound state (three Na^+ ions

bound and substrate), HP2 is closed and forms interactions with HP1, the substrate, and Na2.

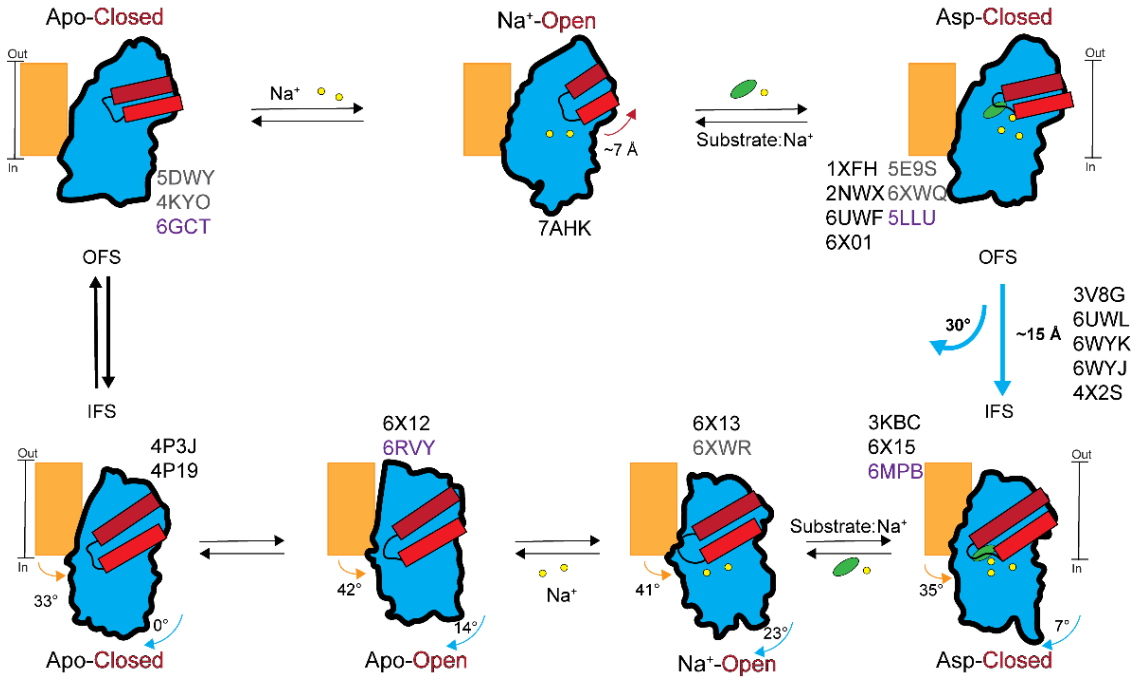

Figure 1.10. Transport domain movement along the transport cycle including the one-gate, HP2. Transport domain is the teal-colored shape and the trimerization domain is depicted as the orange rectangle. HP2 is shown in red, substrate as the green oval and Na^+ as the yellow spheres. OFS to IFS arrows in teal indicate the rearrangement that occurs, a twist and lowering into the membrane. Colored arrows reflect conformational features, whether that be HP2 opening (red arrow), twisting of the transport domain (teal), or the swinging angle between the transport domain and the trimerization domain (light orange) for intracellular gating. The four-character codes are the respective pdbs for the relevant state shown in the cycle. Black lettering is Glt_{Ph}, grey is Glt_{Tk}, and purple is human ASCT2 or EAAT1. Adapted from (191).

The 3L4 which interacts with HP2 in the Na^+ bound state also plays a role in the transport cycle. The disordered loop region crosses the transport domain and is not well resolved in a variety of structures. The loop undergoes substrate dependent conformational changes. When the loop is cleaved, transport is abolished or drastically decreased(204). The decrease in overall transport stems from an altered turn-over rate and not substrate affinity, specifically disrupting one or more steps involved in the loaded OFS to IFS transition, but not the Apo OFS to IFS transition(205). An MD simulation looking at the pathway of substrate translocation also confirmed substrate dependent

conformational changes in the 3L4(206). A recent study performed crosslinking experiments in EAAT2 between HP2 and 3L4 to corroborate that both change in spatial proximity throughout the transport cycle(207), but the role of 3L4 along the transport cycle remains unresolved.

Na^+ induced conformational changes in coupled binding

The molecular mechanism for how HP2 movement is regulated during the transport cycle was poorly understood at the start of this thesis research. The available structural data gave snapshots of different conformations which served as clues for the molecular events necessary for extracellular gate opening and closure. The sequential, coupled binding required to fully load a protomer for transport involves changes in HP2 and residues in the binding site. A functional study utilizing EPR, demonstrated that in the Apo state HP2 is closed and Na^+ binding to the Apo protomer causes conformation changes including HP2 opening(208). Therefore, HP2 opening can either result from Na^+ binding and inducing HP2 opening through allosteric means or Na^+ binding to a select conformation of the protomer with HP2 open, thus stabilizing HP2 open state(209). Several functional studies demonstrate that Na^+ binding to the transporter prior to substrate binding is slow and most likely reflects Na^+ inducing conformational changes(210, 211). This is corroborated by structures which show conformational changes in the presence of Na^+ alone. Upon substrate binding in the presence of Na^+, HP2 closes, and substrate binding is relatively fast. The opening of HP2 caused by Na^+ binding and closure upon substrate binding are the keys to the coupling mechanism which ensures only fully loaded ($3Na^+$:1Asp) or Apo protein transverse the membrane. Na^+ alone cannot translocate since HP2 is open and only in the presence of adequate Na^+ is translocation possible by regulating access to the substrate binding site through HP2 movement.

MD simulations of time resolved HP2 movements have proposed various orders of binding events as well as substrate assisted HP2 closure(170, 201, 212, 213). At the start of the thesis research, Na3 was believed to bind first, followed by Na1. These binding events are responsible for transport domain rearrangements which open HP2 and enable high affinity substrate binding. Substrate then binds and helps HP2 close, followed by Na2 binding to fully stabilize HP2 where the transport domain can then isomerize into the IFS and translocate substrate(214). Further MD simulations have uncovered other potential binding orders and the conformational consequence corresponding to those binding events(169, 171, 215-217). Some notable residues in the binding site which have been identified to be key in this coupling process are R397 and M311(154). The role of these residues in accomplishing the Na^+ induced conformation changes have now been established.

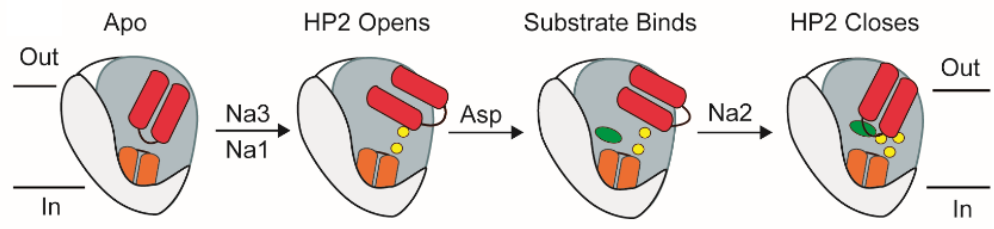

Figure 1.11. HP2 gating in coupled binding required for translocation of substrate.

Summary

Glutamate transporters are vital for normal physiological processes and their dysfunction has been implicated in several pathological states. By understanding how they function, we can both exploit the proteins as therapeutic targets and understand native physiology. Glutamate transporters accomplish the unfavorable translocation of substrate across the membrane by coupling it to the existing Na^+ electrochemical gradient, specifically three Na^+ ions to one molecule of substrates. Through these studies on both glutamate transporters and homologs, the transport cycle and its

structural underpinnings have been resolved for large domain movements. Gaps that existed at the start of this thesis work included the location of the K^+ site and how it fits into the coupling mechanism, the molecular choreography encompassing the Na^+ induced conformational wave and allosteric mechanism for regulating gate movement, and the mechanism for substrate release in the inward facing state. The bulk of the research in this publication is centered on addressing the gap in our understanding of the allosteric coupling mechanism for regulating gate movement.

Chapter 2: Investigation of the allosteric coupling mechanism in a glutamate transporter homolog via unnatural amino acid mutagenesis

This chapter was published in PNAS in 2019 as:

Riederer, E. A. & Valiyaveetil, F. I. (2019). Investigation of the allosteric coupling mechanism in a glutamate transporter homolog via unnatural amino acid mutagenesis. *PNAS*, 201907852. doi:10.1073/pnas.1907852116.

The experiments in this chapter were planned by E.A.R. and F.I.V, E.A.R collected all the data, and E.A.R and F.I.V wrote the manuscript together.

Significance:

Glutamate transporters harness ionic gradients for the concentrative uptake of glutamate. Normal function of glutamate transporters is required for rapid removal of glutamate from the synaptic space, which is required for efficient neurotransmission and preventing excitotoxicity. A key question in glutamate transporters is the mechanism by which the ionic gradient is coupled to glutamate uptake. Previous studies have proposed a role for hairpin-2 in this coupling mechanism. Here, we use unnatural amino acid mutagenesis to develop a fluorescence assay for HP2 movement in the archaeal homolog, Glt_{Ph}. Using this assay, we show how key residues in the substrate binding site modulate the movement of HP2 and thereby identify the sequence of events involved in the coupled binding of sodium and substrate.

Abstract:

Glutamate transporters harness the ionic gradients across cell membranes for the concentrative uptake of glutamate. The sodium coupled Asp symporter, Glt_{Ph} is an archaeal homolog of glutamate transporters and has been extensively used to understand the transport mechanism. A critical aspect of the transport cycle in Glt_{Ph} is the coupled binding of sodium and aspartate. Previous studies have suggested a major role for hairpin-2 (HP2), which functions as the extracellular gate for the aspartate binding site, in the coupled binding of sodium and aspartate to Glt_{Ph}. In this study, we

develop a fluorescence assay for monitoring HP2 movement by incorporating tryptophan and the unnatural amino acid, *p*-cyanophenylalanine into Glt_{Ph}. We use the HP2 assays to show that HP2 opening with Na^+ follows an induced-fit mechanism. We also determine how residues in the substrate binding site affect the opening and closing of HP2. Our data, combined with previous studies, provides the molecular sequence of events in the coupled binding of sodium and aspartate to Glt_{Ph}.

Introduction:

Secondary active transporters harness pre-existing ionic gradients to transport their substrates across cellular membranes(157, 218). A central question in the study of transporters has been the mechanism by which the ionic gradients are harnessed to power the transport of substrate. Here we investigate this question of ion–substrate coupling in the context of glutamate transporters.

Glutamate is the primary excitatory neurotransmitter in the central nervous system(14). Following release into the synaptic space during neurotransmission, glutamate is rapidly cleared by the action of glutamate transporters that are also referred to as Excitatory Amino Acid Transporters (or EAATs)(61, 219, 220). EAATs harness the energy from the pre-existing gradients of Na^+, H^+ and K^+ across the cell membrane to drive the concentrative uptake of glutamate(100, 101). Normal function of EAATs is vital for efficient synaptic transmission and for preventing excitotoxicity(14).

Key insights into the structure and the transport mechanism in EAATs have come from studies on the archaeal homolog Glt_{Ph} (and the closely related Glt_{Tk})(149, 165). Glt_{Ph} is a sodium coupled Asp symporter in which the uptake of Asp is coupled to the symport of 3 Na^+ ions(152). The structural studies show that Glt_{Ph} is a homotrimer (Figure 2.1A) with each subunit consisting of eight transmembrane helices (TM1-8) and two helical hairpins (HP1, 2) that form two distinct domains: a central trimerization domain and a peripheral transport domain (Figure 2.1B)(149, 150, 158). The transport

domain is comprised of TMs 3, 7, and 8 along with HP1 and 2 and contains the binding sites for Asp and the three Na^+ ions (the Na^+ sites are referred to as Na1, Na2 and Na3, Fig. 1B).

The transport mechanism in Glt_{Ph} involves the elevator-like movement of the transport domain between the outward facing state, OFS, and the inward facing state, IFS, while the trimerization domain stays stationary in the membrane(158, 181-184). The transport cycle involves the binding of Na^+ ions and Asp to the transport domain in the OFS, followed by the elevator like movement to the IFS. Following release of Na^+ ions and Asp from the IFS, the transport domain reorients from the IFS to the OFS to complete the cycle.

A critical aspect of the transport mechanism is that the binding of Na^+ and Asp is strongly coupled(150, 151, 202). Due to this coupling, the binding affinity of Glt_{Ph} for Asp is strongly dependent of the Na^+ concentration and conversely the binding affinity for Na^+ is dependent on the presence of Asp(202). The crystal structures of Glt_{Ph} and Glt_{Tk} show no direct contact between the bound Asp and the Na^+ ions indicating that the coupling mechanism involves allosteric changes (Figure 2.1B)(150, 164). Structures of Glt_{Ph} and Glt_{Tk} combined with computational, spectroscopic and functional studies have suggested a scheme for the coupled binding of Na^+ and Asp (Figure 2.1C)(61). Central to this scheme is the movement of HP2, which acts as the external gate to the substrate binding site(150, 170, 200, 201, 208, 213, 221, 222). In the Apo state, the crystal structures show that HP2 is closed thereby preventing access to the substrate binding site(164, 165). The binding of two Na^+ ions, presumably to the Na3 and the Na1 sites, remodels the substrate binding site and causes HP2 to open for the binding of Asp(154, 164, 169). In contrast to this model, computational studies suggest that HP2 is dynamic in the Apo state(170, 221). The binding of Asp is followed by the closure of HP2, which is further enhanced by the binding of the third Na^+ ion to the Na2 site. The Na^+ and Asp

bound transport domain then reorients from the OFS to the IFS for the transport of Na^+ ions and Asp into the cell(158). There are important aspects of this binding scheme that are not understood. Chief among these are the mechanisms by which the binding of Na^+ and Asp is linked to the movement of HP2.

Here, we develop a fluorescence-based assay to track the movement of HP2. We use this assay to show that the opening of HP2 with Na^+ follows an induced-fit mechanism. We use the HP2 assay to identify key residues in the Asp binding site that modulate the movement of HP2. Our experimental data suggests an intricate sequence of events in the coupled binding of Na^+ and Asp to Glt_{Ph}.

Results:

A fluorescence assay to probe the movements of HP2

We developed a fluorescence-based assay to probe the opening and closure of HP2. In developing this assay, we examined the crystal structures of Glt_{Ph} (and Glt_{Tk}) in the various states to identify a pair of residues, V355 in HP2 and S279 in HP1, which change inter-residue distance with the movement of HP2 (Figure 2.1D, Table S2.1). A change in distance between V355 and S279 with HP2 movement was also reported using EPR(208). For the fluorescence assay, we substituted V355 with Trp and S279 with the unnatural amino acid, 4-cyano-phenylalanine (Phe_{CN}). We anticipated that a change in distance between Trp and Phe_{CN} will alter the Trp fluorescence and thereby provide a selective probe to monitor the movement of HP2. We substituted S279 with Phe_{CN} using the nonsense suppression approach (Figure S2.1A)(223, 224). The S279Phe_{CN} +V355W Glt_{Ph} [or Glt_{Ph}(Phe_{CN} +W)] showed similar biochemistry to the wild type transporter and was functional in Asp uptake albeit at a lower level compared to the wild type transporter (Figure S2.1B-D).

To determine if fluorescence of Glt_{Ph}(Phe_{CN}+W) was sensitive to Na^+ and Asp binding, we purified the Glt_{Ph}(Phe_{CN}+W) protein and monitored the Trp fluorescence

emission following excitation at 295 nm in detergent solution. We observed that the fluorescence emission of $Glt_{Ph}(Phe_{CN}+W)$ was responsive to Na^+, with an increase in the fluorescence (33% at 345 nm) and a red-shift of the emission maxima on the addition of Na^+ to the Apo protein (Figure 2.1E). The increase in fluorescence was specific for Na^+ as no change in fluorescence was observed with the addition of an equal amount of K^+ (Figure 2.1F). To determine whether the change in fluorescence is due to the opening of HP2, we tested the effect of TBOA (D,L-threo-β-benzyloxy-aspartate), which binds similarly to Asp but keeps HP2 propped open due to the presence of the benzyloxy group in the side chain(150, 153). Addition of TBOA in the presence of 200 mM Na^+ gave a 45 % increase in the fluorescence confirming that the increase in fluorescence seen on Na^+ addition is indeed due to the opening of HP2. The fluorescence change with TBOA was roughly 12 % greater than the fluorescence change seen with Na^+ alone, which is consistent with the suggestion that TBOA can prop HP2 open further than the opening of HP2 with Na^+(150, 154). The change in fluorescence with TBOA was only observed in the presence of Na^+ suggesting that initial Na^+ binding is required for the binding of TBOA.

Closure of HP2 takes place on binding of Asp and Na^+. We observed for $Glt_{Ph}(Phe_{CN}+W)$ that the addition of Asp in the presence of 200 mM Na^+ caused a decrease in fluorescence and a blue-shift of the emission maxima. The fluorescence observed in the presence of Na^+ and Asp was 18% lower than the value measured for the Apo protein. The further decrease in fluorescence observed in the Asp bound state compared to the Apo state is consistent with the closer proximity of S279 and V355 observed in crystal structures of the Asp bound Glt_{Ph} and Glt_{Tk} compared to the Apo structures(154, 164, 165). The change in fluorescence with Asp was only seen in the presence of Na^+ consistent with the initial binding of Na^+ being required for Asp to bind.

Changes in fluorescence with Na^+ and Asp were also observed for the Glt_{Ph} single mutants, S279Phe_{CN} and V355W (Figure S2.2A/B). The magnitude of the fluorescence changes observed for the single mutants were different in magnitude and direction compared to the changes observed for Glt_{Ph}(Phe_{CN} +W) (Figure S2.2B). Phe_{CN} can act as a FRET donor to Trp,(225) however the changes observed for Glt_{Ph}(Phe_{CN} +W) were more consistent with Phe_{CN} acting as a distance dependent quencher of the Trp residue at 355. In support, we observed that Phe_{CN} in solution acts as a quencher for Trp (Figure S2.2C).

To further confirm that the changes in fluorescence observed originate due to distance dependent quenching of Trp by Phe_{CN}, we created an alternative Phe_{CN}/ Trp pair in which the V355 in HP2 was substituted with Phe_{CN} and A127 in the 3-4 loop was substituted with Trp (Figure S2.3). In the 355/127 pair, the opening of HP2 on the binding of Na^+ decreases the distance between these residues while the closure of HP2 on binding of Asp increases the distance. For the 355/127 pair, we observed that the addition of Na^+ or Na^+/TBOA caused a decrease in fluorescence, while the addition of Asp in the presence of Na^+ caused an increase in fluorescence. The changes in fluorescence for the 355/127 pair on Na^+, TBOA and Asp addition were in the opposite direction of the changes observed for 279/355 pair, which is consistent with a distance dependent quenching effect. The magnitude of the changes for the 355/127 pair were smaller than the fluorescence changes for the 279/355 pair.

The increase in fluorescence for Glt_{Ph}(Phe_{CN} +W) on the addition of Na^+ was fit with a Hill equation and gave a $K_{0.5}^{Na}$ of 177.9 mM (Figure 2.1G, Table S2.2). The Hill coefficient was determined from a double log plot of the ratio of the fraction bound to fraction unbound with the Na^+ concentration as previously described (Figure S2.4)(226, 227). The $K_{0.5}^{Na}$ value measured using the HP2 assay compares to a value of 99.3 mM

reported for Na^+ binding to the wild type transporter using a dye assay and 120 mM measured using the changes in fluorescence of the F273W–Glt_{Ph}(202, 210). Similarly, the decrease in fluorescence due to closure of HP2 was fit to give a $K_{0.5}^{Asp}$ for Asp binding of 36.9 nM in the presence of 200 mM Na^+ (Figure 2.1H), while a K_D^{Asp} of 2 nM has been reported for the wild type Glt_{Ph}(150, 202). The difference in Asp affinity could be due to the presence of the Phe_{CN} and Trp in the vicinity of the substrate binding site in the Glt_{Ph}(Phe_{CN} +W) protein.

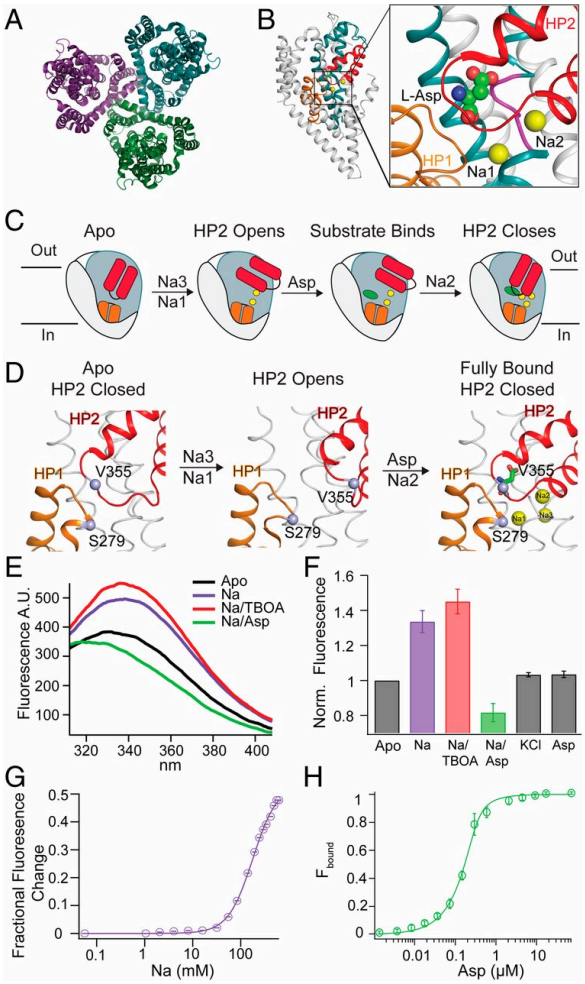

Figure 2.1. A fluorescence-based assay for HP2 movement A) Structure of the Glt_{Ph} trimer (pdb: 2nwx). **B**) Structure of a single subunit of Glt_{Ph}. TM 7 and TM8 are colored green, Close-up view of the Na^+ and Asp binding site is shown in inset. The bound Asp molecule is shown in space fill. **C**) Cartoon representation of the scheme for the coupled binding of Na^+ ions and Asp (green oval). In B and C, HP1 is shown in orange, HP2 is in red, and the Na^+ ions as yellow spheres**. D**) Close up view of the binding site in the Apo, Na^+ bound, and the Na^+ and Asp bound state. The Apo (pdb: 5dwy) and the Na^+/Asp fully bound (pdb: 5e9s) structures are of Glt_{Tk} while the Na^+ bound structure with HP2 open is

of Glt_{Ph} with TBOA bound (pdb: 2nww). Residues in the Glt_{Tk} structures are shown with Glt_{Ph} numbering. S279 in HP1 (orange) substituted with Phe_{CN} and V355 in HP2 (red) substituted with Trp are shown as lavender spheres. The structures highlight the change in distance between the fluorescence probes, Phe_{CN} and Trp, in the different states (Apo 7.6Å, Na^+ 13.6 Å, Asp/Na^+ 6.5 Å). **E**) Fluorescence emission spectra of Glt_{Ph} (Phe_{CN}+W) in the following conditions: Apo, 200 mM NaCl, 200 mM NaCl/10 µM TBOA, and 200 mM NaCl/100 µM Asp. **F**) Fluorescence at 345 nm for Glt_{Ph} (Phe_{CN}+W) with the addition of 200 mM NaCl, 200 mM NaCl/10 µM TBOA, 200 mM NaCl/100 µM Asp, 200 mM KCl and 100 µM Asp. The fluorescence values are normalized to the Apo protein. **G**) Na^+ titration of Glt_{Ph} (Phe_{CN}+W). The normalized change in fluorescence at 345 nm on addition of Na^+ is plotted. The solid line represents a fit using the Hill equation with $K_{0.5}^{Na}$ of 177.9 mM. **H**) Asp titration of Glt_{Ph} (Phe_{CN}+W) in the presence of 200 mM NaCl. The normalized fluorescence change on addition of Asp is plotted and fit (solid line) with a quadratic binding equation with $K_{0.5}^{Asp}$ of 36.9 nM. Error bars in D-F are ± S.E.M., N $\geq$ 3.

HP2 movement in Glt_{Ph} has also been probed using spin labelling and EPR spectroscopy, however, the introduction of the spin labels resulted in a non-functional transporter(208). Further, in contrast to EPR spectroscopy, the fluorescence assay allows for easy titration of the effects of Na^+ and Asp binding on HP2 movement. The fluorescence assay provides a means to evaluate how residues in Glt_{Ph} influence HP2 movement.

Kinetic measurements indicate an induced fit mechanism for HP2 opening with Na^+

The $K_{0.5}^{Na}$ measured using the steady state titrations of the Glt_{Ph}(Phe_{CN}+W) transporter with Na^+ are a composite of the binding affinity for Na^+ (K_D) and the equilibrium constant ($E=k_f/k_r$) for HP2 opening. We used kinetic measurements to estimate these parameters. The time course of the increase in fluorescence with Na^+ addition in the HP2 assay was relatively slow while the decrease in fluorescence with Asp in Na^+ was relatively fast and could not be resolved with our instrumentation (Figure 2.2A). The slow association of Na^+ ions to the transporter followed by the rapid binding of Asp is consistent with previous reports evaluating the kinetics of Na^+ and Asp binding to Glt_{Ph}(210, 211). The time course of the fluorescence increase with Na^+ was fit to a single exponential to obtain k_{obs} and the change in k_{obs} with Na^+ concentration informs on the mechanism of HP2 opening on Na^+ binding (Figure 2.2B/D) (228). The extreme

possibilities are an induced fit mechanism in which Na^+ binding causes the opening of HP2 or a conformational selection mechanism in which Na^+ binds to transporters with HP2 open and stabilizes the HP2 open state (Figure 2.2C). The induced fit mechanism dictates that the k_{obs} should increase with increasing Na^+ as there is more Na^+ to open HP2 while the conformational selection model dictates that k_{obs} should decrease with increasing Na^+, reflecting the decreasing pool of transporters with HP2 open for Na^+ to bind. We observed an increase in k_{obs} with increasing Na^+ that plateaued at higher Na^+ concentrations thereby indicating that Na^+ induced opening of HP2 is consistent with the induced fit model (Figure 2.2D). The variation in k_{obs} with Na^+ can be fit using equation 4 based on the induced-fit model to obtain the values of K_D and *E* (Table S2.3) (228). For the Glt_{Ph}(Phe_{CN}+W) protein, the fit gave a K_D of 322 mM and an *E* of 103 (Figure 2.2D). The kinetics measurements provide the ability to determine whether the mutations introduced in the Asp binding site affect the intrinsic binding of Na^+ or the transition of HP2 opening.

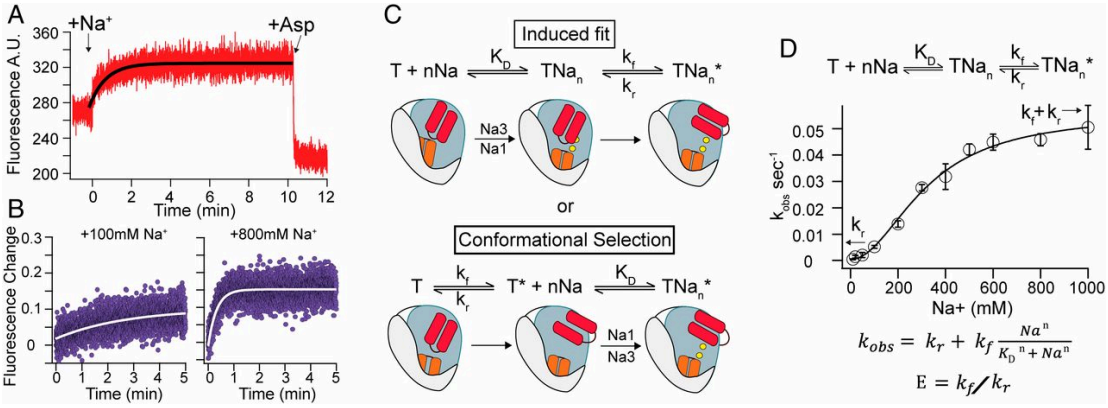

Figure 2.2. Kinetic measurements and mechanism of HP2 movement A) Time course of the fluorescence change in Glt_{Ph}(Phe_{CN}+W) at 345 nm. Addition of 200 mM Na^+ results in a gradual increase in fluorescence due to the slow opening of HP2 while addition of 100 µM Asp results in a rapid decrease in fluorescence due to the fast closure of HP2. The solid black line represents the single exponential fit used to obtain k_{obs} for HP2 opening by Na^+. **B)** Fluorescence changes for Glt_{Ph} (Phe_{CN}+W) upon addition of 100 mM and 800 mM Na^+. Solid white line is single exponential fit. **C)** Schematic of the two potential mechanisms of induced fit and conformational selection for HP2 opening by Na^+. **D)** k_{obs} for HP2 opening measured at different Na^+ concentrations are plotted and fit to the equation shown to give K_D of 322 mM and *E* of 103. Error bars are ± S.E.M., N $\geq$ 3.

Residues that participate in Na^+-Asp coupling

To identify residues that participate in the coupling of Na^+ and Asp binding, we looked for residues in the Asp binding site that showed a conformational change between the Apo and the Asp bound states (Figure 2.3A/B). This comparison for Glt_{Ph} (and Glt_{Tk}) identified R397, T314 and M311. In the Apo structure, the R397 side chain partially occupies the substrate binding site while it flips out and coordinates the Asp molecule in the bound structure. Compared to the Apo structure, the T314 side chain moves closer to the binding site to coordinate the Asp molecule while the M311 side chain rotates from facing the lipid bilayer in the Apo structure to facing HP1 in the bound structure. To evaluate whether these residues participate in Na^+-Asp coupling, we measured the Asp affinity for the R397A, T314 A and M311A mutants at 10 and 200 mM Na^+ to calculate a coupling coefficient (Figure S2.5). We define the coupling coefficient as the ratio of the Asp affinity at low to high concentrations of Na^+. For the WT transporter, we measured a coupling coefficient of 155, indicating the strong coupling between Na^+ and Asp binding. All the Ala mutants showed substantially lower coupling coefficients indicating that the R397, T314 and M311 residues participate in coupling Na^+ and Asp binding (Figure S2.5, Table S2.4).

R397 and T314 have opposite effects on HP2 opening

To investigate the effect of R397 on HP2 movement, we generated an Ala, Gln and Lys substitution at this position in the $Glt_{Ph}(Phe_{CN}+W)$ background. We carried out steady state Na^+ titrations using the HP2 assay and observed that the R397 mutants showed lower $K_{0.5}^{Na}$ values ($K_{0.5}^{Na}$ for R397A = 44.3 mM, R397Q = 56.2 mM, R397K = 98 mM) compared to the WT $Glt_{Ph}(Phe_{CN}+W)$ ($K_{0.5}^{Na}$ = 177.9 mM) (Figure 2.3C). The lower $K_{0.5}^{Na}$ values suggest that the opening of HP2 is facilitated when the R397 side chain is substituted. Next, we used kinetic measurements to determine whether the effect of the

R397 substitutions is through changes in the Na^+ affinity (K_D) and/or the HP2 opening transition (*E*). At 100 mM Na^+, the kinetics of the fluorescence change in the HP2 assay for the R397A and R397Q mutants were dramatically faster than the wild type (Figure 2.3D). A fit of the k_{obs} at different Na^+ concentrations showed large increases in Na^+ affinity (K_D for R397A = 9.5 mM, R397Q = 12.8 mM) and dramatic increases in the HP2 opening transition (*E* for R397A = 2332, R397Q = 2454) (Figure 2.3E). For the Lys mutant, we observed only a marginal increase in the kinetics of the fluorescence change. A fit of the Na^+ dependence of k_{obs} for the Lys mutant indicated a two-fold increase in the Na^+ affinity (K_D = 149 mM) and a modest decrease in the HP2 opening transition (*E* = 65) (Figure 2.3F). The Ala and the Gln substitutions alter both the charge and the side chain sterics while the charge is maintained, and the length of the side chain is altered in the Lys substitution. The effects observed for the R397 mutants suggest that the charge on the R397 side chain plays a role in determining the Na^+ binding affinity. Analysis of the structure of Apo Glt_{Tk}, using the HOLE program identifies a potential pathway for Na^+ ions to access the Na3 and the Na1 sites(229). Na^+ ions traversing along this pathway will encounter the R397 side chain (Figure S2.6). The positive Arg side chain along the pathway will be electrostatically unfavorable for Na^+ access to the Na3 and Na1 sites. In this scenario, mutational deletion of the positive charge will favor Na^+ access to the Na^+ sites and thereby explain the increase in the Na^+ affinity observed in the R397A and the R397Q mutants. The results with the R397 mutants indicate that the steric nature of the side chain also influences the opening of HP2. The mechanism underlying this effect is presently not obvious as there is no direct contact between the R397 side chain and residues on HP2. However, the effects of the R397 mutations, on K_D and *E* indicate that perturbations of the R397 side chain facilitate HP2 opening, which suggest that the R397 side chain plays a role in keeping HP2 closed in the Apo state.

To investigate the effect of the T314 side chain on HP2 movement, we generated an Ala, Val and Ser substitution at this position. Using steady state Na^+ titrations, we observed that the $K_{0.5}^{Na}$ value for the T314S mutant was similar to the wild type while $K_{0.5}^{Na}$ values for the T314A and the T314V were greater than the wild type (Figure 2.3G, Table S2.2). The higher $K_{0.5}^{Na}$ values suggest that the opening of HP2 is hindered in the T314A and V mutants compared to the wild type. The kinetics of the fluorescence change in the HP2 assay for the T314 mutants were slower than the wild type (Figure 2.3H/I). A fit of the k_{obs} measured at different Na^+ concentrations for the S and the V mutants showed a small effect on Na^+ affinity (K_D for T314S = 524 mM, T314V =632 mM) but a substantial effect on the HP2 opening transition (*E* for T314S = 28, T314V = 15) (Figure 2.3I). The kinetics data for the T314A mutant did not saturate and so we were unable to determine the K_D and *E*. The mutational analysis at T314 suggests that the hydroxyl group and the steric bulk of the T314 side chain are both important for the opening of HP2 as alteration of either property hinders the opening of HP2. A comparison of the structures of Glt_{Tk} in the Apo and the Asp bound state indicates that the T314 side chain in the Asp bound conformation will clash with the Arg397 side chain in the Apo conformation as previously proposed (164) indicating the requirement for the steric bulk of the side chain. Further, the T314 side chain can be stabilized in the bound conformation by a H-bond with the N401 side chain and thereby the requirement for the hydroxyl group (Figure S2.7). The results with the T314 mutants in the HP2 assay indicate an effect on the opening of HP2 by influencing mainly the opening transition without affecting the Na^+ affinity. Our results therefore indicate that R397 and T314 have opposite roles, R397 is important for keeping HP2 closed while T314 is responsible for the opening of HP2.

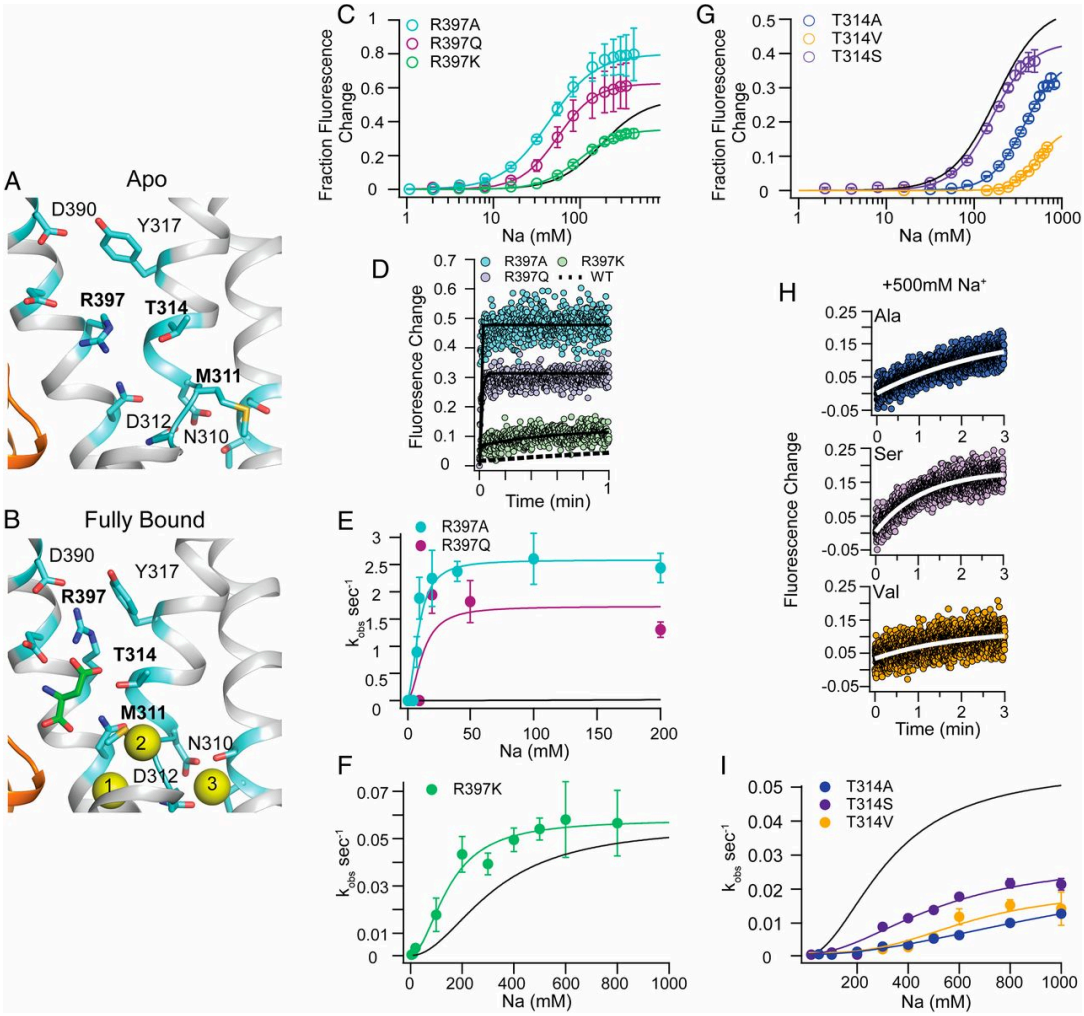

Figure 2.3. Effect of R397 and T314 on HP2 movement. Structures of Glt_{Tk} in the Apo state (**A**, pdb: 5dwy) and the fully bound state with Asp and 3 Na^+ ions (**B,** pdb: 5e9s). Residues that show a conformational shift between these two states are indicated in bold. While the Glt_{Tk} structures are used due to higher resolution, the residues are shown with Glt_{Ph} numbering. **C)** HP2 opening by Na^+ in the R397 mutants. Steady state titration of the R397 mutants in the (Phe_{CN}+W) background by Na^+ is plotted and fit (solid line) to give $K_{0.5}^{Na}$ of 44.3 mM for R397A, 56.2 mM for R397Q and 98 mM for R397K. **D)** Change in fluorescence for the R397A, R397Q, R397K, and WT (black dotted line) Glt_{Ph} (Phe_{CN}+W) upon 100mM Na^+ addition. Solid black line corresponds to the single exponential fit used to determine k_{obs}. **E)** k_{obs} for HP2 opening for R397A and R397Q Glt_{Ph} (Phe_{CN}+W) measured at different Na^+ concentrations are plotted and fit to give K_D of 9.5 mM and *E* of 2332 for R397A and K_D of 12.8 mM and *E* of 2454 for R397Q. **F)** k_{obs} for HP2 opening in R397K Glt_{Ph} (Phe_{CN}+W) measured at different Na^+ concentrations is plotted and fit to give K_D of 149 mM and *E* of 65. **G**) HP2 opening by Na^+ in the T314 mutants. Steady state titration of the T314 mutants in the (Phe_{CN}+W) background by Na^+ is plotted and fit (solid line) to give $K_{0.5}^{Na}$ of 373.6 mM for T314A, 162.8 mM for T314S and 539.1 mM for T314V. **H)** Change in fluorescence for the T314A, T314S, and T314V Glt_{Ph} (Phe_{CN}+W) upon addition of 500 mM Na^+. Solid white line corresponds to the single exponential fit used to determine k_{obs}. **I)** k_{obs} for HP2 opening for T314A, T314S and T314V Glt_{Ph} (Phe_{CN}+W) measured at different Na^+ concentrations are plotted and fit to give K_D of 524 mM and *E*

of 28 for T314S and K_D of 632 mM and *E* of 15 for T314V. Data for the wild type control in panels C, E, F, G and I is shown as a black line. Error bars are ± S.E.M., N ≥ 3.

D390 and Y317 facilitate HP2 opening by stabilizing R397 in the flipped conformation

For Asp binding, the R397 side chain has to flip out of the Asp binding site. In the flipped conformation, the R397 side chain interacts with D390 and Y317 and coordinates Asp (Figure 2.4A). If the flip of R397 facilitates HP2 opening, then we expect that D390 and Y317, which interact with R397 in the flipped conformation, will also affect HP2 movement. Steady state Na^+ titrations for the D390A and the Y317L mutant showed very small fluorescence changes compared to the control indicating that HP2 opening was severely perturbed. The Y317F mutant showed HP2 opening that was relatively similar to the wild type but with a slightly lower $K_{0.5}^{Na}$ (Figure 2.4B). The crystal structure of Apo Glt_{Tk} shows an H-bond between D390 and Y317. The lower $K_{0.5}^{Na}$ value for the Y317F mutant suggests that the opening of HP2 may be coupled to the breaking of the H-bond between D390 and Y317. The dramatic perturbation on Asp binding seen in the Y317L mutant compared to the Y317F mutant indicates the requirement for an aromatic residue at 317 and is consistent with a cation-π interaction between R397 and Y317 in the flipped conformation as previously proposed (Figure 2.4C)(165).

To directly probe for a cation-π interaction, we substituted Y317 with 4-bromo-phenylalanine (Phe_{Br}) and 4-cyano-phenylalanine (Phe_{CN}) using the nonsense suppressor approach. The Br- and the CN- substituents have roughly similar steric sizes but different electron withdrawing properties; with the CN- group being more electron withdrawing than the Br- group(230). The Phe_{CN} side chain is therefore less–capable of participating in cation-π interactions compared to the Phe_{Br} side chain. We could not use the HP2 assay with these mutants as we cannot use the amber suppression approach to simultaneously incorporate Phe_{Br} at 317 and a Phe_{CN} at 279. Instead, we assayed the

effect of the unnatural substitution by evaluating Asp binding by using the L130W assay(150). We observed that the Phe_{CN} substitution had a greater effect on K_D^{Asp} compared to the Phe_{Br} substitution (Figure 2.4D). We also observed that the differential effects of the Phe_{CN} and the Phe_{Br} substitutions on K_D^{Asp} required the R397 side chain as this effect was not observed in the context of the R397A mutant (Figure S2.8). These results strongly suggest a cation-π interaction between R397 and Y317 in the Asp bound state. Overall, these results indicate that the interactions of D390 and Y317 with R397 modulate HP2 movement and are consistent with the existence of a cation-π interaction between R397 and Y317.

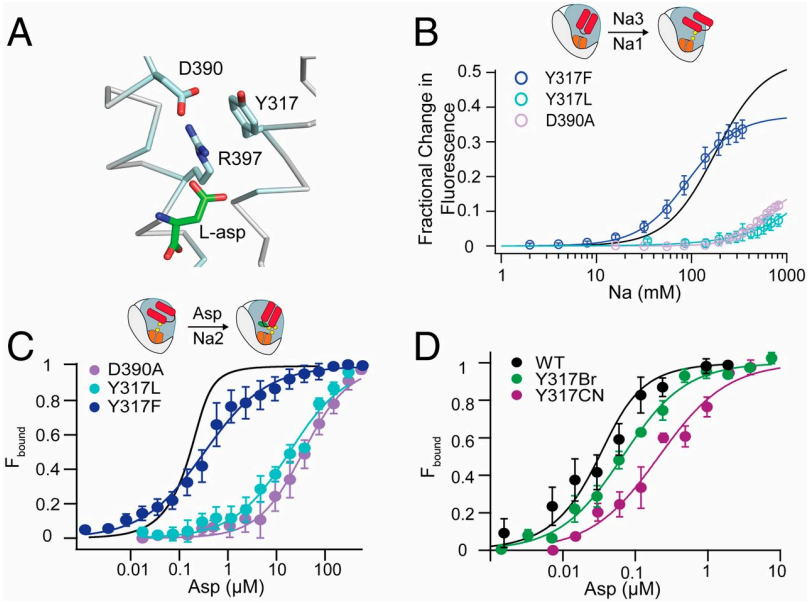

Figure 2.4. Interactions of R397 in the flipped conformation A) Close-up view of the Asp binding site in Glt_{Ph} (pdb: 2nwx) shows that R397 in flipped conformation interacts with D390 and Y317. HP2 opening by Na^+ (**B**) and HP2 closing by Asp (**C**) in Glt_{Ph} Y317L, Y317F and D390A. HP2 opening was assayed by Na^+ titration of these mutant proteins in the (Phe_{CN}+W) background while HP2 closing was assayed by Asp titration in the presence of 200 mM NaCl. Fit of the Na^+ titration data gave $K_{0.5}^{Na}$ of 91 mM for the Y317F while fits of the Asp titration data gave $K_{0.5}^{Asp}$ of 0.48 μM for the Y317F, 18.5 μM for the Y317L and 35.5 μM for the D390A mutants. Solid black lines in B and C correspond to the wild type control. **D)** Unnatural amino acid substitutions at Y317. Asp binding was assayed by the fluorescence change in the wild type, $Y317Phe_{Br}$ and $Y317Phe_{CN}$ Glt_{Ph} with a L130W substitution in the presence of 100 mM Na^+. The binding assays gave a K_D^{Asp} of 15 nM for the wild type, 66 nM for the $Y317Phe_{Br}$ and 210 nM for the $Y317Phe_{CN}$. Error bars are ± S.E.M., N ≥ 3.

M311 acts as a wedge to prop HP2 open

To evaluate the effect of M311 on HP2 movement, we generated a M311A substitution in the Glt_{Ph}(Phe_{CN} +W) background. In the HP2 assay, we did not observe a change in fluorescence on the addition of Na^+ but observed an increase in fluorescence on addition of TBOA (Figure 2.5A). This increase in fluorescence with TBOA was only observed in the presence of Na^+ (Figure 2.5B). The opening of HP2 is required for TBOA to bind and the Na^+ requirement for TBOA binding indicates that Na^+ dependent opening of HP2 must take place in the M311A mutant. The binding of TBOA props HP2 open therefore the fluorescence signal observed with TBOA corresponds to the opening of HP2. We took advantage of the ability of TBOA to prop HP2 open and carried out the HP2 assay for the M311A(Phe_{CN}+W) mutant in the presence of 10 μM TBOA. We observed a $K_{0.5}^{Na}$ of 3.7 mM for the M311A mutant while a value of 12.6 mM was measured in the HP2 assay for wild type Glt_{Ph}(Phe_{CN}+W) in the presence of 10 μM TBOA (Figure 2.5C). Additionally, we used the dye assay to probe Na^+ binding to the Glt_{Ph}-M311A mutant((202). We observed Na^+ binding to the Apo-M311A mutant with an approximate K_D^{Na} of 73 mM (Figure 2.5D). This value is an approximation as we did not observe saturation of the signal. In the presence of 1 mM Asp, we observed a K_D^{Na} of 0.78 mM. The K_D^{Na} values obtained for the M311A mutant are comparable to the wild type, however the binding of Na^+ to the M311A mutant showed lower cooperatively than the wild type. These results indicate that Na^+ binding is relatively unperturbed in the M311A mutant but that HP2 opening on Na^+ binding is severely affected.

The HP2 assay provides a time-averaged readout of the position of HP2. For the wild type Glt_{Ph}(Phe_{CN}+W) transporter, the increase in fluorescence observed in the HP2 assay on Na^+ addition indicates that HP2 changes from being closed in the Apo state and to mainly open in the Na^+ bound state. For the M311A mutant, the lack of a change

in the fluorescence signal on the addition of Na^+ suggests that HP2 remains predominantly in the closed state with only very brief openings in the presence of Na^+. These results indicate that in the absence of the M311 sidechain, HP2 is not propped open on Na^+ binding.

We observed a decrease in fluorescence on the addition of Asp to the M311A(Phe_{CN}+W) mutant in the presence of Na^+. This decrease in fluorescence indicates the closure of HP2 and was only observed in the presence of Na^+ (Figure 2.5B). Using the HP2 assay, we measured a $K_{0.5}^{Asp}$ of 160 nM, which compares to a value of 36.9 nM measured for the wild type, thereby indicating that the closure of HP2 on Asp binding is relatively unperturbed in the M311A mutant (Figure 2.5F).

M311 is in the conserved NMDGT motif and modelling studies indicate that conformational changes in M311 must take place in concert with the movement of HP2 as the flip in the conformation of the M311 side chain is not compatible with the HP2 in the closed state as previously reported (Figure S2.9)(154, 212, 222). Our studies suggest a role for the M311 side chain in keeping HP2 propped open. Na^+ coupled Asp binding has been previously reported for a M311L Glt_{Ph}(154). We tested the M311L mutant in the HP2 assay and observed that the opening of HP2 with Na^+ and closure of HP2 on Asp binding took place similar to the wild type (Figure 2.5E/F) indicating a role for the length of the M311 side chain in keeping HP2 propped open. In the M311A mutant, the methyl side chain is too small to accomplish this role.

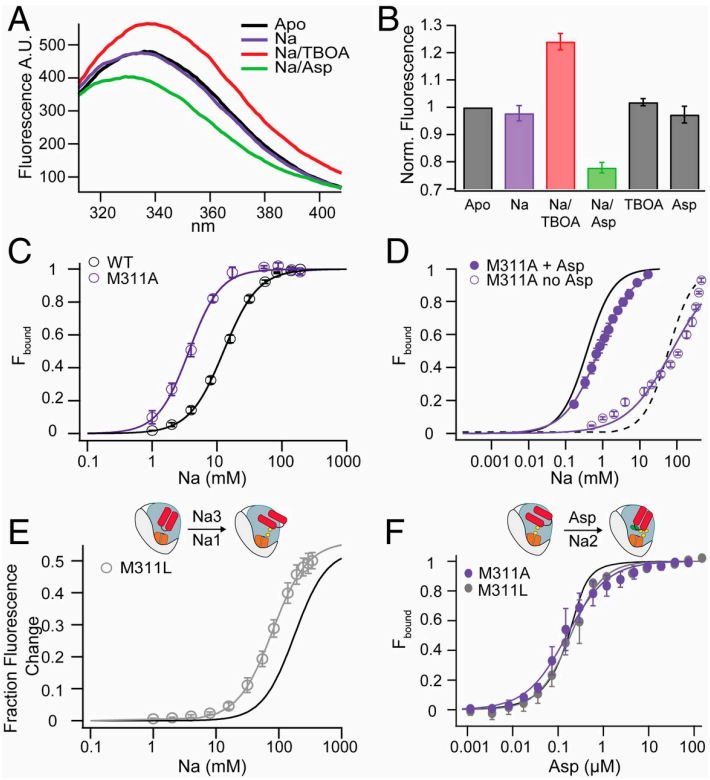

Figure 2.5. M311 affects the opening of HP2 A) Fluorescence emission spectra of M311A (Phe_{CN}+W) on excitation at 295 nm in the following conditions: Apo, 200 mM NaCl, 200 mM NaCl/10 μM TBOA, and 200 mM NaCl/100 μM Asp. **B**) Fluorescence at 345 nm for the M311A (Phe_{CN}+W) with the addition of 200 mM NaCl, 200 mM NaCl/10 μM TBOA, 200 mM NaCl/100 μM Asp, 10 μM TBOA and 100 μM Asp. The fluorescence values are normalized to the M311A (Phe_{CN}+W) Apo protein. **C**) Na^+ titration of M311A (Phe_{CN}+W) and wild type Glt_{Ph} (Phe_{CN}+W) with 10 μM TBOA present. A fit of the titration data gave a $K_{0.5}^{Na}$ of 3.7 mM and 12.6 mM for the M311A and the wild type respectively. **D**) Na^+ binding assay for Glt_{Ph} M311A. Na^+ binding was measured using the RH421 dye in the presence and absence of 1 mM Asp. The M311A mutant shows K_D^{Na}s of 73 mM without Asp and 0.78 mM in the presence of 1 mM Asp. The black lines corresponds to the Na^+ binding curve for the wild type Glt_{Ph} (dashed: without Asp, K_D^{Na} = 58.8 mM; solid: with 1 mM Asp, K_D^{Na} = 0.33 mM). **E**) HP2 opening in Glt_{Ph} M311L by Na^+. Titration of M311L (Phe_{CN}+W) by Na^+ is plotted and fit to give $K_{0.5}^{Na}$ of 79.3 mM. **F**) HP2 closing in M311A and M311L Glt_{Ph}. Titration of M311A (Phe_{CN}+W) and M311L (Phe_{CN}+W) by Asp in the presence of 200 mM NaCl. The titration data was fit as described in methods to give a $K_{0.5}^{Asp}$ of 0.16 μM for M311A and 0.19 μM for M311L. The solid black line is the Na^+ titration curve (E) and the Asp titration curve (F) for the wild type Glt_{Ph} (Phe_{CN}+W) protein. B-F) Error bars are ± S.E.M., N ≥ 3.

Discussion:

The opening and closing of HP2, the extracellular gate, is a key aspect of coupling Na^+ and Asp binding in Glt_{Ph}. In this study, we developed a fluorescence assay

to track the movement of HP2. Using this assay, we show that the opening of HP2 on the binding of Na^+ to the Apo transporter is a slow process while closure of HP2 on the binding of Asp in the presence of Na^+ is very rapid. These results are consistent with previous finding which indicate that Na^+ binding is accompanied by a slow conformational change(210, 211). We find that the opening of HP2 by Na^+ follows an induced fit mechanism. We investigate how residues in the Asp binding site modulate HP2 movement and our studies demonstrate that R397 plays a role in keeping HP2 closed while T314 plays a role in the opening of HP2 and M311 acts as a wedge to keep HP2 propped open following the binding of Na^+.

Combining our results with previous studies on Glt_{Ph} and Glt_{Tk} (153, 154, 164), we propose the following scheme for the coupled binding of Na^+ and Asp to Glt_{Ph} (Figure 2.6). In the Apo state, HP2 is closed and R397 partially occupies the Asp binding site while M311 points towards the lipid bilayer. The first step in the process is the binding of Na^+ to the Na3 and the Na1 sites. The Na3 and the Na1 sites consists of amino acid side chains and the protein backbone from the conserved NMDGT motif and Na^+ binding causes a conformational change in this motif. One component of the conformational change in the NMDGT motif is a switch of the M311 side chain from facing the lipid bilayer to pointing towards HP1. In this conformation, M311 acts as a wedge to break interactions between the tip of HP1 and HP2, which are important for keeping HP2 closed in the Apo state. The conformational switch in the M311 side chain on Na^+ binding therefore allows HP2 to open, as previously proposed(154). Another component of the conformational change in the NMDGT motif on Na^+ binding is the movement of T314 into the Asp binding site where it clashes with R397, as previously proposed(153, 164). This clash pushes R397 from the Apo conformation, wherein it partially occupies the Asp binding site, into the flipped conformation. In the flipped conformation, R397 is stabilized by a salt bridge interaction with D390 and through a cation-π interaction with

Y317. The R397 side chain in the Apo conformation helps keeps HP2 closed and the change to the flipped conformation allows the opening of HP2. The conformational changes in R397 and M311 side chain are therefore the key steps required for the Na^+ coupled opening of HP2. All of these events which involve the opening of HP2 and side chain rearrangements setup the binding site for coordinating Asp. The binding of Asp results in the closure of HP2 which is further facilitated by the binding of the third Na^+ ion to the Na2 site. The binding of Asp following the binding of Na^+ is expected to follow a conformational selection mechanism. A recent study using kinetics to look at Asp binding (in the inward facing state) determined that the mechanism of Asp binding is consistent with a conformational selection model(231). The Na^+ and Asp bound transport domain that result from the coupled binding process can then transition to the inward facing state in an elevator like movement for the transport of Na^+ and Asp into the cell.

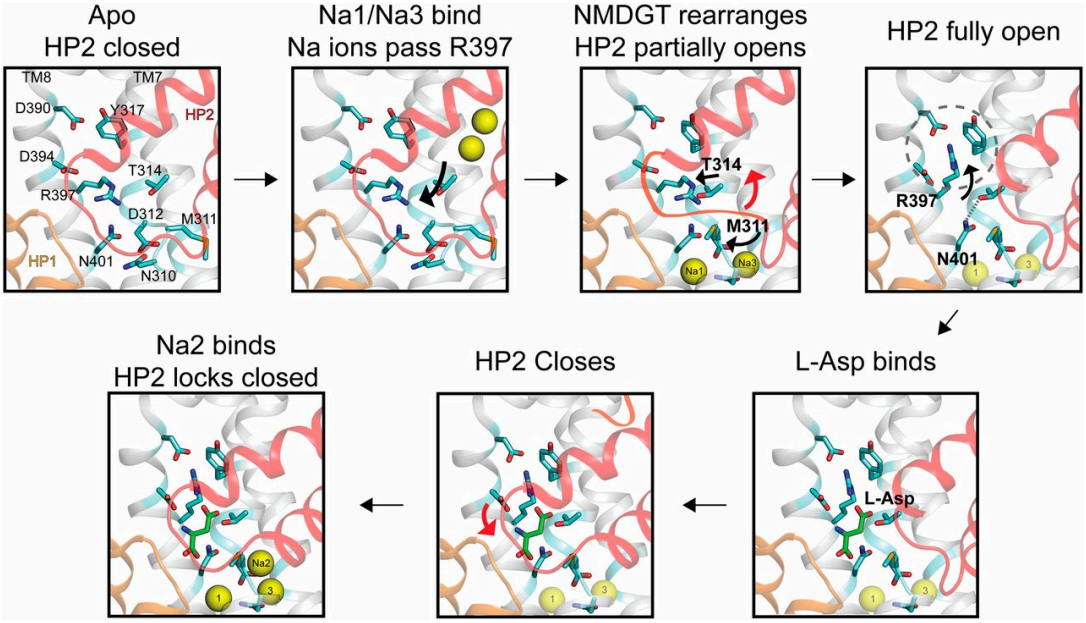

Figure 2.6. Proposed scheme for the coupled binding of Na^+ and Asp to $GltPh$. In the Apo state, the R397 side chain partially occupies the Asp binding site while the M311 side chain points away from the binding site. Binding of Na^+ ions to the Na3 and the Na1 sites causes conformational changes in the NMDGT motif which involves the shift of the M311 side chain towards HP1 and the movement of T314 towards the binding site. The movement of M311 helps break HP1 and HP2 interactions to partially open HP2. The movement of T314 towards the substrate binding site is stabilized by interacting with N401

and flips R397 out of the substrate binding site. R397 in the flipped conformation is stabilized by interactions with D390 and Y317. The movement of R397 into the flipped conformation fully opens HP2 and HP2 is propped open by M311. Following the opening of HP2 by Na^+, Asp binds to the protein and closes HP2 through various interactions of HP2 with Asp. The third Na^+ binds to the Na2 site to fully lock HP2. The fully loaded Glt_{Ph} isomerizes to the inward facing state for translocation of the Na^+ and Asp into the cell.

While the overall binding scheme is supported by this study and previous investigations, the mechanisms underlying key steps are presently unresolved. These include the molecular details of how the R397 side chain in the Apo conformation keeps HP2 closed or how the M311 conformational switch allows HP2 to open. High resolution structure determination of the various states combined with focused computational studies will be necessary to understand these mechanisms.

The residues in Glt_{Ph} that we investigated in this study are conserved in EAATs and so we anticipate that the general binding process described will also be valid for EAATs(61, 193). Importantly, the HP2 assay developed in this study can be adapted to probe HP2 movement in EAATs. Further, re-entrant loops in the form of helical hairpins gate the substrate-binding site for a variety of transporters(157). We anticipate that the strategy used herein will be applicable to investigating the movement of helical hairpins in these diverse transporters.

Acknowledgements: This research was supported by NIH Grants R01GM087546 and R37NS085318 (to Dr. Olga Boudker, Principal Investigator and F.I.V., Coinvestigator). E.A.R. was supported by a Predoctoral Fellowship from the American Heart Association (AHA 19PRE34380950).

Methods:

Definition of the terminology used. Binding parameters determined using the HP2 assay for Na^+ and Asp are denoted by $K_{0.5}^{Na}$ and $K_{0.5}^{Asp}$ respectively. The intrinsic Na^+ dissociation constant determined from the kinetic measurements using the HP2 assay is denoted by K_D. Asp dissociation constant determined using the Glt_{Ph} L130W assay is

denoted by K_D^{Asp} while the Na^+ dissociation constant determined using the RH421 dye assay is denoted by K_D^{Na}.

Expression and purification of Glt_{Ph}. The Glt_{Ph} construct referred to as wild type (Glt_{Ph}-WT) in this study consisted of seven point mutations to histidine(149), a C321A substitution (unless otherwise specified) and a His_8 tag at the C-terminus. Site directed mutagenesis was carried out using the PCR overlap or Quickchange mutagenesis protocols. The Glt_{Ph} constructs were cloned and expressed from the pBCH/G4 vector (kindly provided by Dr. Eric Gouaux) in *Escherichia coli* TOP10 cells (Fisher Scientific).(149) Protein expression and membrane preparation was carried out as previously described.(155) The membrane vesicles were solubilized using dodecyl-β-D-maltopyranoside [DDM, 2% (w/v)] and the Glt_{Ph} protein purified by affinity chromatography (Ni NTA resin, Qiagen) and size exclusion chromatography (SEC).(155) SEC was carried out on a Superdex S-200 column (GE Biosciences) using 20 mM Tris-HEPES pH 7.5, 200 mM NaCl, and 0.1% DDM as the column buffer.

***Unnatural amino acid incorporation*.** Incorporation of Phe_{CN} (4-Cyano-Phenylalalnine) or Phe_{Br} (4-Bromo-Phenylalanine) was carried out by *in vivo* nonsense suppression using the Phe_{CN} tRNA synthetase/tRNA pair for *Escherichia coli* expression.(223, 224) The Phe_{CN} synthetase/tRNA pair also incorporates Phe_{Br}.(232) Briefly, an amber (TAG) stop codon was introduced at the desired position in the Glt_{Ph} construct. The plasmid carrying the Glt_{Ph} construct with the stop codon was co-transformed into *Escherichia coli* TOP10 cells with a plasmid carrying the Phe_{CN} synthetase and tRNA. The transformed cells were grown at 37 °C in 2YT or TB medium containing 2 mM of Phe_{CN} or Phe_{Br} (Chem-Impex) and the antibiotics required for maintenance of both the plasmids until an OD_{600} of ~1.0, at which time the expression of Glt_{Ph} [0.1% arabinose] and the synthetase (1 mM IPTG) was induced. Following induction, cell growth was carried out for an

additional 4 hours at 37 ºC. Purification of Glt_{Ph} containing the unnatural amino acid was carried out as described for Glt_{Ph}-WT. In initial experiments, we used the Phe_{CN} synthetase/tRNA pair on a pSUP plasmid (kindly provided by Dr. Peter Schultz) while the latter experiments used a pULTRA plasmid (pULTRA-CNF was a gift from Dr. Peter Schultz, Addgene plasmid # 48215). The spectinomycin resistance gene on the pULTRA-CNF plasmid was replaced by the kanamycin resistance gene from pRSF1b (EMD Millipore) for use in TOP10 cells.

Hairpin 2 movement assays*.* Prior to the HP2 assays, the $Glt_{Ph}(Phe_{CN}+W)$ proteins were exchanged into HP2 assay buffer (20 mM Tris-HEPES pH 7.5, 100 mM KCl and 0.1% DDM). The steady-state titrations were carried out using ~100 µgs Glt_{Ph} in assay buffer at 30 ºC. The change in fluorescence was monitored at 345 nm after excitation at 295 nm. For the opening of HP2, we added aliquots of NaCl to the Apo protein in the assay buffer and monitored the fluorescence (F). The fluorescence values measured were corrected for dilution, normalized to the fluorescence of the Apo protein and fit using the Hill equation (equation 1) to determine the values of $K_{0.5}^{Na}$.

$$F = \frac{[Na]^n}{[K_{0.5}^{Na}]^n + [Na]^n} \qquad \textit{Equation 1}$$

The fraction bound was determined by normalizing the change in fluorescence following Na^+ addition to the maximum change observed and the Hill coefficient for the HP2 opening by Na^+ was determined as the slope at the intercept along the x-axis in a plot of the $Log[F_b/(1-F_b)]$ vs $Log[Na^+]$.(226, 227)

For closure of HP2, we added aliquots of Asp to the Glt_{Ph} (Phe_{CN}+W) protein in assay buffer containing 200 mM NaCl. The fraction bound was calculated by normalizing the change in fluorescence following Asp addition to the maximum change observed and $K_{0.5}^{Asp}$ was determined by a fit to the equation 2:

$$F_b = \frac{[Asp]}{K_{0.5}^{Asp}+[Asp]}. \quad \textit{Equation 2}$$

In cases where the protein concentration (P) was similar to or greater than the $K_{0.5}^{Asp}$, the following quadratic equation was used:

$$F_b = \frac{\left(K_{0.5}^{Asp}+[P]+[Asp]\right)-\sqrt{\left(K_{0.5}^{Asp}+[P]+[Asp]\right)^2-(4\ [P]\ [Asp])}}{2[P]} \quad \textit{Equation 3}$$

Kinetics for HP2 opening. Kinetics of HP2 opening was monitored using ~100 µgs Glt_{Ph} in the HP2 assay buffer (20 mM Tris-HEPES pH 7.5, 100 mM KCl and 0.1% DDM) at 30 ºC. The change is fluorescence at 345 nm (excitation at 295 nm) was monitored after the addition of NaCl (from a 3M stock prepared in assay buffer) to the desired concentration with fast stirring. The change in the fluorescence signal was corrected for dilution and fit with a single exponential to determine the k_{obs}. k_{obs} values determined over a range of Na^+ concentrations were fit with the equation for an induced-fit mechanism.(228).

$$k_{obs} = k_r + k_f \frac{Na^n}{[K_D]^n+Na^n} \quad \textit{Equation 4}$$

The value of k_r was fixed as the average of the k_{obs} at lower Na^+ and n was fixed as 2 for all mutants except for T314V. For a satisfactory fit of the k_{obs} vs Na^+ plot for the T314V mutant, the value of n was set as 3.

Aspartate binding assays. Aspartate binding assays were carried out on Glt_{Ph} constructs with a L130W substitution.(150) Prior to the binding assay, the Glt_{Ph} sample was extensively dialyzed against the assay buffer [20 mM Tris-HEPES pH 7.4, 200 mM Choline Chloride, 0.1% DDM] to lower Na^+ concentration below 0.5 mM and to remove bound Asp. The binding assays were carried out using ~80 µgs of Glt_{Ph} at 30 ºC in assay buffer. Binding of Asp was monitored by the change in the fluorescence emission at 334 nm following excitation at 295 nm. The fraction bound was calculated by normalizing the

change in fluorescence following Asp addition to the maximum change observed and K_D^{Asp} was determined by a fit to the equation 2 or with equation 3 (with $K_{0.5}^{Asp}$ substituted with K_D^{Asp}). Equation 3 was used when the value of K_D^{Asp} determined was on par or lower than the protein concentration used in the assay.

Na⁺ binding assays. Na^+ binding to the Glt_{Ph} constructs was assayed using the voltage sensitive dye, RH421 as previously described.(154, 202) Briefly, 200 nM of RH421 was added to 300 µgs of Glt_{Ph} in 10 mM HEPES/KOH, 100 mM KCl and 0.01% DDM. The protein solution with the dye was allowed to equilibrate for at least 1 hour before the start of the titration. Aliquots of NaCl were then added and binding was monitored by change in the fluorescence emission at 628 nm with excitation at 532 nm. After the addition of each aliquot of NaCl, the sample was allowed to equilibrate (~ 15 min) until the fluorescence signal stabilized. For Na^+ titrations in the absence of Asp, the fluorescence changes observed during the titration were normalized to the change in fluorescence on addition of 1 mM Asp at the end of the titration. The normalized fluorescence changes were corrected for dilution to determine the fraction bound and the dissociation constant K_D^{Na} was determined from a fit to the Hill equation (equation 1 with $K_{0.5}^{Na}$ substituted with K_D^{Na}).

Aspartate transport assays. Glt_{Ph} was reconstituted at into lipid vesicles comprised of a 3: 1 ratio of *Escherichia coli* polar lipids to 1-palmitoyl-2-oleoyl-glycero-3phosphatidylcholine (POPC) as previously described.(151) The transport assays were carried out in 20 mM Tris-HEPES pH 7.5, 200 mM NaCl, 1 µM valinomycin at 30 °C as previously described.(155) 100 nM of ^{14}C Asp (Moravek Biochemicals) was used for transport assays with Glt_{Ph}-WT while 200 nM of ^{14}C Asp was used for assays with Glt_{Ph} (Phe_{CN}+W). Background levels of Asp transport were determined by performing the

transport assay in absence of NaCl, with 100 mM KCl in the assay buffer, as well as 200mM NaCl on each side.

Appendix A: Supplementary Information:

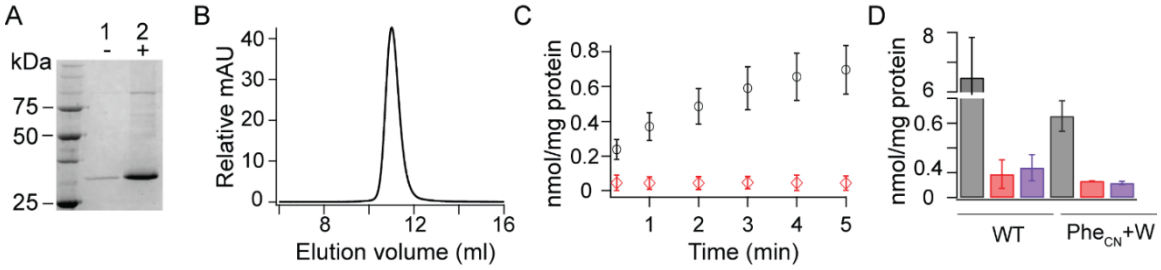

Figure S2.1. Biochemistry of Glt$_{Ph}$ (Phe$_{CN}$+W). 4-Cyano-Phenylalanine (Phe$_{CN}$) was site specifically incorporated into Glt$_{Ph}$ at residue 279 using the amber suppression system as described in methods. **A**) SDS-PAGE gel showing that expression of the Glt$_{Ph}$-S279Phe$_{CN}$ +V355W [referred to as Glt$_{Ph}$ (Phe$_{CN}$+W)] is only obtained in the presence of Phe$_{CN}$. Lane 1 shows that the Glt$_{Ph}$ protein is not expressed without the addition of Phe$_{CN}$ to the media while Lane 2 is the protein expressed with 2 mM Phe$_{CN}$ present. **B**) Size exclusion chromatography showing the elution profile for Glt$_{Ph}$ (Phe$_{CN}$+W). **C**) Asp uptake activity of Glt$_{Ph}$ (Phe$_{CN}$+W). The time course of [^{14}C]-Asp uptake for Glt$_{Ph}$ (Phe$_{CN}$+W) in the presence of a Na^+ gradient (black circles) while no uptake is observed in the absence of a Na^+ gradient (red diamonds). The activity of Glt$_{Ph}$ (Phe$_{CN}$+W) is ~10% that of wild type Glt$_{Ph}$. Error bars for the uptake data in the presence of a Na^+ gradient correspond to S.E.M. (for $N \geq 3$) while the error bars for the data in the absence of a Na^+ gradient corresponds to range of values from two independent measurements. **D)** Bar graph showing uptake of [^{14}C]-Asp in 5 mins by WT and Glt$_{Ph}$ (Phe$_{CN}$+W) with a Na^+ gradient (black), 100 mM K^+ on both sides of the membrane (red), and 200 mM Na^+ on both sides (purple). Error bars are S.E.M. (for $N \geq 3$)

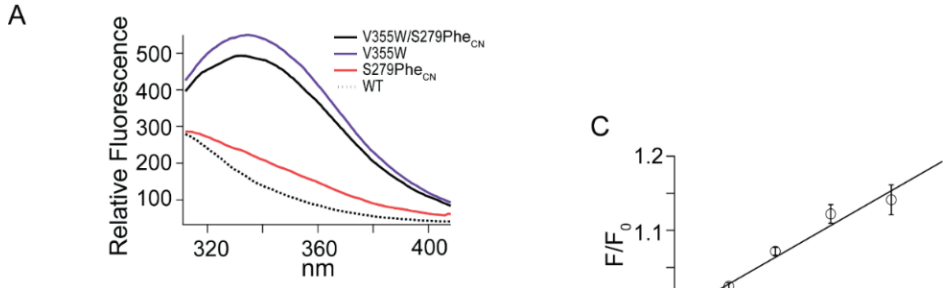

B

Sample	Percent Change From Apo		
	+Na	+TBOA/Na	+Asp/Na
Glt$_{Ph}$(Phe$_{CN}$+W)	33 ± 2.5	45 ± 3.1	-18 ± 1.7
Glt$_{Ph}$(Phe$_{CN}$)	5.5 ± 1.4	6.3 ± 1.6	8.5 ± 0.9
Glt$_{Ph}$(W)	5.1 ± 0.6	8.5 ± 0.9	29 ± 9.9

.

Figure S2.2. Fluorescence properties of the Glt_{Ph} mutants A) Fluorescence emission spectra of S279Phe_{CN}+V355W Glt_{Ph} [Glt_{Ph}(Phe_{CN}+W)], S279Phe_{CN} Glt_{Ph} [Glt_{Ph}(Phe_{CN})], V355W Glt_{Ph} [Glt_{Ph}(W)], and wild type Glt_{Ph} on excitation at 295 nm in 20 mM HEPES-Tris (pH 7.5), 100 mM KCl, and 0.1% DDM. **B)** Table showing the percent change in fluorescence at 345 nm from Apo state on the addition of 200 mM NaCl, 200 mM NaCl/10 µM TBOA, and 200 mM NaCl/100 µM Asp for the wild type and mutant Glt_{Ph} proteins. **C)** Phe_{CN} in solution acts as quencher of Trp. PheCN was titrated into a 5 µM solution of Trp and the fluorescence emission at 360 nm was measured following excitation at 295 nm. The contribution due to the Phe_{CN} was subtracted from the fluorescence signal and corrected for the inner filter effect (233). Shown is a Stern-Volmer plot with the line representing $F_o/F = K_a[Phe_{CN}]+1$, where $K_a = 0.008$.

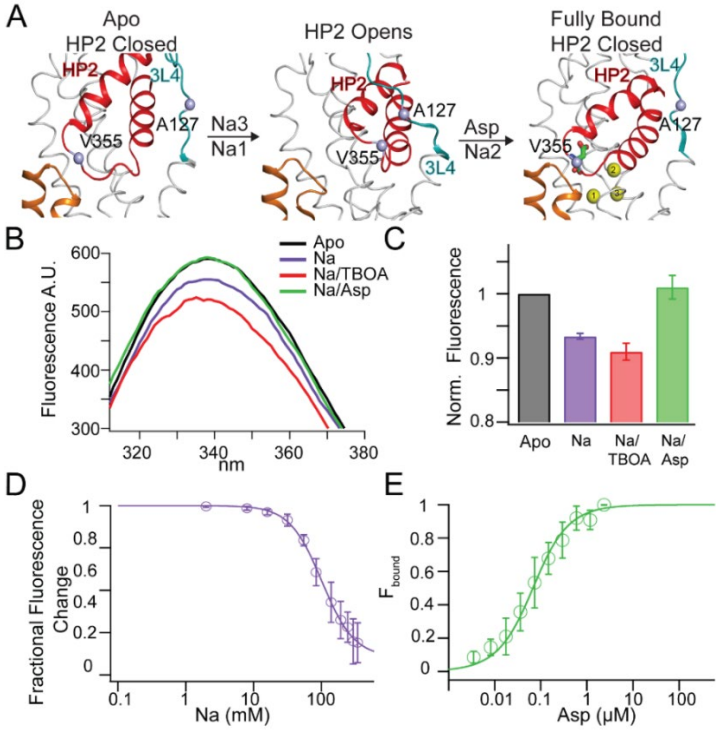

Figure S2.3. The A127W+V355Phe_{CN} pair for fluorescence tracking of HP2 movement A) Close up view of the binding site in the Apo, Na^+ bound, and the Na^+ and Asp bound state. The Apo (pdb: 5dwy) and the Na^+/Asp fully bound (pdb: 5e9s) structures are of Glt_{Tk} while the Na^+ bound structure with HP2 open is of Glt_{Ph} with TBOA bound (pdb: 2nww). Residues in the Glt_{Tk} structures are shown with Glt_{Ph} numbering. A127 in 3-4 loop (teal) substituted with Trp and V355 in HP2 (red) substituted with Phe_{CN} are shown as lavender spheres. The structures highlight the change in distance between the fluorescence probes, Phe_{CN} and Trp, in the different states. Cα-Cα distances are Apo: 20.2Å, Na^+/TBOA: 7.5Å, Na^+/Asp: 23.4 Å **B**) Fluorescence emission spectra of Glt_{Ph} (A127W+V355Phe_{CN}) in the following conditions: Apo, 200 mM NaCl, 200 mM NaCl/10 µM TBOA, and 200 mM NaCl/100 µM Asp. **C**) Fluorescence at 345 nm following the addition of 200 mM NaCl, 200 mM NaCl/10 µM TBOA, 200 mM NaCl/100 µM Asp. The fluorescence values are normalized to the Apo protein. **D**) Na^+ titration of Glt_{Ph}(A127W+V355Phe_{CN}). The normalized change in fluorescence at 345 nm on addition

of Na^+ is plotted. The solid line represents a fit using the Hill equation with $K_{0.5}^{Na}$ of 101.7 mM, n of 1.8. **E**) Asp titration of Glt_{Ph}(A127W+V355Phe_{CN}) in the presence of 200 mM NaCl. The normalized fluorescence change on addition of Asp is plotted and fit (solid line) with a quadratic binding equation to give a $K_{0.5}^{Asp}$ of 52.7 nM. Error bars in C-E are ± S.E.M., N ≥ 3.

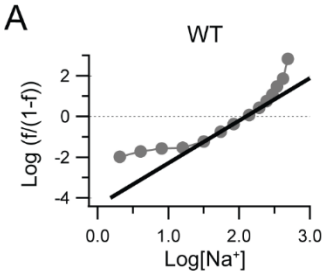

B

Protein	Hill Coefficient from linear region of Log[Na^+] vs Log(f/(1-f))
WT	2.1
R397A	1.6
R397Q	1.9
R397K	2.1
T314S	2
M311L	1.7
Y317F	1.9

Figure S2.4. Hill coefficient for HP2 opening by Na^+ A) Hill plot of Log[(fraction bound) /(1-fraction bound)] vs Log[Na^+] for the WT Glt_{Ph}(Phe_{CN}+W). The Hill coefficient for HP2 opening by Na^+ was determined from the slope (solid line) at the intercept along the x-axis.(226, 227) **B**) Values of the Hill coefficient determined for the different Glt_{Ph} mutants using this approach.

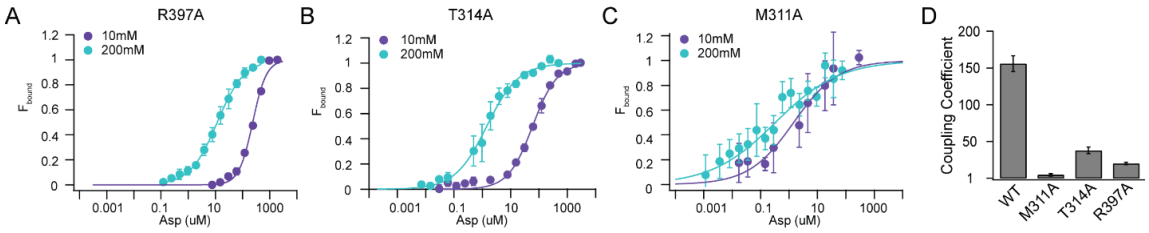

Figure S2.5. Asp titrations of R397A, T314A, and M311A Glt_{Ph}. Asp binding was assayed by the fluorescence changes in R397A (**A**), T314A (**B**) and M311A Glt_{Ph} (**C**) with a L130W substitution in 10 and 200 mM NaCl. The binding assays gave K_D^{Asp} values in 10 mM and 200 mM NaCl for WT: 0.28 μM and 1.8 nM, R397A: 238 μM and 11.8 μM, T314A: 58 μM and 1.44 μM, and M311A: 1.5 μM and 0.33 μM. **D**) Coupling coefficients for the wild type, R397A, T314A and M311A Glt_{Ph}. The coupling coefficient is defined as the ratio K_D^{Asp}(10 mM Na^+)/K_D^{Asp}(200 mM Na^+). Error bars correspond to S.E.M., N ≥ 3.

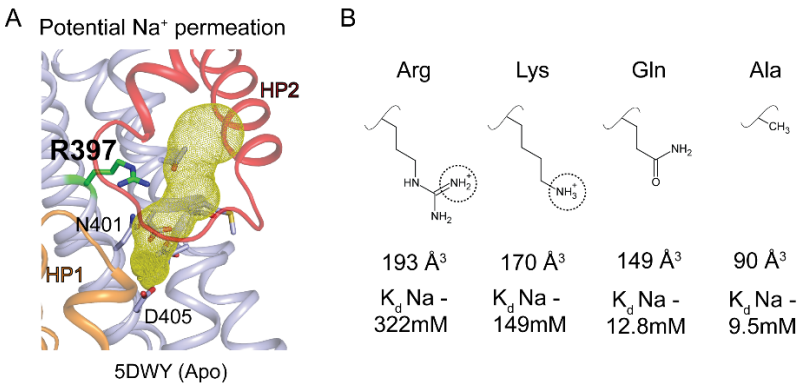

Figure S2.6. Proposed role for R397 in HP2 opening A) Analysis of the structure of Apo Glt_{Tk} (pdb: 5dwy), using the HOLE program (229) identifies a potential pathway (indicated by yellow spheres) for Na^+ ions to access the Na3 and the Na1 sites. The R397 side chain is present along this pathway and will electrostatically disfavor Na^+ access to the Na3 and Na1 sites. **B**) Amino acid substitutions at R397. Structures of the amino acid substitutions tested at R397. The K_D-Na^+ values determined from the kinetic assays as well as the residue volumes (234) are shown. The Ala and the Gln side chains are not positively charged and will not hinder Na^+ access to the binding sites. Correspondingly, the R397A and R397Q mutants show a large increase in Na^+ affinity. The Lys side chain is positively charged but the shorter length of Lys compared to the Arg side chain results in sub-optimal positioning along the Na^+ permeation pathway. Due to this sub-optimal positioning, only a small affect on the Na^+ affinity is observed in the Lys mutant.

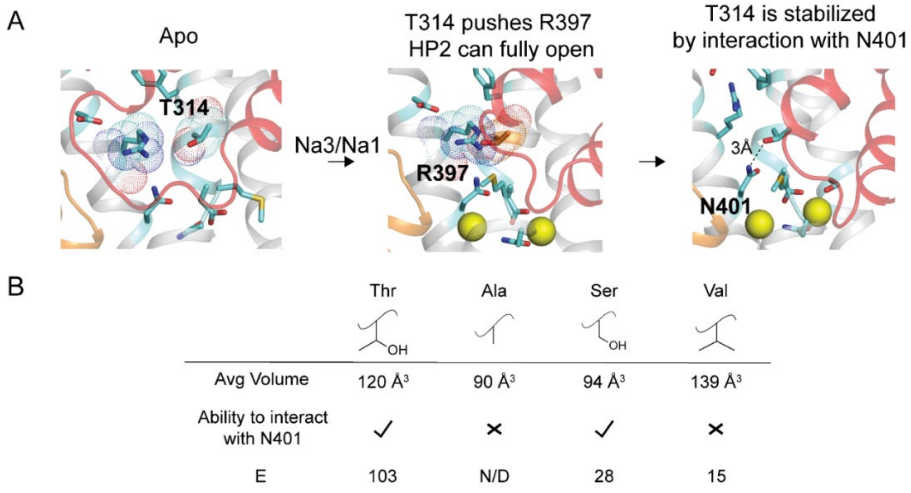

Figure S2.7. Proposed role of T314 in HP2 opening A) In the Apo state, the T314 side chain is away from the Asp binding site. The Apo binding site (pdb: 5dwy) is shown in the left panel. The shift in the T314 towards the substrate binding site when Na^+ ions bind to the Na3 and the Na1 sites forces a reorientation of R397 due to a steric clash between T314 and R397 as previoulsy described.(164) The middle panel depicts a model with the R397 side chain in the Apo conformation (from pdb:5dwy), HP2 open (from pdb: 2nww) and the T314 side chain in the Asp binding conformation (from pdb: 5e9s) to illustrate the steric clash between the T314 and the R397 side chains. T314 in the Asp binding

conformation is stabilized by a H-bonding interaction between the hydroxyl group of T314 and the N401 side chain. The potential H-bond between T314 and N401 is illustrated in the right panel which depicts a model with the R397 and the T314 side chains in the Asp binding conformation (from pdb: 5e9s) and with HP2 open (from pdb: 2nww). The changes in the T314 and R397 side chains result in a reorganization of the binding site for coordinating Asp. Glt_{Tk} structures are used for the Apo and the Asp bound structures due to higher resolution but are shown with Glt_{Ph} numbering. **B)** Amino acid substitutions tested at T314. Structures of the amino acids substituted at T314 are shown along with the effect of the substitutions on HP2 opening as deduced from the HP2 kinetics assay. The data indicate a requirement of both the steric bulk of the T314 side chain and the ability to form a H–bond in HP2 opening by Na^+.

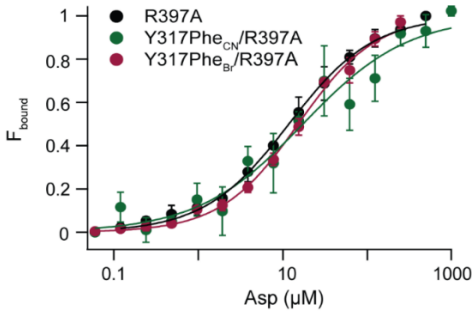

Figure S2.8. Testing cation-π interactions between R397 and Y317. Asp binding was assayed by the fluorescence changes in R397A, R397A+Y317Phe$_{CN}$ and R397A+Y317Phe$_{Br}$ Glt_{Ph} with a L130W substitution in 200 mM Na^+. The binding assays gave K_D^{Asp} values of 11.8 μM for R397A, 17.1 μM for R397A+Y317Phe$_{CN}$, and 15.2 μM for R397A+Y317Phe$_{Br}$. The binding data show that the difference in K_D^{Asp} values observed for the Y317Phe$_{CN}$, and Y317Phe$_{Br}$ substitution require the R397 side chain, consistent with the presence of a cation –π interaction between R397 and Y317. Error bars correspond to S.E.M (N ≥ 3).

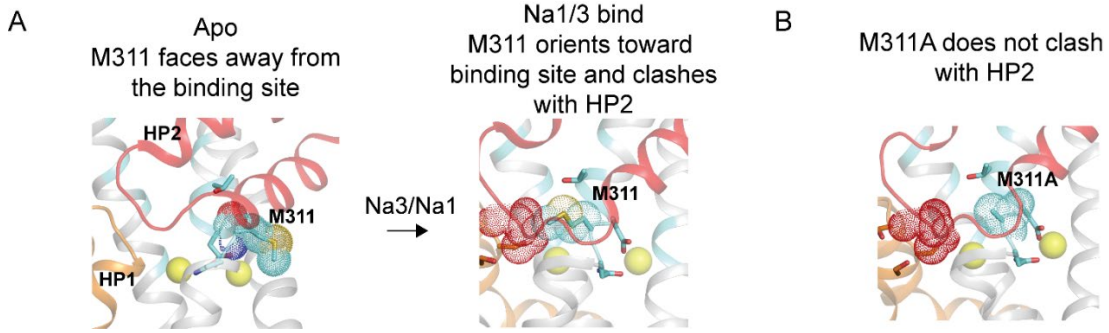

Figure S2.9. Proposed role of M311 in HP2 opening A) In the Apo state, the M311 side chain is positioned away from the Asp binding site. The Apo binding site, with M311 depicted in space fill (pdb: 5dwy) is shown in the left panel. Rearrangements in the NMDGT sequence due to Na^+ binding to the Na1 and the Na3 sites flips M311 to facing

the substrate binding site. In this flipped conformation, there is a steric clash between M311 and the closed HP2, which favors the opening of HP2 as previously described.(154) The middle panel shows a model with HP2 in the Apo (closed) conformation (from pdb: 5dwy) while the TM7 and the NMDGT region are shown in the Na^+ bound conformation (from pdb:5e9s). The steric clash between M311 in the flipped conformation and the closed HP2 is highlighted. **B)** The Ala side chain in the M311A mutant does not cause a steric clash with HP2. The flip of the Ala side chain therefore does not prop HP2 open.

Table S2.1. Distance between two probes for fluorescence-based HP2 movement assay

Cα- Cα Distances between V355 and S279			
Protein	pdb	Condition	Distance (Å)
Glt_{Ph}	2NWL	L-Asp	6.47
Glt_{Ph}	2NWW	TBOA and Na^+	13.58
Glt_{Ph}	2NWX	L-Asp and Na^+	6.53
Glt_{Tk}	4KY0	Apo	7.66
Glt_{Tk}	5DWY	Apo	7.55
Glt_{Tk}	5E9S	L-Asp and Na^+	6.38

Table S2.2. Parameters for HP2 opening determined by steady-state Na^+ titration of WT and mutant Glt_{Ph} (Phe_{CN}+W) transporters using the HP2 assay

Protein	$\mathbf{K_{0.5}^{Na}}$ (mM)
WT	177.9 ± 6.49
R397A	44.32 ± 0.95
R397Q	56.15 ± 0.99
R397K	98.01 ± 1.96
T314A*	373.63 ± 18.2
T314V*	539.08 ± 51.7
T314S	162.8 ± 6.27
M311L	79.32 ± 3.22
Y317F	91.04 ± 2.93

Values are given as mean ± S.E.M. for N ≥ 3. * $K_{0.5}^{Na}$ values for these mutants are approximations as saturation was not observed.

Table S2.3. Best fit parameters for the kinetics of HP2 opening by Na^+ in the WT and mutant Glt_{Ph} (Phe_{CN}+W) transporters

Protein	k_f (sec^{-1})	k_r (sec^{-1})	E $(\frac{k_f}{k_r})$	K_D (mM)
WT	0.0552 ± 0.002	0.00053	103	322 ± 18
R397A	2.59 ± 0.18	0.0011	2332	9.5 ± 1.6
R397Q	1.76 ± 0.5	0.00074	2454	12.8 ± 8.5
R397K	0.0572 ± 0.002	0.00089	65	149 ± 18
T314V	0.0184 ± 0.003	0.0013	15	632 ± 92
T314S	0.0279 ± 0.003	0.00098	28	524 ± 75

Values are given as mean ± S.E.M. for N ≥ 3.

Table S2.4. Affinities for Asp at high Na^+ determined by the L130W assay

Protein	K_D^{Asp} (200 mM Na^+) μM
WT	0.002 ± 0.000
R397A	11.759 ± 0.433
T314A	1.436 ± 0.111
M311A	0.334 ± 0.053
*Y317Phe$_{CN}$	0.21 ± 0.02
*Y317Phe$_{Br}$	0.066 ± 0.004
R397A+Y317Phe$_{CN}$	17.1 ± 3
R397A+Y317Phe$_{Br}$	15.2 ± 0.08

Values are given as mean ± S.E.M. for N ≥ 3.

*K_D^{Asp} values were determined in 100 mM NaCl. K_D^{Asp} for wild type Glt$_{Ph}$ in 100 mM NaCl is 0.015 ± 0.008 μM.

Chapter 3: Na^+ induced conformational choreography comprising the allosteric coupling in a glutamate transporter homolog

The experiments in this chapter were planned by E.A.R. and F.I.V, E.A.R collected all the data, and E.A.R and F.I.V wrote the results and discussion together.

Introduction

Harnessing pre-existing Na^+ gradients to transport solute across a membrane is a common theme across all branches of life. The inherent coupling between the electrochemical gradient and substrate translocation is poorly understood even though it is a fundamental mechanism for a variety of proteins. Na^+ symporters are a class of transporters responsible for a wide variety of vital functions such as Na^+ coupled transport of nucleosides(2), vitamins(3), amino acids(4, 5), neurotransmitters(6, 7), and sugars(1). One of the major excitatory neurotransmitters is glutamate and the proteins responsible for the rapid uptake of glutamate into cells are excitatory amino acid transporters or EAATs(14). Because of their importance in normal and pathological physiology, we have chosen to study how EAATs couple the Na^+ gradient to accomplish transport (61, 62). The transporters stoichiometrically use three Na^+ ions to translocate one molecule of glutamate along with a H^+ and a K^+ ion is required to accomplish counter transport(99-101). We chose to exploit the archaeal homolog, Glt_{Ph}, to investigate the molecular mechanisms for coupling since this protein has a large base of literature from both functional and structural studies as well as being amenable for spectroscopy studies.

In Glt_{Ph}, the overall stoichiometry of Na^+ ions to substrate is maintained (3 Na^+:1 substrate), but the substrate selectivity is altered to being highly selective for Asp and there is no K^+ dependent countertransport(150-152). The overall transport mechanism is known to be an elevator mechanism in which the transport domain moves within the

membrane and the trimerization domain acts as a scaffold (Figure 3.1B)(157, 158, 185). Each protomer can function independently and can isomerize from the outward facing state, OFS, to the inward facing state, IFS, in the Apo or fully loaded ($3Na^+$:1Asp) state (163, 181-184). Due to this feature, a key to the transport mechanism lies in sequential coupled binding. The proposed order of binding starts with two Na^+ ions (Na1/Na3) binding to the outward facing state of the transporter, causing necessary conformational changes to support substrate binding including binding site rearrangements and the extracellular gate opening. With access to the binding site, substrate can bind and HP2 closes followed by the final binding of third Na^+ ion (Na2) (Figure 3.1D). The fully loaded protein then can isomerize into the inward facing state and translocate the substrate across the membrane. The three Na^+ ion binding sites have been identified through several structures of both Glt_{Ph} and the closely related homolog, Glt_{TK} (Figure 3.1C)(150, 164, 165). Structures have given some insight into Na^+ induced conformational changes which occur during the coupling process within the transport domain of the protein. The most noticeable changes are the rearrangement of the highly conserved NMDGT motif which participates in Na^+ coordination, the R397 movement out of the binding site once Na^+ binds, and HP2 open and closed states with different ligands (Figure 3.1C).

Even with the wealth of knowledge on the overall transport mechanism, the conformational wave proceeding Na^+ binding to the Na3 and Na1 sites is still unknown. We have the structure of the starting state, Apo-OFS, and the end state with both Na^+ and Asp bound, Na^+/Asp-OFS. A new high-resolution structure was solved with only Na^+ bound to help shed light on this process, but both the binding site and NMDGT motif look essentially the same as the fully bound structure (Figure 3.1C)(203). HP2 is also open to a similar extent as a previously solved structure with the substrate analogue TBOA. The new structure gives no further insight into how binding to the Na3 and Na1 site induce the conformational wave necessary to make the binding site competent for Asp binding

and to open HP2. Our strategy to address the gap in knowledge was to perturb Na3 and Na1 sites individually and study their effects on different steps in the coupling process.

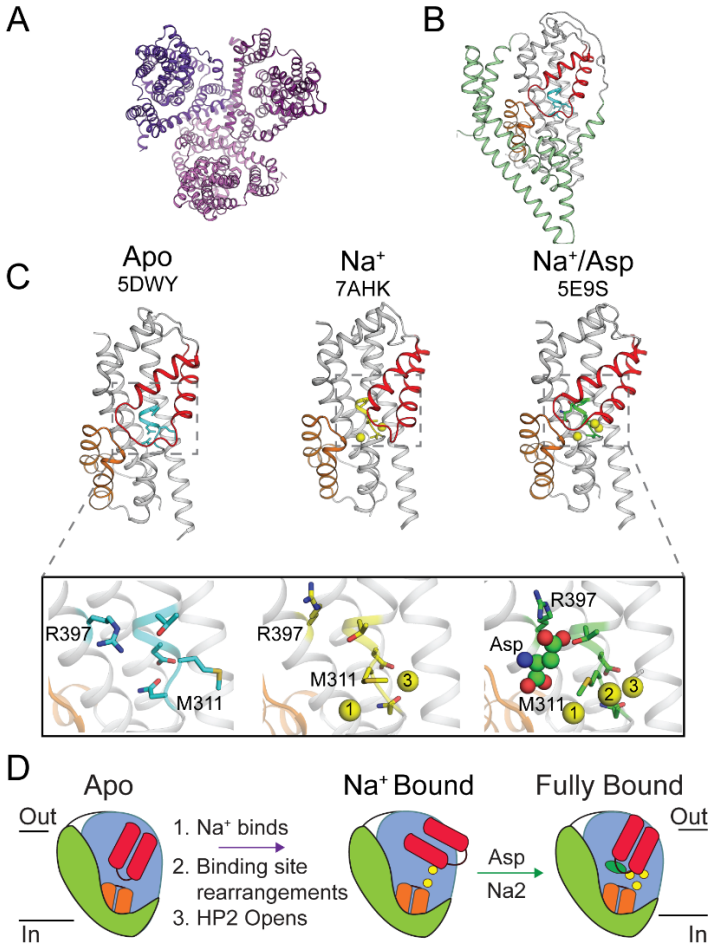

Figure 3.1. Sequential binding order for coupled transport and available structures of steps in the process. A) Trimer of Glt_{Ph} in top-down orientation, each protomer is colored a different shade of purple **B)** Single protomer with trimerization domain colored in green, transport domain shown in grey with key hairpin moieties colored in orange (HP1) and in red (HP2) (pdb 5dwy) **C)** Structures of transport domain in different ligand bound states of the OFS labeled Apo, Na^+ bound, Na^+/Asp bound with the corresponding pdb code. Both Apo and fully bound structures are from Glt_{Tk} with Glt_{Ph} numbering. The NMDGT motif is colored in each transport domain. Insets are close ups of the binding sites, with HP2 removed for clarity, and focus on the orientation of R397 and NMDGT and ligand binding sites **D)** Proposed order of binding with cartoon highlighting HP2 state.

In the present study, we developed novel assays to expand the steps of the coupling process we can study. In conjunction with established assays, we were able to cover the coupling process from Na^+ binding to HP2 opening. Both Na3 and Na1 sites were perturbed individually and from the effects on Na^+ induced conformational

changes, we were able to infer their role in the coupling process. Overall, Na^+ binding breaks several interactions which stabilize the non-binding, Apo form and replaces most of those interactions with protein-ion interactions which both start and partake in the coupling mechanism. We demonstrate that Na1 and Na3 have different roles in the coupling process where Na3 drives NMDGT rearrangements while Na1 binding causes partial HP2 opening to support low affinity substrate binding. Both Na^+ sites are necessary for full HP2 opening.

Results:

Tyr fluorescence of Glt_{Ph} reports on Na^+ binding to the Na1 and the Na3 sites

We initially optimized an assay for monitoring Na^+ binding to Glt_{Ph}. It has been reported that Na^+ binding to Glt_{Ph} can be monitored by changes in protein fluorescence(211). Glt_{Ph} does not contain any Trp residues but contains 18 Tyr residues that are distributed throughout the protein (Figure 3.2A)(149). The Tyr fluorescence of Glt_{Ph} shows a ~10% increase in emission intensity with Na^+(Figure 3.2B). This effect is selective for Na^+ as no change in fluorescence is observed with K^+ (Figure 3.2B). The change in fluorescence is also specific for Na^+ binding as addition of Asp following Na^+ (which causes closure of HP2) does not result in a further change in fluorescence (Figure 3.2B). Of the 18 Tyr residues in Glt_{Ph}, Y88, Y89 and Y247 are in the vicinity (< 7 Å) of the Na1 and the Na3 sites (Figure 3.2A). To probe whether the fluorescence changes in Glt_{Ph} reflect Na^+ binding to the Na1 and the Na3 sites, we substituted these Tyr residues with Phe. As a control, we also generated a Phe substitution at Y317 that was distant from the Na^+ binding sites. We observed that the Y88F and the Y89F substitutions reduced the fluorescence change with Na^+ while no fluorescence changes with Na^+ were observed for a Y88F/Y89F double mutant (Figure 3.2C). We could not evaluate the effect of Y247 on the fluorescence change due to poor biochemistry of the Y247F mutant while the Y317F substitution did not affect the fluorescence response with

Na^+ (Figure 3.2C). These results indicate that the changes in Tyr fluorescence of Glt_{Ph} reflect Na^+ binding to the Na1 and the Na3 site and that changes in Tyr fluorescence provides a facile assay to monitor Na^+ binding to these sites.

Using the Tyr fluorescence assay, we measured a K_D of 45 mM for Na^+ binding to Glt_{Ph} (Figure 3.2D). This in the same range of 60-90 mM reported using a dye-based assay (202, 209). Na^+ binding to Glt_{Ph} has also been evaluated by the HP2 movement assay to give values of 178 mM (209) and 120 mM by using a F273W substitution (210). The affinity of Na^+ was increased to 1.2 mM in the presence of 100 μM Asp, as expected for this transporter (Figure 3.2D).

To perturb the Na1 and the Na3 sites, we substituted the amino acid side chains that coordinated Na^+ (Figure 3.2E). At the Na3 site, Na^+ is coordinated by the side chains of T92, S93, N310 and the D312. We introduced both conservative and non-conservative substitutions at these side chains and evaluated the effect on Na^+ binding. We observed that conservative substitutions such as T92S or S93T did not substantially perturb Na^+ binding and instead improved affinity around two-fold (Figure 3.2E, Table S3.1). The non-conservative substitutions showed two distinct effects. Substitutions at T92, N310 and D312 showed a dramatic shift in K_D and the maximal fluorescence response observed was roughly half the value observed for the wild type protein (Figure 3.2E, Table S3.1). For the S93 mutants, we also observed a shift in the Na^+ binding affinity but the maximal fluorescence response was similar to the wild type. These data support the T92C, D312N, and N310D/S substitutions abrogating Na^+ binding to the Na3 site while the S93 substitutions decreases the Na^+ binding affinity at the Na3 site. At the Na1 site, D405 is the only sidechain involved in Na^+ coordination. It has been previously demonstrated using structural approaches and Asp binding that the D405N substitution perturbs Na^+ binding to the Na1 site(150). We tested Na^+ binding to the D405N substitution using the Tyrosine assay. We observed a decrease in the maximal response

and a shift in the K_D to 214 mM confirming the perturbation of Na^+ binding to the Na1 site in the D405N mutant (Figure 3.2E, Table S3.1). We also used the dye-based assay to monitor Na^+ binding in these Na^+ site mutants (Figure S3.1). The dye assay also reported perturbed Na^+ binding in the Na^+ site mutants consistent with the data obtained by the tyrosine fluorescence assay. These experiments provide us with Glt_{Ph} mutants that were perturbed in the Na1 or the Na3 sites.

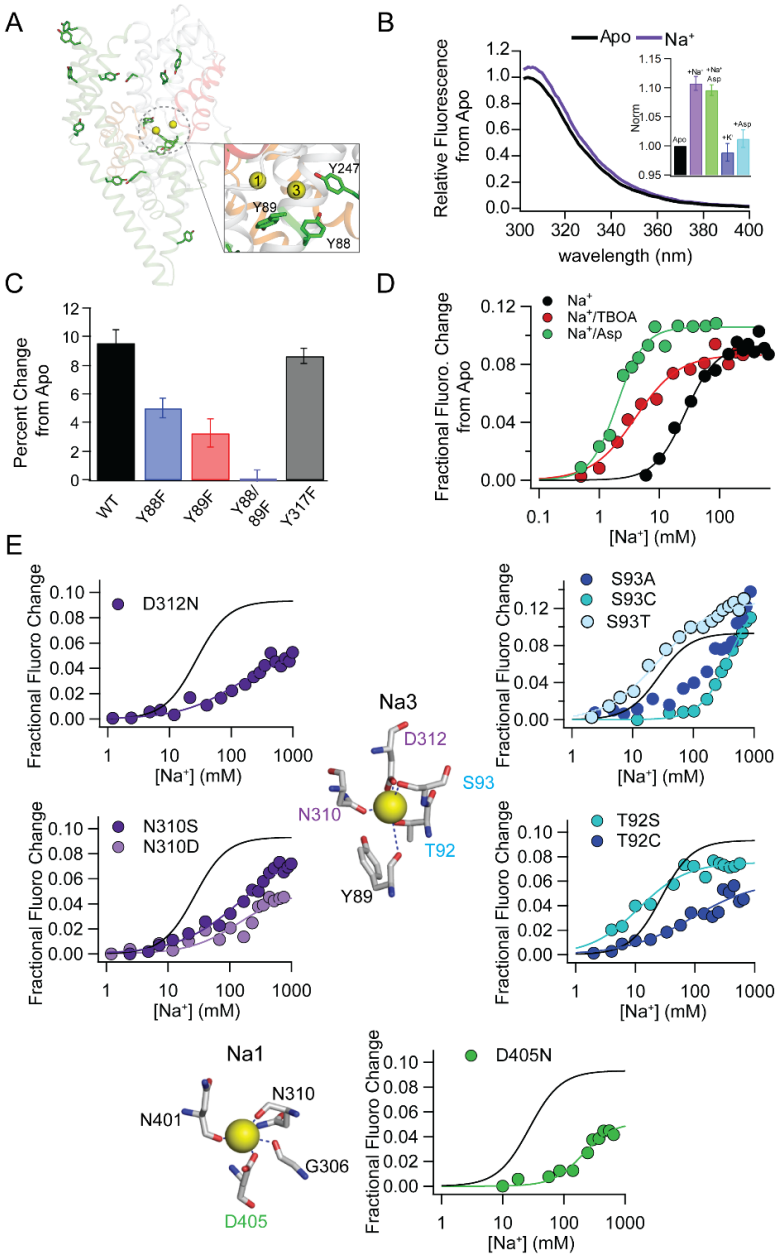

Figure 3.2. Tyrosine-based fluorescence assay to monitor Na^+ binding affinity A) Single protomer showing tyrosine residues in green and those that are close to Na1/3 sites are labeled in the inset **B)** Emission spectra after excitation at 289 nm for Apo and 300 mM Na^+, the inset is the fractional fluorescence change normalized to Apo (black) for various ligand additions. Additions are Na^+(purple): 300 mM NaCl, Na^+/Asp (green): 300 mM Na^+/100 µM Asp, K^+ (blue): 300 mM KCl, Apo/Asp (teal): 100 µM Asp) **C)** Fractional fluorescence change for specific proteins after 300 mM Na^+/100 µM Asp addition **D)** Sample titrations of Na^+ alone, Na^+ with 10µM TBOA or 100 µM Asp present for WT Glt_{Ph} (K_D: Na^+ alone 45 mM, Na^+/TBOA 4 mM, Na^+/Asp 1.2 mM) **E)** Na1 and Na3 ion binding sites with coordination spheres composed of side chains and backbone carbonyls. Sample titrations for Na^+ site mutants using the tyrosine-based fluorescence assay to assess Na^+ affinity effects. WT response to Na^+ is the black line in all panels. Error bars in (B/C) are S.E.M. and all representative and averaged data is from N ≥ 3.

Perturbation of the Na3 site affects HP2 movement

Next, we investigated the effect of perturbing the Na^+ sites on HP2 movement. We had previously developed a fluorescence assay to monitor the movement of HP2(209). This assay involves the incorporation of two probes into Glt_{Ph}, a Trp in HP2 and a Phe_{CN} in HP1. We substituted V355 in HP2 with Trp and used nonsense suppression approaches to substitute S279 in HP1 with cyanophenylalanine (Phe_{CN}). In the Apo state, HP2 is (predominantly) closed and the probes are close together. In this state Phe_{CN} quenches the Trp fluorescence due to the proximity of the two probes. The binding of Na^+ opens HP2, which increases the separation between probes and increases Trp fluorescence due to reduced quenching of Trp by Phe_{CN}. Binding of Asp closes HP2, which decreases the separation between the probes and is indicated by a decrease in fluorescence (Figure 3.3A/B). Monitoring the changes in fluorescence therefore provides us with a means to evaluate the opening of HP2 with Na^+ and the closure of HP2 with Na^+/Asp.

We tested the effect of the Na3 site mutants on HP2 movement. For the N310S and the D312N mutants, we observed very small (3-5%) fluorescence changes with Na^+ in the HP2 assay (Figure 3.3C). The lack of a change in fluorescence in the HP2 assay can be attributed to either HP2 not opening or HP2 not being able to remain open after

the binding of Na^+. To distinguish between these possibilities, we tested the effect of TBOA on HP2 opening and the extent of fluorescence change with HP2 closure. TBOA binds to Glt_{Ph} similarly to Asp but keeps HP2 propped open due to the presence of the benzyloxy group in the side chain. Addition of Na^+/TBOA to the wild type Glt_{Ph} gives an increase in fluorescence which is greater than the fluorescence changes seen with Na^+ alone (Figure 3.3B/D). Addition of Na^+/TBOA to the N310S or the D312N mutants showed fluorescence changes that were only slightly higher than the changes observed with Na^+ alone, which indicates that HP2 opening is severely perturbed in these mutants (Figure 3.3D). For S93A and T92C, we observed fluorescence changes with Na^+ and with Na^+/TBOA in the HP2 movement assay (Figure 3.3D). However, the changes observed were smaller than the changes observed in the wild type indicating impaired HP2 opening in these mutants. Consistent with limited extent of opening, HP2 closure experiments in the presence of Na^+ had correspondingly reduced extents of fluorescence change for the Na3 mutants (Figure 3.3E). These results indicate that Na^+ binding to the Na3 site is required for HP2 opening and that the magnitude of the effect depends on the specific side chain that is perturbed. We see a severe effect for substitutions in the N310 and D312 residues that are in the NMDGT motif compared to substitutions in the T92 and S93 in the TM3 helix.

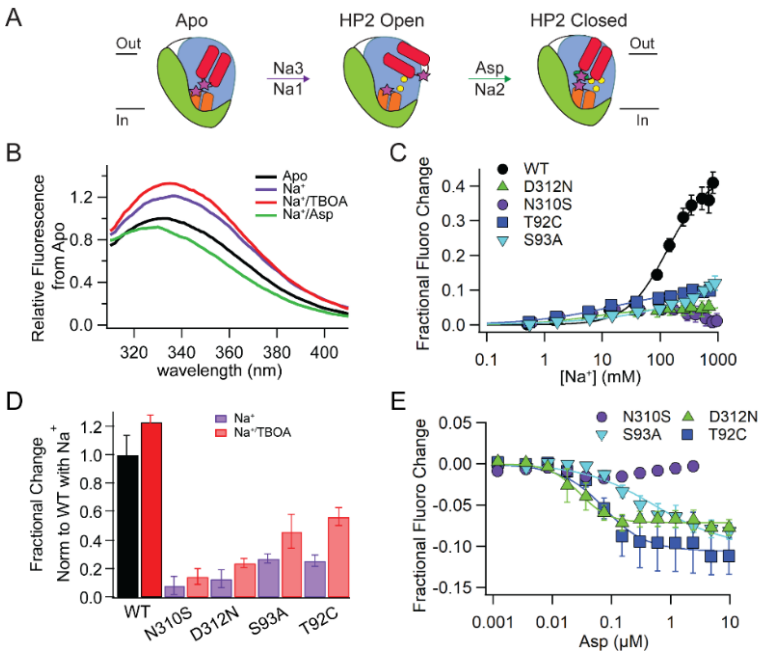

Figure 3.3. Reintroducing assay to monitor extracellular gate movement and consequences of Na3 perturbation on HP2 opening A) Scheme for distance changes of probes (magenta stars) in HP2 movement assay throughout the binding process, probes are Phe_{CN} at 279 on HP1 (orange) and Trp at 355 on HP2 (red) **B)** Emission spectra after excitation at 295 nm (Na^+ is 200 mM, Na^+/TBOA is 200 mM Na^+/10 μM TBOA, Na^+/Asp is 200 mM Na^+/100 μM Asp) **C)** Steady state titrations of HP2 opening with Na^+ alone, WT is in black, Na3 mutants are referred to in legends: N310S, D312N, T92C, S93A ($K_{0.5}^{Na}$ WT: 132 ± 20 μM) **D)** HP2 steady state fluorescence changes for HP2 opening with and without the presence of 10 μM TBOA normalized to the fluorescence change of WT with Na^+ **E)** Steady state HP2 closure titrations in the presence of 500 mM Na^+ ($K_{0.5}^{Asp}$ WT: 0.012 ± 0.002 μM, T92C: 0.046 ± 0.1 μM, S93A: 0.53 ± 0.2 μM, D312N: 0.03 ± 0.003 μM). Error bars throughout the figure are S.E.M. and N ≥ 3.

A conformational switch in the NMDGT motif couples Na^+ binding to HP2 movement

A highly conserved sequence in EAATs is the NMDGT motif. This motif forms the un-wound region present in the middle of TM7 and participates in the coordination of the Na1 and Na3 sites (Figure 3.4A). The NMDGT region shows a different conformation in Apo-Glt_{Ph} compared to Na^+- or Na^+/Asp-Glt_{Ph} and it stands to reason that the NMDGT motif couples Na^+ binding to the opening of HP2. In order to functionally investigate this, we developed an assay to monitor the conformational switch in the NMDGT motif. We identified a residue in the vicinity of the NMDGT motif which undergoes a change in

environment with the conformational switch in this motif. At this Leu 99 residue, we substituted the native residue for a Trp to serve as a fluorescence reporter. The L99W-Glt_{Ph} showed similar biochemistry to the wild type transporter and was functional in Asp uptake (Figure S3.2A). We observed that the fluorescence emission L99W-Glt_{Ph} was sensitive to Na^+ and showed a substantial 21% decrease in fluorescence intensity and a blue shift in the emission maximum on the addition of Na^+ (Figure 3.4B). The blue shift in the fluorescence intensity indicates a shift to an environment with a lower polarity. There were no further changes in fluorescence on the addition of Asp, which is anticipated as there are no changes in the NMDGT region between Na^+ bound and Na^+/Asp bound states (Figure 3.4B/C). The structures of Glt_{Ph} in the Apo and Na^+ bound states indicate that the change in the environment around L99 with the NMDGT conformational switch is due a change in the relative positioning of the L316 side chain (Figure 3.4D). To confirm, we investigated the fluorescence changes in a L99W/L316A mutant. We observed that the fluorescence changes were greatly attenuated compared to the L99W mutant (Figure 3.4E). In control experiments, we confirmed that the L316A substitution did not dramatically affect HP2 movement (Figure S3.2B). These experiments confirm that the fluorescence changes of L99W are indeed reporting on the NMDGT conformational switch.

We introduced various Na3 site substitutions into the L99W-Glt_{Ph} and determined the effect on the NMDGT conformational switch. We found that the D312N substitution eliminated any fluorescence changes with Na^+ or Na^+/Asp addition (Figure 3.4F). The fluorescence changes in the T92C and the N310S mutants were greatly attenuated compared to the control wild type, L99W-Glt_{Ph} (Figure 3.4F). Changes similar to the control were observed for the S93A mutant though the changes were observed at a much higher Na^+ concentration (Figure 3.4F). The studies of these mutants highlight the requirement of Na^+ binding to the Na3 site for the conformation switch of the NMDGT

motif. We find that the effects of the Na3 mutants on the NMDGT conformational switch mirror the effects on HP2 opening. Therefore, the NMDGT conformational switch couples Na^+ binding at the Na3 site and HP2 opening.

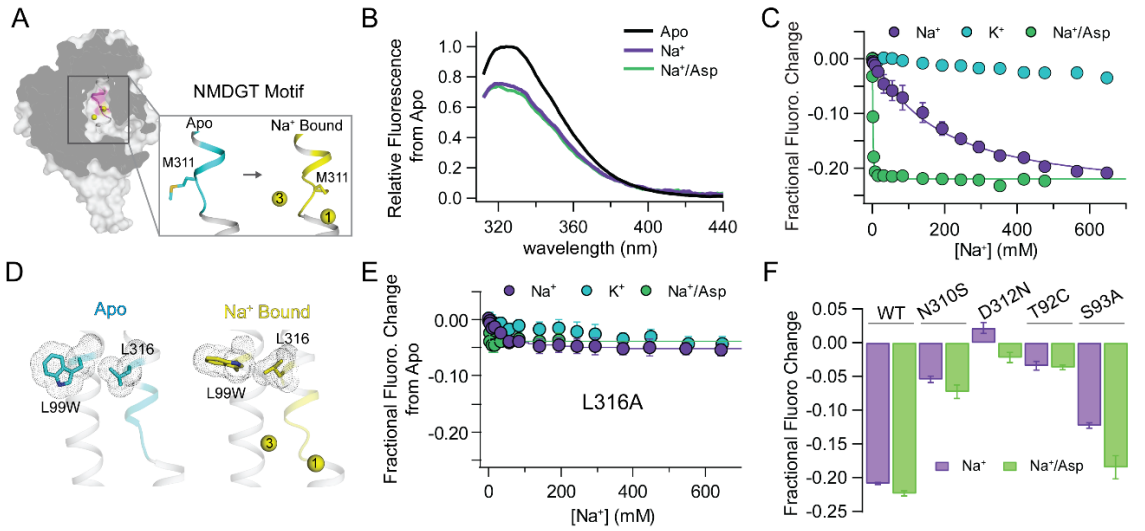

Figure 3.4. Novel assay to monitor key Na^+ induced conformational changes in the conserved NMDGT motif A) Singe protomer in surface representation with NMDGT inset both in Apo (cyan) and Na^+ bound conformations (yellow) where major movements can be seen and highlighted by M311 positioning **B)** Emission spectra after excitation at 295 nm (Na^+ is 500 mM and Na^+/Asp is 500 mM Na^+/100 µM Asp) **C)** Steady state titrations of Na^+ alone, K^+, and Na^+ with 100 µM Asp present **D)** L99W position relative to L316 and the Na^+ sites in Apo (cyan) and Na^+ bound conformations (yellow) **E)** Decreased fluorescence signal in the NMDGT rearrangement assay when L316 is substituted with Ala in all ligand conditions **F)** NMDGT rearrangement data for the respective Na3 mutant (N310S, D312N, T92C, S93A) taken from steady state titrations (Figure S3.3). Error bars throughout the figure are S.E.M and N ≥ 3.

S93-M311 steric clash assists in propping HP2 open

M311 is a key residue for coupling in the NMDGT motif. We have previously shown that on Na^+ binding, M311 acts as a wedge to keep HP2 propped open(209). In Glt_{Ph} structures, the M311 side chain has been visualized in two conformations that we refer to as the extended and the flipped conformation. In the Apo state, the M311 side chain is dynamic and samples both these conformations while in the Na^+ or the Na^+/Asp bound state, the M311 side chain is in the flipped conformation (Figure 3.5A). A structural inspection suggests that Na^+ binding at the Na3 site can influence the

conformation of the M311 side chain. This occurs because in the Na^+ bound conformation, the S93 side chain sterically clashes with the extended conformation of the M311 side chain (Figure 3.5A). To confirm this steric clash mechanism, we probed the effect of substitutions at S93 and M311 that changed the steric properties of these side chains. We substituted S93 with T to increase the steric bulk of this side chain. For the S93T mutant, we observed that the opening of HP2 took place at a lower Na^+ concentrations and to a larger extent than the wild type (Figure 3.5B). At M311, a Leu substitution, which has a similar side chain volume(234) to Met but with different sterics, showed that HP2 opens in a relatively WT-like manner (Figure 3.5C). In the M311L/S93T double mutant, we observed that the opening of HP2 took place at a substantially lower Na^+ concentration and the extent of opening was greater than observed for the single mutants (Figure 3.5C). These results are in accordance with a steric interaction between the S93 and the M311 side chains when Na^+ binds to the Na3 site. This steric interaction helps switch the M311 side chain into the flipped conformation, wherein it acts as a wedge to keep HP2 open on Na^+ binding. The M311 flip provides another means by which Na^+ binding to the Na3 site is transduced to opening HP2 for substrate binding.

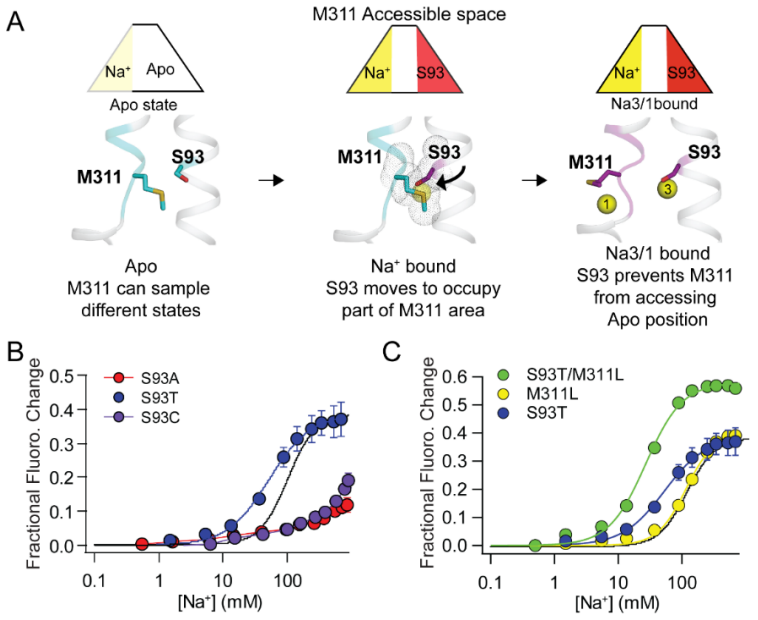

Figure 3.5. S93-M311 steric interaction demonstrate one way Na^+ binding to the Na3 site is transduced to opening HP2 A) Depiction of Na^+ regulation for state of M311 in binding process with Na3 coordinator S93. Apo is pdb 5dwy with only one conformation of M311 shown and colored cyan. Na^+ bound state is pdb 7ahk colored in purple **B)** Steady state HP2 opening for S93X substitutions, black line is WT HP2 opening **C)** Steady state HP2 opening for double mutation of S93 and M311 along with corresponding single substitutions, black line is WT HP2 opening ($K_{0.5}^{Na}$ S93T: 53 ± 3.4 mM, M311L: 115 ± 4.7 mM ST/ML: 27 ± 2 mM) Error bars are S.E.M. and N ≥ 3.

Na1 site substitution at D405 uncouples HP2 opening from Na^+ binding

After investigating the consequences of Na3 binding and confirming that D405N perturbs Na^+ binding, we used the D405N substitution to evaluate the effect of perturbing the Na1 on HP2 movement (Figure 3.6A). In the HP2 assay for the D405N mutant, we did not observe a fluorescence change upon the addition of Na^+ although there was a decrease in fluorescence with Na^+/Asp (Figure 3.6B/C). The decrease in fluorescence indicates Asp binding and the closure of HP2. Therefore, the lack of a fluorescence signal corresponding to the opening of HP2 with Na^+ could stem from HP2 not being stable in the open state (as previously observed for the M311A mutant) or HP2 being already open. We used TBOA binding to distinguish between these possibilities (as previously described in Chapter 2 with M311A). We found that the addition of Na^+/TBOA did not result in a significant fluorescence change compared to Apo- or the Na^+-D405N

Glt_{Ph} (Figure 3.6B). For the wild type control, we observed an additional 9% change in intensity when comparing the fluorescence response to Na^+ versus Na^+/TBOA. We confirmed that TBOA binds to the D405N Glt_{Ph} in the presence of Na^+ by measuring a shift in the Asp affinity in the presence of TBOA (Figure S3.5B). The lack of an effect of Na^+ or Na^+/TBOA in the HP2 assay for the D405N Glt_{Ph} suggests that HP2 is already open in the Apo state. We also investigated another substitution at D405 and observed a similar result (Figure S3.4).

We speculated that if HP2 is already open, then the mutant should be able to bind Asp in the Apo state as well as with Na^+ bound. We tested Asp binding by the Apo D405N transporter and observed a decrease in fluorescence indicating that Asp binding and closure of HP2 took place in the absence of Na^+. Asp binding to the Apo D405N transporter took place with a $K_{0.5}^{Asp}$ of 124 μM compared to a value of 0.033 μM in the presence of 200 mM Na^+ (Figure 3.6C). To confirm Asp binding to D405N-Glt_{Ph} in different states, we used Isothermal titration calorimetry (ITC). In the presence of 10 mM Na^+, we observed strong Asp binding with a K_D of 0.19 μM to the wild type transporter while the Asp binding to the D405N transporter took place with a K_D of 3.4 μM and a smaller heat change (Figure 3.6D/E). We tested Asp binding in the absence of Na^+ and observed no binding to the wild type transporter (Figure 3.6F). In contrast, we observed Asp binding to the D405N transporter at a decreased affinity of 11 μM and a corresponding further decrease in the magnitude of heat change (Figure 3.6G). ITC confirms that D405N-Glt_{Ph} can indeed bind Asp without Na^+, but the different heat changes along with shifted affinities indicate that the conformational change upon Asp binding are not the same as with WT-Glt_{Ph}. The combined data from the HP2 assay and the ITC experiments suggest that D405N substitution perturbs the Na^+ coupled opening of HP2 and allows the binding of Asp to the Apo transporter.

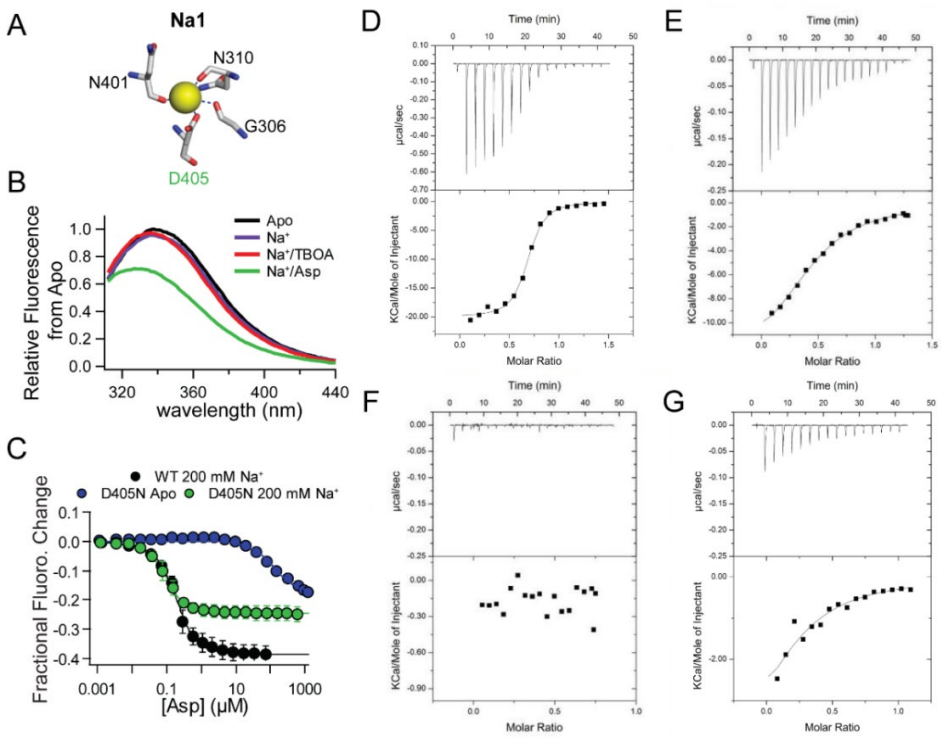

Figure 3.6. Perturbing Na1 results in uncoupled substrate binding A) Coordination of Na1 with the only side chain, D405, highlighted in green **B)** Emission spectra for Na1 site mutant D405N in HP2 movement background. Excitation at 295 nm (Na^+ is 200 mM, Na^+/TBOA is 200 mM Na^+/10 μM TBOA, Na^+/Asp is 200 mM Na^+/100 μM Asp) **C)** Closure titrations with Asp with and without Na^+ present ($K_{0.5}^{Asp}$ WT: 56 ± 2 nM, D405N Na^+: 33 ± 2 nM D405N Apo: 124 ± 21 μM) **D-G)** ITC data for Asp binding with or without 10 mM Na^+ **D)** WT Asp titration with 10 mM Na^+ (0.19 μM) **E)** D405N Asp titration with 10 mM Na^+ (3.4 μM) **F)** WT Asp titration with no Na^+ **G)** D405N Asp titration with no Na^+ present (100 mM KCl) (11 μM). All error bars are S.E.M. and all representative data comes from N ≥ 3.

We used CW-EPR experiments to further probe the movements of HP2 when the Na1 site was perturbed. We introduced spin probes at V355 and S279 as previously described to monitor the distance distributions of HP2 in the different states (Figure 3.7A). The positions the spin probes are introduced are the same positions at which fluorescence probes were introduced for the HP2 movement assay and previous EPR studies(208). When the spin labels are in close proximity, there is a broadening of the EPR spectra by dipolar relaxation. The separation between the spin probes is reflected by the relative amplitude of the central peak in the EPR spectra and in the shape of the spectra. In wild type Glt_{Ph}, HP2 is closed in the Apo state and open when Na^+ is bound.

Correspondingly, we observed an increase in the relative amplitude of the central peak in the EPR spectra of the Na^+ bound state compared to the Apo state (Figure 3.7B/D). An additional increase is seen in the Na^+/TBOA bound state while a decrease is observed in the Na^+/Asp bound state, which is as anticipated based on the distance distribution of HP2 in these states in wild type Glt_{Ph} (Figure 3.7D). For the D405N-Glt_{Ph}, we observed a similar amplitude for the central peak in the Apo, Na^+ bound and the Na^+/TBOA bound states indicating a similar distance distribution for HP2 in these states (Figure 3.7B/D). We observed a decrease in the relative peak amplitude in the Na^+/Asp bound state compared to the Apo state, indicating the closure of HP2 on the binding of Na^+/Asp. However, the change in amplitude between the Na^+ bound and the Na^+/Asp state for the D405N transporter was smaller than the corresponding change in the wild type transporter suggesting a limited opening of HP2 in the D405N mutant compared to the wild type. The splitting pattern in the EPR spectra for the Apo and Na^+ bound wild type Glt_{Ph} are different, reflecting the different states of HP2. In contrast, we observed a similar splitting pattern for the D405N transporter indicating no change in the state of HP2 in the D405N transporter on the binding of Na^+. We also measured the EPR spectra for the Apo transporter after the addition of Asp (Figure 3.7C). We did not see any change for the wild type Glt_{Ph} consistent with the inability of the wild type transporter to bind Asp in the absence of Na^+. For the D405N transporter, we observed a decrease in the peak amplitude on Asp addition to the Apo state consistent with the ability of the D405N transporter to bind of Asp in the absence of Na^+.

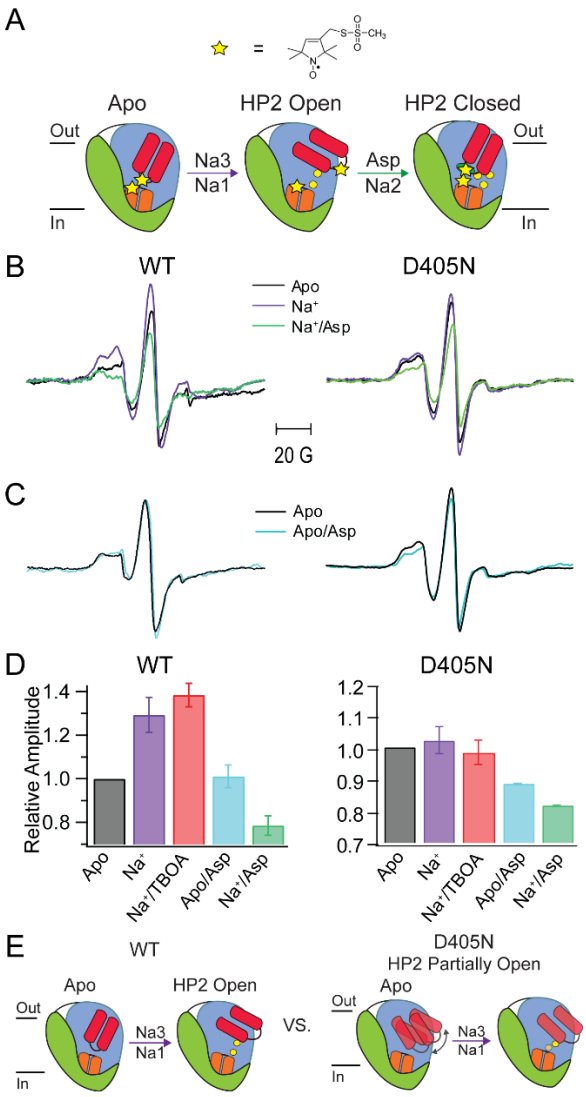

Figure 3.7. HP2 opening is uncoupled in Na1 mutant A) Scheme for distance changes of spin probe, MTSL, throughout the binding process. Probes are represented through yellow stars and attached at 279 on HP1 (orange) and 355 on HP2 (red) **B)** WT CW-EPR spectra and D405N CW-EPR spectra (Apo: 300 mM KCl, Na^+: 200 mM NaCl, and Na^+/Asp: 200 mM Na^+/500 µM Asp) **C)** EPR spectra of Apo: 300 mM KCl and Apo/Asp: 300 mM K^+/500 µM Asp for WT and D405N Glt_{Ph} **D)** EPR WT and D405N relative amplitudes normalized to Apo values, error bars are S.E.M. from an N ≥ 3 **E)** Cartoon representation of HP2 states for Apo and Na^+ bound states in WT vs D405N-Glt_{Ph}.

D405N mimics a Na1 bound state of Glt_{Ph}

The opening of HP2 in the wild type transporter requires Na^+ binding to the Na1 and the Na3 sites. In the D405N transporter, we see HP2 opening in the absence of Na^+ indicating that the D405N substitution mimics the effect of Na^+ binding. As D405

contributes to the Na1 site, we expect that D405N mimics Na^+ binding to the Na1 site. To probe whether the D405N substitution also mimics Na^+ binding to the Na3 site, we investigated whether the switch in the NMDGT motif that is induced by Na^+ binding to the Na3 site is involved in the HP2 opening observed in the D405N-Glt_{Ph} Apo state. A key aspect of the NMDGT switch is the flip of the M311 side chain. M311 in this flipped conformation is important for keeping HP2 wedged open on Na^+ binding and in the M311A substitution HP2 cannot stay open. We investigated the effect of the M311A substitution in the D405N background to determine if the M311 residue plays a role in HP2 opening in the Apo-D405N transporter. In the M311A/D405N mutant, there is no observable signal for HP2 opening as in the D405N single mutant. We inferred the state of HP2 by investigating Asp binding in the absence of Na^+ since Asp binding can only take place if HP2 is already open. We observed Asp binding to M311A/D405N mutant in the Apo state and the binding took place with a higher affinity than observed for the D405N mutant (Figure S3.6). Asp binding to the M311A mutant in the Apo state was not detected (Chapter 2, Figure 2.5). Asp binding to the M311A/D405N mutant in the Apo state indicates that substituting the M311 side chain does not hinder the HP2 opening observed in the Apo-D405N Glt_{Ph}. This result indicates that the conformational changes corresponding to the binding of Na^+ to the Na3 site are not involved in HP2 opening in the D405N transporter. We therefore conclude that the D405N substitution does not reflect the effect of Na^+ binding to the Na3 site and it mainly mimics a transporter with Na^+ bound to the Na1 site. These results suggest that HP2 opening in Glt_{Ph} can take place with Na^+ binding to only the Na1 site. However, the results from the HP2 assay and the EPR studies indicate a limited HP2 opening when Na^+ is bound to the Na1 site in contrast to the full opening of HP2 that is observed when Na^+ is bound to both the Na1 and the Na3 sites. Furthermore, the changes in Asp affinity in Apo-D405N compared to the D405N and the wild type transporter in the presence of Na^+ indicate a sub-optimal

substrate binding site in the Apo-D405N transporter in which the side chain structural changes necessary for high affinity substrate binding have not taken place. These additional changes necessary for high affinity substrate binding are therefore attributed to Na3 binding rearrangements.

Na^+ binding to the Na1 site perturbs the H-bond network of D405

In the Apo state, the D405 side chain participates in a H-bond network with direct interactions with N310 and Y89 which is broken on Na^+ binding (Figure3.8A). To probe the role of this H-bond network in coupling Na^+ binding to HP2 opening, we disrupted the D405-Y89 H-bond by substituting Y89 with Phe. Using the Tyr fluorescence assay, we measured a higher Na^+ affinity in the Y89F mutant compared to the wild type (Figure 3.8B). As Y89 is partially responsible for the Tyr fluorescence signal change on Na^+ binding, we confirmed the increase in Na^+ affinity in the Y89F mutant by also using the dye-based assay (Figure 3.8C). Furthermore, we observed that the NMDGT rearrangement and the opening of HP2 on Na^+ binding took place at lower Na^+ concentrations in the Y89F mutant compared to the wild type (Figure 3.8D/E). The observation of higher Na^+ affinity and of lower Na^+ concentrations for carrying out the Na^+ dependent conformational changes suggest that disruption of the D405-Y89 H-bond on Na^+ binding is part of the structural changes involved in coupling Na^+ binding to the opening of HP2.

The H-bond network formed with the D405 residue at its nexus extends to the N401 residue. In the Apo state, N401 forms a H-bond with the carbonyl backbone of G313 in the NMDGT motif (Figure 3.8A). In the Na^+ bound state, this H-bond is broken and the N401 residue forms a H-bond with the T314 side chain in the NMDGT motif. The structural analysis suggests that changes in the N401 side chain are linked to the conformational switch in the NMDGT motif. To probe the role of the N401 side chain

interactions, we tested a number of amino acid substitutions at this position. Of the substitutions tested, only the Asp substitution was biochemically stable. We found that Na^+ binding to the N401D mutant took place with a higher affinity (Figure 3.8B). Additionally, the NMDGT conformation switch took place at a lower Na^+ concentration and HP2 opening also took place at a lower Na^+ concentration (Figure 3.7D/E). These data are consistent with a rearrangement of the H-bonds of the N401 residue as a part of the structural changes induced by Na^+ binding. Both the D405N substitution and breaking the H-bond network in a manner similar to Na1 binding, provide key information on the role of Na1 in the coupled binding process.

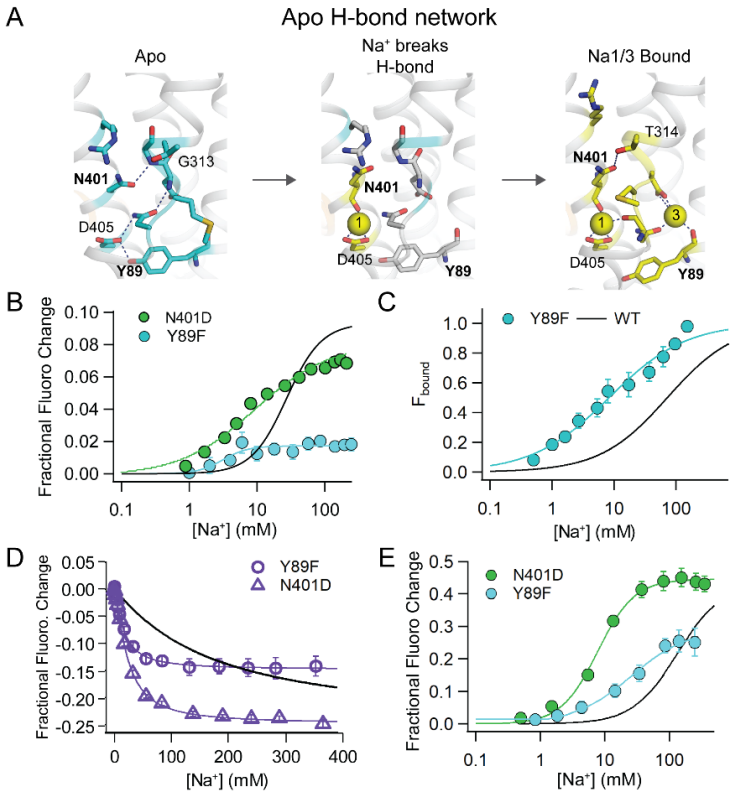

Figure 3.8. Essential role of Na^+ binding is to break the Apo H-bond network A) Apo state with residues involved in H-bond shown and network indicated through dashes. Apo is in cyan, residues which participate in interactions that would theoretically be broken by Na1 binding are colored gray in the intermediate figure, Na^+ bound state is in yellow **B)** Na^+ binding data for Y89F and N401D compared to WT shown as a black line with only Na^+ in the tyrosine based assay (K_D WT: 45 mM, Y89F: 8.2 ± 0.9 mM, N401D: 11.6 ± 2.6 mM) **C)** Na^+ binding data for Y89F compared to WT shown as a black line with only Na^+.

This data is from dye-based Na^+ binding assay (K_D WT: 72 ± 10 mM vs Y89F: 8.2 ± 0.9 mM). **D)** Y89F and N401D in NMDGT rearrangement assay (L99W-Glt_{Ph}) (Y89F K_{nmdgt} Na^+: 17 ± 0.8 mM, K_{nmdgt} Na^+/Asp: 0.01 ± 0.02 mM and N401D K_{nmdgt} Na^+: 23.5 ± 0.5 mM, K_{nmdgt} Na^+/Asp: 21.5 ± 0.7 mM) **E)** Steady state HP2 opening for Y89F and N401D compared to WT represented as a black line ($K_{0.5}^{Na}$ Y89F: 25 ± 6 mM and $K_{0.5}^{Na}$ N401D: 7.9 ± 0.5 mM). Error bars are S.E.M. and N ≥ 3.

Kinetic measurements with newly developed conformational assays confirm Na^+ induced HP2 opening

The focus of this study was to monitor the effects of Na^+ site perturbation on Na^+ binding, NMDGT conformational switch, and HP2 opening to determine the molecular consequences of binding individually to the Na1 and Na3 sites. Using the assays developed in this study, we aimed to gain further mechanistic insight into the native process by determining the kinetics of each step (Figure 3.9A/C/E). The Tyr fluorescence assay was used to monitor the kinetics of Na^+ binding and we observed that Na^+ binding took place at rates substantially faster than the rates of HP2 opening (Figure 3.9A/E). The kinetics of the NMDGT conformational switch are also faster than HP2 opening on Na^+ binding, all indicating that HP2 opening is the rate limiting step in the Na^+ binding step of the coupling mechanism (Figure 3.9C/D). By plotting the rates versus their respective Na^+ concentrations, it is apparent that with increasing concentrations both NMDGT rearrangements and HP2 opening occur at faster rates. These results are consistent with an induced fit- mechanism wherein Na^+ binding causes the conformational switch in the NMDGT motif (Figure 3.9D/F)(228). Both NMDGT rearrangements and HP2 opening are Na^+ induced conformational changes.

We have previously reported that in the R397A mutant, HP2 opening takes place at a faster rate compared to the wild type control, while HP2 opening takes place at a slower rate in the T314A mutant. We measured the rate of Na^+ binding to the R394A and the T314A mutant and observed similar rates of Na^+ binding comparable to the rates of Na+ binding to the wild type transporter (Figure 3.9B). The differences in the rate of HP2 opening in the R397A and the T314A mutants therefore do not arise from differences in

the Na^+ binding kinetics but from the subsequent steps involved in transducing Na^+ binding to HP2 opening. These data further support HP2 opening in an induced fit mechanism instead of conformation selection mechanism. The kinetics data for different steps of the coupling process confirm steps in the WT process (Figure 3.9G). With the kinetics data along with our Na^+ site perturbation data, we can generate a molecular mechanism for the conformational wave proceeding Na^+ binding to Na1 and Na3 sites.

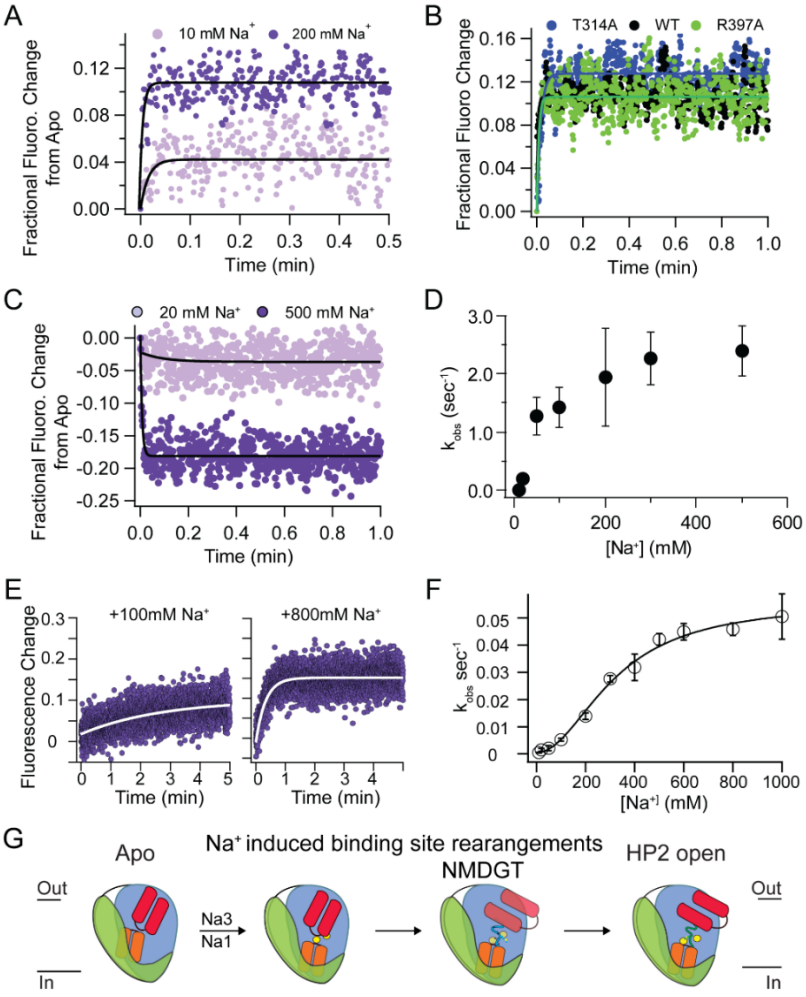

Figure 3.9. Interrogation of the coupled binding process through kinetics measurements with novel assays A) Kinetics after low and high Na^+ addition using the same excitation and emission wavelengths as steady state titrations (k_{obs} 10 mM 1.08 sec^{-1} and 200 mM 2.47 sec^{-1}) **B)** Kinetics of Na^+ binding for T314A, WT, R397A at [Na^+] 5x K_D (T314A at 600 mM Na^+, WT at 200 mM Na^+, R397 at 50 mM Na^+ **C)** L99W-Glt_{Ph} Kinetics time course at high and low Na^+ (k_{obs}: 20 mM is 0.2 sec^{-1} and at 500 mM is 2.4 sec^{-1} using the same excitation and emission wavelengths as steady state titrations **D)** Plot of rates collected at different Na^+ concentrations for L99W-Glt_{Ph}. Error bars are S.E.M. with N ≥ 3

E-F) Replotted kinetics data from HP2 opening in Chapter 2 **G)** Binding scheme with Na^+ induced changes for the WT coupling process.

Discussion:

Coupled, sequential binding is a key component in the transport mechanism of glutamate transporters. In the allosteric mechanism for coupled binding, the binding of two Na^+ ions to the Na1 and Na3 sites make the protein competent to bind substrate. An unresolved component of the coupling process was the conformational consequences of binding to each of the two Na^+ sites preceding substrate binding. To address this gap in our understanding, we interrogated the role of each Na^+ site by perturbing the Na3 and Na1 sites individually and studying the functional consequences on the different steps in the coupling process. Our developed fluorescence-based assays allow for the beginning of the process, Na^+ binding (tyrosine-based assay), as well as the key subsequent Na^+ dependent changes in the NMDGT motif (L99W- Glt_{Ph}) and the extracellular gate to be probed (HP2 movement assay). These assays also enabled the collection of kinetics data for these different steps to confirm that Na^+ binding induces the NMDGT conformational switch as well as HP2 opening. Through the collective data on the WT process and the effect of Na^+ site perturbations, we demonstrate that binding to the Na1 and Na3 sites have different roles in priming the protein for substrate binding and that binding to both Na^+ sites is essential for full HP2 opening and high affinity substrate binding.

We provide evidence that Na3 binding is necessary for both NMDGT rearrangements and full HP2 opening. The differing effects of non-conservative substitutions at the Na3 site also revealed an additional role of one of the Na3 coordinating residues, S93. When Na^+ binds to the Na3 site and switches the M311 side chain into the flipped conformation, the S93 and the M311 side chains have a steric interaction. M311 flipped conformation is key for keeping HP2 open on Na^+ binding and

this steric regulation of M311 positioning provides a means by which Na^+ binding to the Na3 site is transduced to opening HP2 for substrate binding. We were able to attribute the functional consequences of D405N substitution to Na1 binding by exploiting the Na3 induced movement of M311. By pairing D405N substitution with M311A, we established that the conformational changes corresponding to the binding of Na^+ to the Na3 site are not involved in HP2 opening in the Apo-D405N transporter. Therefore, the conformational consequences of binding to the Na1 site consist of disruptions to the Apo H-bond network, in which D405, Y89, and N401 participate, to accomplish partial HP2 opening while binding to the Na3 site causes the NMDGT conformational switch which couples Na^+ binding at the Na3 site and HP2 opening.

We herein propose a molecular mechanism for how Na^+ binding to the Na1 and Na3 site accomplishes HP2 opening and high affinity substate binding (Figure 3.10). First, Na1 binds to the Apo transporter where HP2 is predominantly closed. Na1 binding disrupts the Apo H-bond network by breaking interactions between D405 and Y89/N310 as well as interactions between the side chain of N401 and G313 of the NMDGT. We posit these disruptions are transduced to alter the Apo position of R397 which leads to partial HP2 opening and low affinity substrate binding. Na3 then binds and causes NMDGT rearrangements necessary to coordinate Na^+ and fully open HP2. These rearrangements including the previously established M311 repositioning towards the binding site to act as a wedge and T314 moving towards the binding site to help position R397 out of the binding site. Our data with various MD simulations support Na1 binding first, proceeded by binding to the Na3 site through Na1 site pathway or an alternative pathway revealed in the Na1 bound state (203, 215, 217, 222). Na3 induced changes are stabilized by the Na1 site coordination through N401-T314 side chains interactions and N310 backbone carbonyl interactions with Na1. Both Na1 and Na3 binding are necessary for full HP2 opening and high affinity substrate binding. Our mechanism

allows for a mix of two Asp binding modes to take place, Na1/Asp/Na3 and Na1/Na3/Asp. These simultaneous pathways to fully load the transporter explain how substrate can bind at low Na^+ concentrations, the dependence on Na^+ for substrate binding, and how the presence of substrate can increase Na^+ affinity.

The same key residues which have been identified in the Na^+ induced conformational wave are conserved across EAATs and therefore, our newfound understanding of the coupling process in Glt_{Ph} can be applied to EAATs. Another indication that our findings are applicable to EAATs is the fact that these key conserved players have similar secondary structure placement since we now have several structures of human SLC1 members including the substrate and ion binding sites. By comparing Glt_{Ph} and EAATs, we can also understand differences in transport between Glt_{Ph} and EAATs, such as the differences in functional consequences of D405N substitution. With in-depth mechanistic studies such as these along with MD simulations and new human transporter structures, we can fully understand how these transporters couple ions and substrate to accomplish their function.

Figure 3.10. Proposed mechanism for coupled binding required for successful substrate translocation. Na^+ binds to the Na1 site and disrupts the Apo H-bond network which maintains the Apo state. The disruption is enough to allow for partial HP2 opening, potentially through alteration of the Apo-R397A positioning. With HP2 partially open in the Na1 bound state, either Asp can bind at low affinity and cause partial HP2 closure or Na3 binds. Na3 can bind via the Na1 pathway or through an alternative path which is revealed upon Na1 based HP2 opening. The Na1/Na3 bound state has HP2 in the fully open state as well as full binding site rearrangements which support high substrate affinity binding. If Asp binds after Na1, Na3 can subsequently bind and fully close HP2 and if Na3 binds after Na1, the protein can bind Asp. Substrate binding causes HP2 closure which is stabilized through Na2 binding. Substrate translocation can take place with full $3Na^+$:1Asp. Trimerization domain of a protomer is represented as a green box while the transport domain is represented by the blue colored shape. HP2 is shown in red, Asp as the green sphere, and sodium ions as yellow spheres. Insets of binding site conformations are generated from Apo Glt_{Tk} pdb 5dwy shown in cyan and Na^+ bound from Glt_{Ph} pdb 7ahk shown in yellow. Figure on the following page.

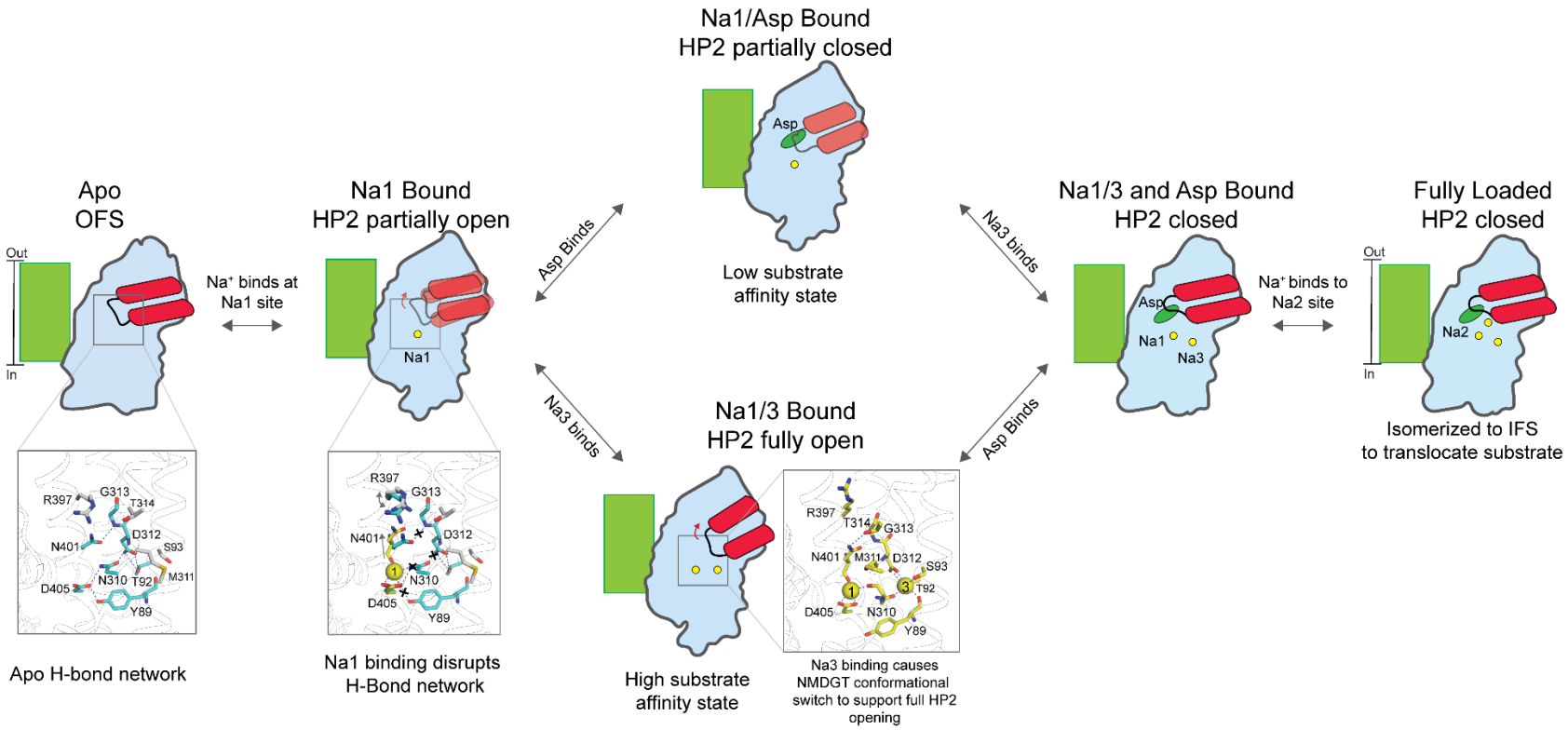
Apo
OFS
Out
In
Na⁺ binds at
Na1 site
Na1 Bound
HP2 partially open
Na1
Asp Binds
Na3 binds
Na1/Asp Bound
HP2 partially closed
Asp
Low substrate
affinity state
Na3 binds
Asp Binds
Na1/3 Bound
HP2 fully open
High substrate
affinity state
Na1/3 and Asp Bound
HP2 closed
Asp
Na1
Na3
Na⁺ binds to
Na2 site
Fully Loaded
HP2 closed
Na2
Isomerized to IFS
to translocate substrate
R397
G313
T314
D312
N401
S93
N310
T92
M311
D405
Y89
Apo H-bond network
Na1 binding disrupts
H-Bond network
Na3 binding causes
NMDGT conformational
switch to support full HP2
opening

Acknowledgements: This research was supported by NIH Grants R01GM087546, R21NS113561 (to F.I.V) and R37NS085318 (to Dr. Olga Boudker, Principal Investigator and F.I.V., Coinvestigator). E.A.R. was supported by a Predoctoral Fellowship from the American Heart Association (AHA 19PRE34380950). We thank Dr. Eric Gouaux for access to the ITC, Dr Vikas Navratna for his generous training in how to use the ITC, and Dr. Pierre Moenne-Loccoz for access to the EPR and training.

Methods:

Expression and purification of Glt_{Ph}. The Glt_{Ph} construct referred to as wild type consisted of seven point mutations to histidine(149), a C321A substitution (unless otherwise specified), a His_8 tag at the C-terminus and any additional substitutions required for the specific assay. Site directed mutagenesis was carried out using the PCR overlap or Quickchange mutagenesis protocols. The Glt_{Ph} constructs were cloned and expressed from the pBCH/G4 vector (kindly provided by Dr. Eric Gouaux) in *Escherichia coli* TOP10 cells (Fisher Scientific).(149) Protein expression and membrane preparation was carried out as previously described.(155) The membrane vesicles were solubilized using dodecyl-β-D-maltopyranoside [DDM, 2% (w/v)] and the Glt_{Ph} protein purified by affinity chromatography (Ni NTA resin, Qiagen). The protein was concentrated using an Amicon filter with a 100kDa cutoff and extensively washed with SEC buffer to ensure Na^+ concentration was under 1 mM. The Glt_{Ph} protein was further purified by size exclusion chromatography (SEC) on a Superdex S-200 column (GE Biosciences) using 20 mM Tris-HEPES pH 7.5, 100 mM KCl, and 0.1% DDM as the column buffer.(155) Unnatural amino incorporation for the HP2 movement assay was accomplished by *in vivo* nonsense suppression using the Phe_{CN} tRNA synthetase/tRNA pair for *Escherichia coli* expression. The expression methods used are the same as Chapter 2 except for the addition of 1 mM Phe_{CN} to the growth media instead of 2 mM.

Fluorescence assays: All assays were carried out in 20 mM Tris-HEPES pH 7.5, 200 mM Choline chloride, and 0.1% DDM except for the dye-based Na^+ binding assay.

Tyr-based Na^+ binding assay. Assays were carried out with ~ 40 ugs of Glt_{Ph} in choline buffer,at 30 °C, with 1 min incubation time periods in between Na^+ additions. Fluorescence was monitored at 308 nm after excitation at 289 nm. Data was plotted as fractional fluorescence change from Apo and fit to the hill equation (Equation 1).

$$F = \frac{[Na]^n}{[K_{0.5}^{Na}]^n + [Na]^n} \qquad \textit{Equation 1}$$

The reported K_D values and hill coefficients are an average of individually fitted single titrations.

NMDGT conformational switch assay. Assays were carried with ~80 ugs of Glt_{Ph} in choline buffer at 30 °C, with 1 min incubation time periods in between Na^+ additions. Fluorescence was monitored at 324 nm after excitation at 295 nm. Data was plotted as fractional fluorescence change from Apo and fit to the hill equation (Equation 1). The titration data in Na^+ alone was normalized to the maximal fluorescence response observed for Na^+ titrations in the presence of 100 μM Asp.

HP2 movement assay. Assays were carried out and analyzed in the same manner as presented in Chapter 2 except for longer incubation times in between assay points and choline chloride as the assay buffer instead of KCl. The closure titrations were carried out in the same manner as Chapter 2 but analyzed through change in fluorescence instead of fraction bound normalization.

Kinetics measurements for Na^+ binding and NMDGT conformational shift. Assays were carried out in choline buffer, at 30 °C, with the same amounts of protein as steady state titrations. A stable fluorescence signal from the protein was established before addition of Na^+. Fluorescence was monitored and collected at a single wavelength with 0.1 sec integration. Kinetic experiments carried out with a final Na^+ concentrations above 50 mM were corrected for dilution by subtraction of a kinetics experiment with equivalent K^+ additions carried out in parallel.

Dye-based Na^+ binding assay was carried out as described in Chapter 2.

***ITC*.** Proteins were generated and purified in the same manner as outlined above until after the affinity purification. For ITC experiments, the His tag was cleaved before running on the SEC in KCl buffer with a lower DDM concentration. The DDM concentration was reduced to 0.4 mM DDM. After SEC, the proteins were diluted to 15-40 µM concentrations in the respective assay buffer (20 mM Tris-HEPES pH 7.5, 100 mM KCl, 0.4 mM DDM or 20 mM Tris-HEPES pH 7.5, 90 mM KCl, 10 mM NaCl, 0.4 mM DDM) and tested for Asp binding immediately. The titrant solution with Asp was made in the corresponding assay buffer with or without 10 mM Na^+. The experiments were carried out at 25 °C in a small volume MicroCal iTC200 (Malvern Panalytical). Data was analyzed using MicroCal origin-based software and an independent-binding site model. Generally followed principles and parameters outlined in (202, 235).

EPR. *Spin Labeling.* The double cysteine mutants (V355C/S279C or V355C/S279C/D405N) were expressed and purified as outlined above until after the affinity purification step. Following affinity chromatography, the protein was incubated for 30 min with 500 µM tris(2-carboxyethyl)phosphine (TCEP, from Gold Biotechnology) at room temperature. The protein was then concentrated using an Amicon filter with 100kDa cut off and washed with 20 mM Tris-HEPES pH 7.5, 50 mM NaCl, 0.1% DDM for removal of TCEP and imidazole. The protein concentrations were then determined and spin probe, 1-oxyl-2,2,5,5-tetramethyl-AE3-pyrrolin-3-yl methyl methanethiosulfonate (MTSL, from Toronto Research Chemicals) was added at a 10:1 spin label:protein ratio (mol/mol). The labeling reaction was allowed to proceed at room temperature for 30 min before continuing at 4 °C overnight. The labeled protein was separated from free label through SEC and a subsequent concentration step with an Amicon filter with a 100kDa cut off. Protein was immediately tested at roughly 100 µM after incubation with the respective ligands. *Collecting CW-EPR spectra*. Data was

collected and analyzed following (208). Briefly, continuous wave EPR spectra were collected at room temperature on a Bruker E500-X band EPR spectrometer equipped with a superX microwave bridge and an ER4123D dielectric resonator (Bruker Biospin). Samples were loaded into TPX capillaries (Bruker Biospin) and constantly flushed with N_2. The microwave frequency was 9.78 GHz, microwave power of 2mW, modulation frequency of 100 kHz, and modulation amplitude of 2G. *EPR spectra analysis.* Spectra were baseline subtracted and double integrated to determine the number of spin probes present in each experiment. Spectra were normalized to the spin number for comparison between conditions. Relative amplitudes were determined by subtracting the central peak minima from the maxima.

Aspartate transport Assays. Glt_{Ph} was reconstituted into lipid vesicles comprised of a 3: 1 ratio of *E.coli* polar lipids to POPC as previously described.(151) The transport assays were carried out in 20 mM Tris-HEPES pH 7.5, 200 mM NaCl, 1 µM valinomycin at 30 ^{o}C as previously described.(155) 100 nM of ^{14}C Asp (Moravek Biochemicals) was used for transport assays and background levels of Asp transport were determined by performing the transport assay in absence of NaCl, with 100 mM KCl in the assay buffer.

Appendix B: Supplementary Information

Table S3.1. Na^+ binding affinities using tyrosine-based assay for Na^+ coordinator mutants.

Site		K_D (mM)	Hill Coefficient
	WT	44.7 ±11	1.1 ±0.2
	S93A	> 300	> 2
	S93C*	304 ± 22	2.2 ± 0.2
	S93T	26 ± 1.2	1.1 ± 0.1
Na3	T92C	139 ± 62	1 ± 0.4
	T92S	14 ± 2.8	1.3 ±0.1
	N310S	171± 32	1 ± 0.2
	N310D	179 ± 22	1.3 ± 0.3
	D312N	123 ± 11	1.1 ±0.2
Na1	D405N	214 ± 18	1.7± 0.2

(*) S93C did not saturate well so K_D is approximate. Errors are S.E.M. and N ≥ 3.

A

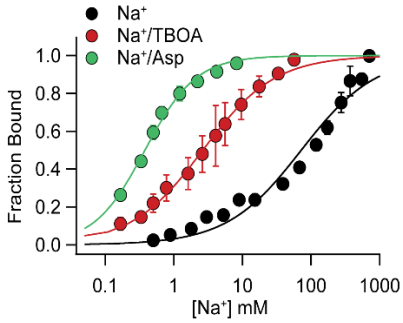

B

Site	Substitution	K_D (mM)	Fold Change from WT Dye	Fold Change from WT Tyr	K_D (mM) +1 mM Asp
	WT	72 ± 10			0.4 ± 0.02
	S93A	352 ± 40	4	~6 *	3.9 ± 0.2
Na3	T92C	237 ± 24	3	3	2.5 ± 0.2
	N310S	279 ± 17	3	3	2.5 ± 0.1
	D312N	234 ± 19	3	2	1.3 ± 0.1
Na1	D405N	224 ± 28	3	4	1.6± 0.1

Figure S3.1. **Na^+ affinity data using established dye-based assay for select Na^+ site mutants A)** Steady state Na^+ binding data for different ligand conditions (Na^+, Na^+/10 μM TBOA and Na^+/1 mM Asp) **B)** Table of Na^+ affinities for select mutants in the dye-based assay as well as fold changes to compare with the tyrosine-based assay, (*) S93A never saturated so fold change of affinity is a rough estimation. Errors are S.E.M. for both A and B and N ≥ 3.

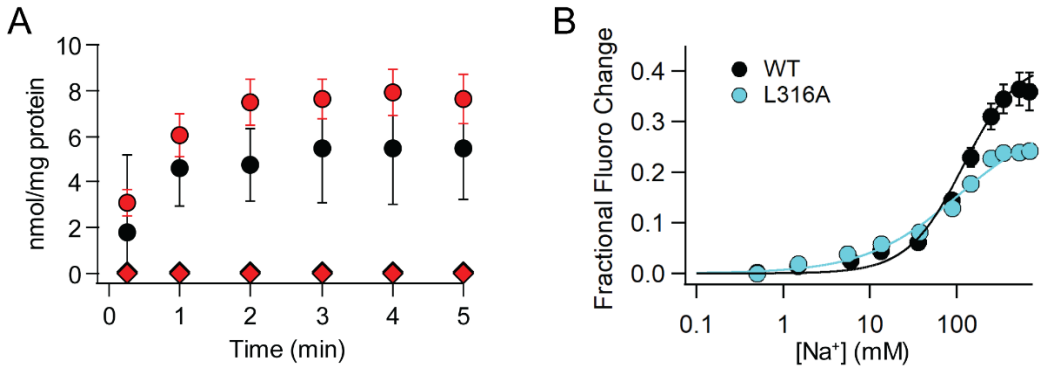

Figure S3.2. **Further characterization of the L99W-Glt_{Ph} construct and control experiments A)** Time course of [^{14}C] L-Asp uptake for WT-Glt_{Ph} (black) and L99W-Glt_{Ph} (red) in the presence of 200 mM Na^+ (circles) and no gradient, 100 mM KCl (diamonds). L99W-Glt_{Ph} in the presence of Na^+ error bars are S.E.M. and sample size of 3 while the other three conditions are from a sample of two and bars are the difference between the two experiments **B)** Confirmed function of L316A in the HP2 movement assay ($K_{0.5}^{Na}$ L316A: 106 ± 45 mM). All error bars are S.E.M. and N ≥ 3.

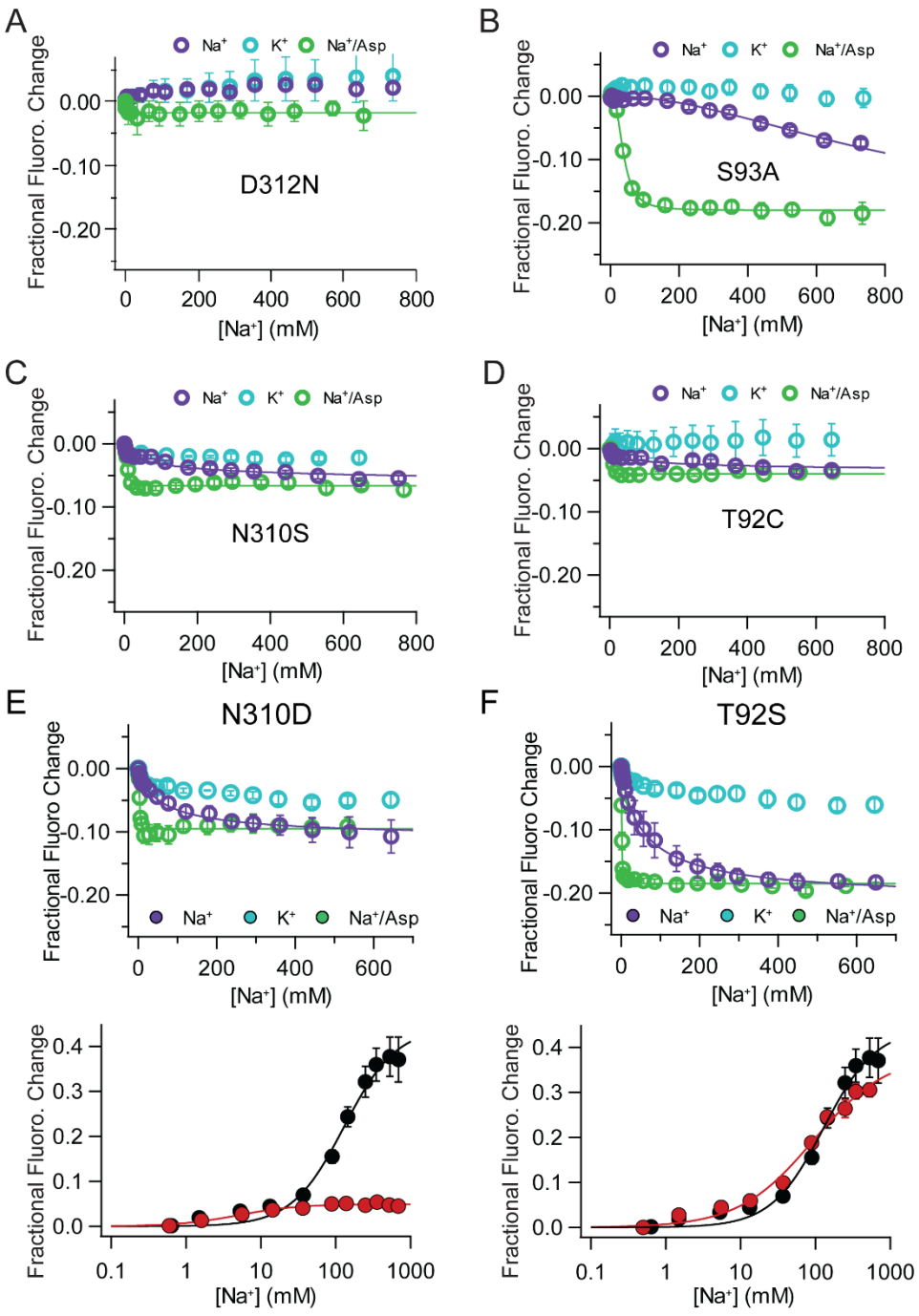

G

	NMDGT Movement						HP2 Movement
	Na+			Na+/Asp			Opening
	K_{nmdgt} (mM)	Hill Coefficient	% Change	K_{nmdgt} (mM)	Hill Coefficient	% Change	% Change
WT	*172 ± 6*	1.1 ± 0.05	21	*2 ± 0.06*	2.2 ± 0.1	23	36
S93A	*804 ± 15*	2 ± 0.1	12	*38 ± 1.1*	2.6 ± 0.2	18	13
T92C	*102 ± 23*	0.6 ± 0.1	4	*8.2 ± 0.4*	3 ± 0.4	4	11
T92S	*60 ± 4.4*	0.9 ± 0.04	18	*1.5 ± 0.06*	1.8 ± 0.1	19	31
N310S	*108 ± 14*	0.6 ± 0.05	5	*7.7 ± 0.6*	2.4 ± 0.4	6.6	3
N310D	*64 ± 5*	0.9 ± 0.05	11	*3.1 ± 0.3*	2.8 ± 0.6	10	5
D312N		no change		*1.8 ± 0.7*	1.3 ± 0.7	2	5

Figure S3.3. Steady state titration data for Na3 site substitutions in the NMDGT conformational switch assay (A-F) with additional mutants as well as HP2 movement data for the other N310 and T92 substitutions **(E-F). G)** Summary table of apparent affinities and the fluorescence changes from Apo. Error bars are S.E.M. and N ≥ 3.

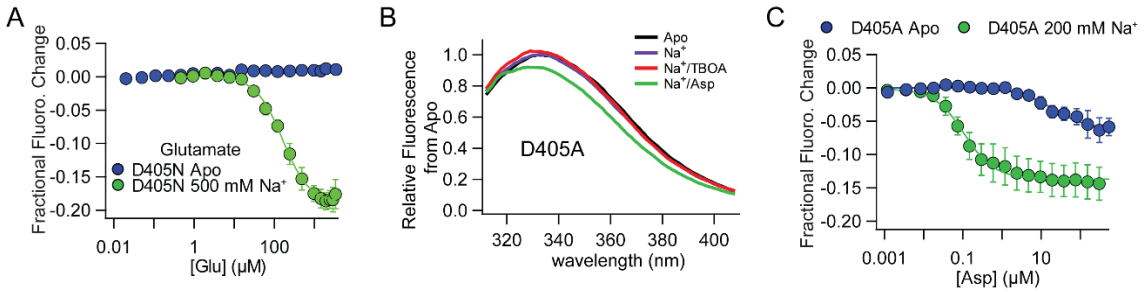

Figure S3.4. Probing HP2 opening in D405X substitutions A) D405N in the HP2 movement background titrating glutamate with and without Na^+ present ($K_{0.5}^{Glu}$ D405N Na^+: 161 ± 9 μM) **B)** Emission spectra for D405A to show similar phenotype to D405N in the HP2 movement assay using the same ligand conditions **C)** Steady state closure data for Asp and D405A with and without Na^+ present in the HP2 movement assay ($K_{0.5}^{Asp}$ D405A Na^+: 84 ± 2 nM, D405A Apo: 19.8 ± 6 μM). All error bars are S.E.M. and N ≥ 3.

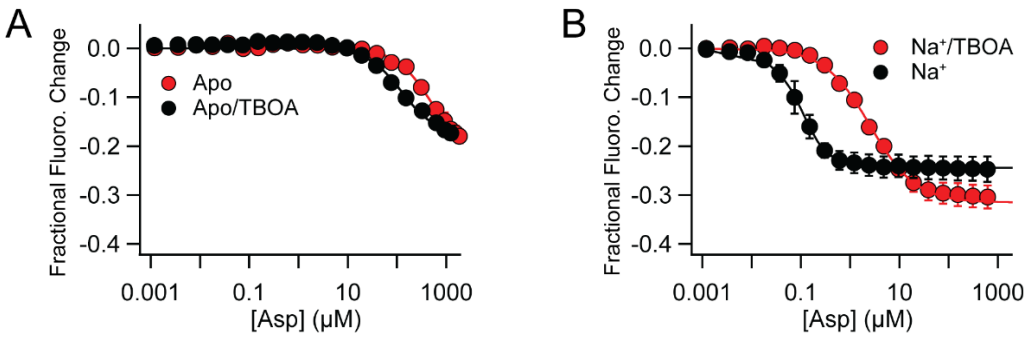

Figure S3.5. Confirmation that D405N does bind TBOA A) Steady state HP2 closure titrations with Asp and no Na^+ with or without 100 μM TBOA present (~3x difference in affinity) ($K_{0.5}^{Asp}$ No TBOA: 124 ± 1.2 μM, With TBOA: 473 ± 74 μM) **B)** Steady state HP2 closure titrations with Asp and 200 mM Na^+ with or without 100 μM TBOA present (~69x difference in affinity) ($K_{0.5}^{Asp}$ No TBOA: 33 ± 2 nM, With TBOA: 2.3 ± 0.08 μM). All error bars are S.E.M. and N ≥ 3.

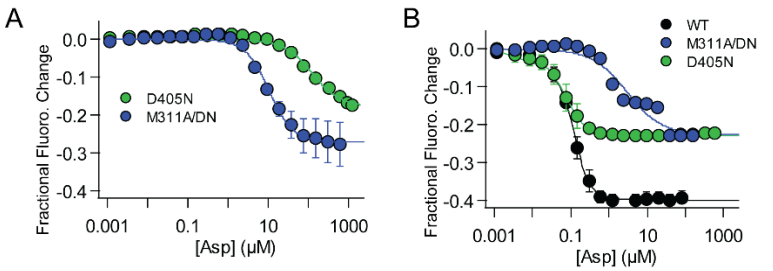

	Apo K_D (μM)	+500 mM Na^+ K_D (μM)
WT	——	0.017
D405N	124	0.02
M311A/ D405N	11	2.9

Figure S3.6. Evidence for D405N reflecting Na1 binding consequences. Double mutant analysis of D405N with M311A in the HP2 movement assay **A)** Steady state closure experiments by titration Asp in the absence of Na^+ **B)** Steady state closure experiments by titration Asp in the presence of 500 mM Na^+ **C)** Apparent affinity values of both sets of HP2 closure experiments for D405N and D405N/M311A Glt_{Ph}. Error bars are S.E.M. from N ≥ 3.

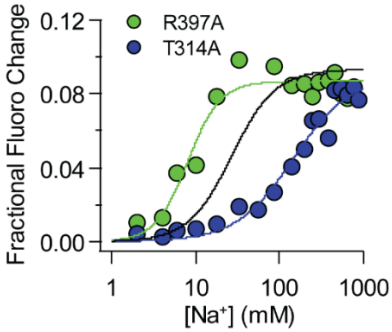

Figure S3.7. Steady state Na^+ binding data for R397A and T314A in the tyrosine-based assay. The affinity for R397A was around 8.1 ± 0.9 mM so ~5x the K_D is 50 mM Na^+. The affinity for T314A was around 146 ± 12 mM so ~5x the K_D is 600 mM Na^+.

Appendix C: Substrate binding and HP2 Closure

The experiments in this appendix were planned by E.A.R. and F.I.V, E.A.R collected all the data, and E.A.R wrote the appendix with input from F.I.V

Introduction and Rationale:

The SLC1 family consists of two distinct clusters based on substrate selectivity: the EAATs which transport glutamate, aspartate, and cysteine (9, 10, 61, 93) and ASCTs which transport neutral amino acids such as alanine, serine, threonine, and glutamine (4, 11, 49, 94, 95). ASCT1 and 2 are ubiquitously expressed throughout the body and can be found in lung, intestine, kidney, skeletal muscle, and brain(11, 49, 50, 54, 59). ASCT2 has been shown to be upregulated across many cancer types such as breast(87), gastric(88), esophageal(89), prostate(90), and more. The upregulation of this transporter in cancer predominately stems from a switch in metabolism in which cells rely on glutamine and glycolysis for energy known as the Warburg Effect(91, 92, 236). Due to its role in cancer cell nutrient acquisition, ASCT2 has been identified as an important therapeutic target. Therefore, there is a drive for selective inhibitors as therapeutics and academic tools. To aid in structurally guided drug design, an understanding of the structure activity relationship between substrate and transporter is necessary.

To establish a structure activity relationship for SLC1 family and gain an in depth understanding of substrate binding, we use Glt_{Ph} as a model system. We have a variety of functional assays to assess substrate binding in Glt_{Ph} and key components of transport are conserved between the family members. The binding site for substrate is similar in the SLC1 family, only differing in a few coordinating residues which determine substrate selectivity (Figure C1A/B). Both ASCT2 and Glt_{Ph} have Na^+ dependent substrate transport where one molecule of substrate is coupled with three Na^+ ions in the

forward direction (96, 97, 151, 152). The proposed order of binding is also the similar in which two Na^+ ions bind first to cause conformational changes in the binding site and HP2 to allow for substrate binding, followed by HP2 closure and the final Na^+ ion binding after substrate binding (Figure C.1C). ASCTs are exchangers and therefore differ in their transport mode compared to EAATs and Glt_{Ph}. Essentially, to resume the OFS state and complete the transport cycles, ASCTs require three Na^+ ions and one molecule of substrate while Glt_{Ph} doesn't require any ligands to transition from IFS to OFS. In Glt_{Ph}, Asp binding assays and indirect methods consistently show a stoichiometry of at least one coupled Na^+ ion to substrate binding (150, 152, 164, 217).

Recently, other papers and our D405N data suggest that Asp can bind with only Na1 ion bound in Glt_{Ph} (150, 217, 231). This led to suggesting a combination of two binding modes: one in which Asp binds after Na1 followed by Na3 and one in which Asp binds after both Na1 and Na3. This potential mix of binding modes helps explain the ability of transporter to bind substrate at low Na^+ and Asp's ability to increase Na^+ binding affinity. Along the coupling process, we have been able to identify key conformational changes which occur from binding at the Na3 and Na1 sites including changes necessary for HP2 to open for substrate binding (Figure C.1C). A remaining gap in our mechanism is the second arm of this process, namely how HP2 is closed. The molecular mechanism of how HP2 is closed is poorly resolved with the main body of information coming from MD studies(170, 201, 213).

Using our innovative, real-time assay, we can monitor HP2 closure as a function of substrate properties. By specifically perturbing protein-substrate interactions, we can gain insight into which interactions and substrate properties are necessary. Pervious chapters have outlined how HP2 opening is accomplished in the coupling mechanism. By probing substrate binding with our HP2 movement assay, we can also gain insight into how substrate assisted HP2 closure is accomplished. In this appendix, we present

preliminary data which suggest substrate backbone interactions are essential for HP2 closure and varying the substrate side chain chemistry results in varied extents of HP2 closure. These data do not encompass the full process and further experiments are necessary to complete this story.

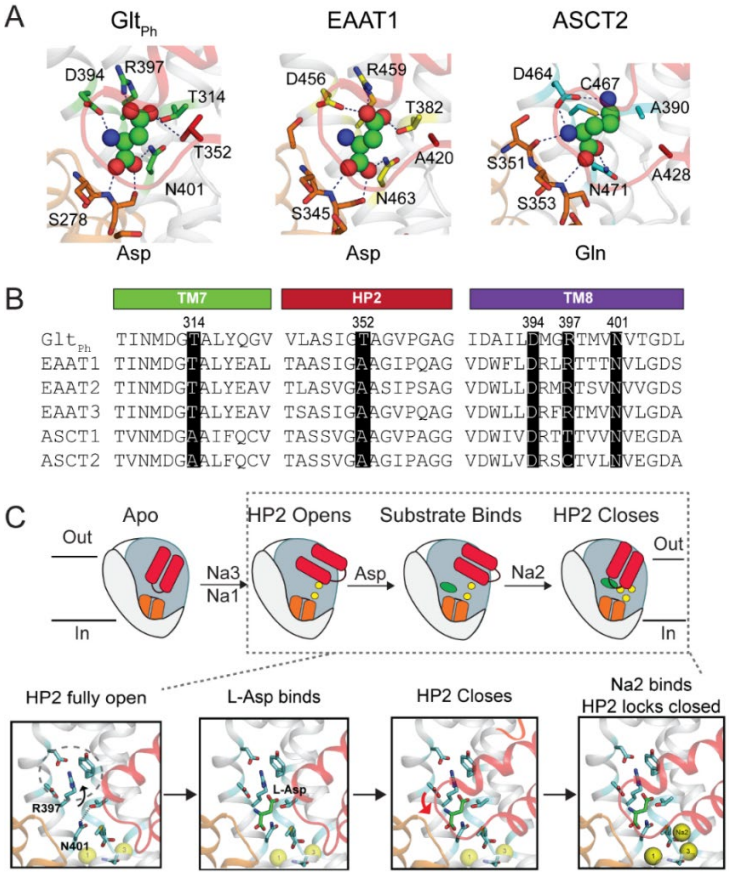

Figure C1. Binding site for substrate and involvement in the coupling mechanism A) Binding sites of substrate. Glt_{Ph} is actually Glt_{Tk} pdb 5e9s with Glt_{Ph} numbering, EAAT1 is pdb 5llu and ASCT2 is pdb 6mpb **B)** Sequence alignment of SLC1A family members with residues involved in substrate coordination highlighted(237). Not shown in the sequence alignment is S278 which is a serine in the other SLC1A family members **C)** Proposed scheme for sequential binding, the box highlights the part of the coupling mechanism to focus on, Asp binding and substrate assisted closure of HP2. The close up reflects some of the molecular choreography of the binding site and HP2 movement.

Results:

All residues which coordinate substrate in the binding pocket are necessary for high affinity substrate binding and full HP2 closure

Our first approach to perturb the Asp binding site was through protein substitutions at the coordinating residues. From structures, we know the coordination

sphere for substrate involves several residues in the core of the transport domain including R397 and T314 to coordinate the sidechain and D394 and N401 to coordinate the backbone (Figure C.1A). We have previously shown that repositioning of R397, T314, and N401 upon Na^+ binding is part of the HP2 opening process. One of the most readily accessible methods to assess substrate binding for Glt_{Ph} is a fluorescence-based assay utilizing a Trp substitution at L130. The assay has been used to probe substrate specificity and affinity while providing further evidence that Asp binding is coupled to two Na^+ ions (Figure C.2A/B)(150). We substituted an Ala at each of the substrate coordinating residues and using the L130W assay confirmed that these substitutions result in a decrease in Asp affinity (Figure C.2C). D394A shows a larger decrease in ability to bind substrate compared to R397A and T314A, indicating a difference between residues which coordinate the side chain or the backbone of the substrate. N401A substitution in the L130W assay did not give reasonable signal changes to indicate substate binding. The preliminary evidence for S278A decreasing Asp affinity also support a role for HP1 serine residues in substate binding.

These substitutions were tested in the construct of the HP2 movement assay. Data was collected for substrate binding/HP2 closure at 200 mM Na^+ for R397A, T314A, and D394A (Figure C.2D). All three substitutions resulted in decreased Asp affinity and showed different extents of fluorescence change (Figure C.2D). Surprisingly D394A showed no decrease in fluorescence to indicate HP2 closure and instead, there was a small increase in fluorescence after 100 μM Asp. The increase in fluorescence seen with substrate addition is either due to a nonspecific fluorescence effect or Asp affinity is so shifted that it can enter the binding site but not form the proper interactions to close HP2 in our assay background. The ability to bind Asp can be further assessed in the D394A mutant through ITC to help resolve the HP2 closure data. It is also possible that D394 itself is required for full HP2 closure irrespective of its coordination of substrate and the

difference seen in Asp binding between L130W and HP2 movement assays stem from monitoring different events. The mechanistic basis for the L130W fluorescence change is unresolved. Overall, these data are consistent with substrate backbone-protein interactions being essential for substrate binding and HP2 closure. If Asp cannot be properly coordinated in the binding site and form the necessary interactions, then HP2 cannot close which is consistent with substrate assisted closure.

The overall signal change upon Asp titration in the HP2 assay is potentially a composite of different factors: the extent of HP2 opening, how well the substrate is situated in the binding site, and extent of HP2 closure. To better interpret HP2 closure data for residues which coordinate the substrate, we must also incorporate their HP2 opening data (Figure C.2E/F). R397A drastically decreases substate binding affinity, but at first glance has a WT-like extent of closure. When closure data is considered within the context of HP2 opening, R397A does not reach the same extent of closure as WT (Figure C.2F). Without R397, Asp affinity is greatly decreased and most likely HP2 does not fully close. T314A is the most WT-like in terms of affinity and extent of closure compared to the other substrate coordinator substitutions even though both substrate affinity and extent of HP2 closure are decreased. Our data is consistent with HP2 closure being a composite of several factors. Since some substrate coordinators also participate in HP2 opening, comparing the Asp induced HP2 closure data across protein substitutions does not offer direct conclusions on the protein-substrate interactions.

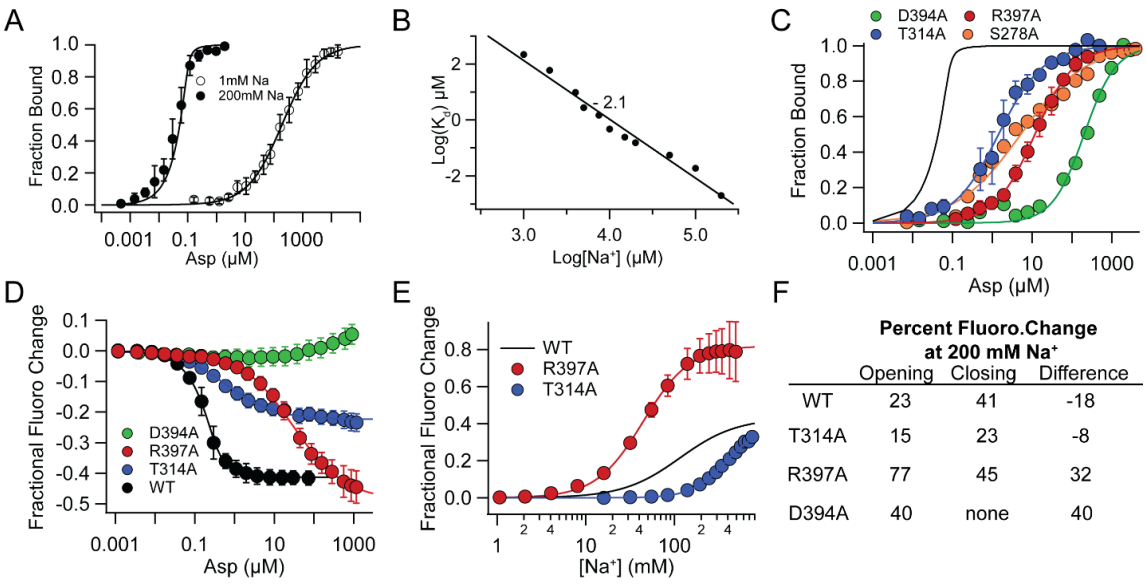

Figure C2. Binding site perturbation through substitutions to substrate coordinators. A) Asp binding at high and low Na^+ using an assay with a Trp substitution at L130 demonstrating affinity dependence of Asp on [Na^+] **B)** Overall coupling of Asp binding is to 2 Na^+ ions indicated by the slope of the log[Na^+] vs logK_d **C)** Steady state L130W Asp titrations for binding site mutants at 200 mM Na^+, black line is WT ($K_{0.5}^{Asp}$: WT 0.0018 ± 0.000 μM, T314A 1.5 ± 0.1 μM, S278A 5.2 ± 0.7 μM, R397A 11.8 ± 0.7 μM, D394A 199 ± 19 μM). All data is from N ≥ 3 except S278A which is from N = 2. **D)** Steady state Asp titrations of the binding site mutants in the HP2 movement assay in 200 mM Na^+ ($K_{0.5}^{Asp}$: WT 0.042 ± 0.007 μM, T314A 2.2 ± 0.2 μM, R397A 11.8 ± 0.7 μM, D394A no binding) **E)** HP2 opening titrations of two binding site mutants R397A and T314A to illustrate different fluorescence changes for extent of opening, black line is WT(data from Chapter 2) **F)** Table of HP2 fluorescence changes in the HP2 movement assay upon addition of 200 mM Na^+ and saturating Asp concentrations. HP2 opening is from Apo to Na^+ and HP2 closure is the signal from Na^+ to Na^+/Asp. All error bars are S.E.M. and N ≥ 3.

Probing the cause in varied extents of change upon substrate binding in the HP2 movement assay

One of the hallmarks of coupled substrate binding is the improvement of affinity with increased Na^+ (Figure C.2A/B). Since we are interested in substrate assisted HP2 closure, we wanted to further characterize HP2 closure for WT-Glt_{Ph} observed in our HP2 movement assay. Like other methods which measure Asp binding, the HP2 movement assay shows improved Asp affinity with increasing Na^+ concentrations (Figure C.3A). The affinities obtained, although slightly decreased compared to the L130W assay, fall within an acceptable range of values across Na^+ concentrations.

Along with differences in substrate affinity, there are differences in the magnitude of fluorescence signal change observed at different Na^+ concentrations. As posited earlier, the overall signal change in the HP2 movement Asp titrations is a composite of the extent of HP2 opening, how well the substrate is situated in the binding site, and HP2 closure. If this holds true, a lower extent of HP2 opening results in a corresponding lower fluorescence change for HP2 closure upon Asp binding. Also, if the substrate is not properly situated in the binding site, then there would also be a corresponding lower signal change for HP2 closure. These conclusions are further supported when comparing HP2 closure at low and high Na^+ with and without the Asp analogue TBOA present. Normally, the addition of TBOA in the presence of Na^+ results in HP2 being propped open and the maximal fluorescence change for HP2 opening. If the extent of HP2 opening is indeed an important component in HP2 closure titrations, then having TBOA present at different Na^+ concentrations should lead to similar extents of change. When TBOA is present in low Na^+ closure titrations, the extent of fluorescence change is increased to similar levels as high Na^+ (Figure C.3B). At high Na^+, the additional increase in fluorescence from the presence of TBOA is minimal in comparison (Figure C.3C). These data also indicate that different Na^+ concentrations result in different extents of HP2 opening with corresponding differences in the substrate binding site (different substrate binding affinities). The complexity of factors which contribute to HP2 closure confirms that determining causation relationships from comparisons between protein substitutions is nontrivial.

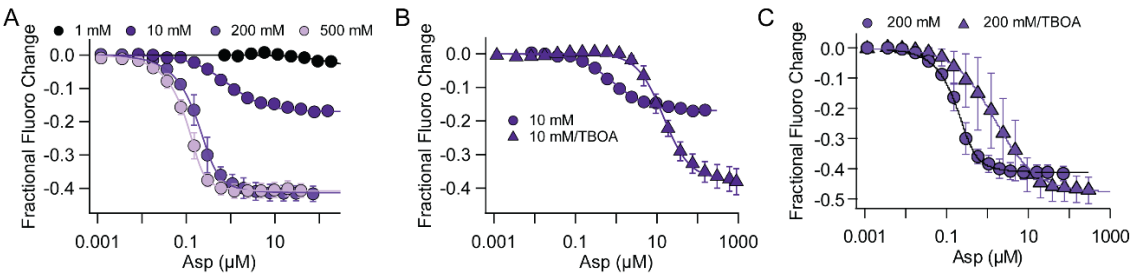

Figure C3. Properties of WT HP2 closure upon substrate binding A) WT steady state titration of Asp binding at different Na^+ concentrations in the HP2 movement assay background ($K_{0.5}^{Asp}$: 1mM 127 ± 57 μM, 10 mM 0.85 ± 0.08 μM, 200 mM 0.042 ± 0.007 μM, 500 mM 0.012 ± 0.002 μM) **B)** Asp binding in the HP2 movement assay at 10 mM Na^+ with or without 100 μM TBOA ($K_{0.5}^{Asp}$: 10 mM 0.85 ± 0.08 μM and with TBOA 15 ± 0.5 μM) **C)** Asp binding in the HP2 movement assay at 200 mM Na^+ with or without 100 μM TBOA ($K_{0.5}^{Asp}$: 200 mM 0.042 ± 0.007 μM and with TBOA 1.53 ± 0.09 μM). All error bars are S.E.M. from an N ≥ 3.

Backbone interactions are essential for binding and side chain moiety modulates the extent of HP2 closure

The substrate coordinator substitution data indicates all substrate-protein binding site interactions are important for binding and HP2 closure. All the residues substituted with Ala are involved in earlier steps of the coupling process and therefore it is non-trivial to draw structure function relationships when comparing between the perturbed proteins. One possible approach to lessen the extent of opening variability between protein mutants is to have TBOA present at the start of the titration with Na^+. TBOA binding would theoretically bring HP2 opening to the same extent across mutants if TBOA can still bind to mutants, thus the extent of closure would only reflect substrate competing off TBOA and HP2 closure. Control experiments are necessary to use the TBOA approach to help interpret binding site mutant's HP2 closure data. To address the HP2 movement assay limitations and further probe the second half of the coupled binding process, we decided to use a substrate analogue series. Using alternative substrates with systematically altered chemical properties, we can compare the functional effects within WT protein to inform on a mechanism for substrate assisted HP2 closure. The series consists of Asp analogues in which the backbone and the side chain properties are altered (Figure C.4).

Analogues which lack either a α-amino or α-carboxyl group could barely bind and close HP2 (Figure C.4B). The affinity for both these substrates is greatly decreased or non-existent, even with full substrate side chain chemistry, suggesting a large part of

affinity for substrate stems from backbone-protein interactions. β-Ala, which lacks the α-carboxyl group, does not show any substantial change as a function of substrate to indicate HP2 closure (Figure C.4B). The lack of succinate binding unless there is over 1.5 mM present agrees with the corresponding protein substitution data in which there is no HP2 closure (D394A). Without backbone coordination, the substrate cannot bind well and little to no HP2 closure.

The substrate analogues with altered substrate side chain chemistry show the same trends as the corresponding protein substitutions in both affinity and extents of HP2 closure. Just as R397A and T314A showed different effects, there is a wide variety of responses when different components of the side chain are changed. When the polar side chain is removed as in L-Ala and Abu, there is a decreased ability to close HP2 at any relevant substrate concentration (Figure C.4C). L-Ala only lacks the terminal side chain functional groups compared to Asp, but shows an inability to fully close HP2, highlighting the role of side chain chemistry in HP2 closure. Abu shows the same phenotype as D394A where excess ligand results in a slight increase in fluorescence and no observable HP2 closure signal. The difference in Abu and L-Ala is only one methyl group and suggests size of the substrate is also important for proper coordination. Only when the substrate has a polar moiety which can hydrogen bond like in L-Cys and L-Glu do we see substantial extents of closure with a reasonable affinity (Figure C.4C). Size of the substrate is also a factor in which the larger the substrate, the less HP2 closes. All these differences in HP2 closure and affinity add to the interpretation that a lower fluorescence change results from less HP2 closure. Since the affinity for the analogues is generally greatly decreased, it would be useful to test the HP2 closure at higher Na^+ concentrations to provide further insight.

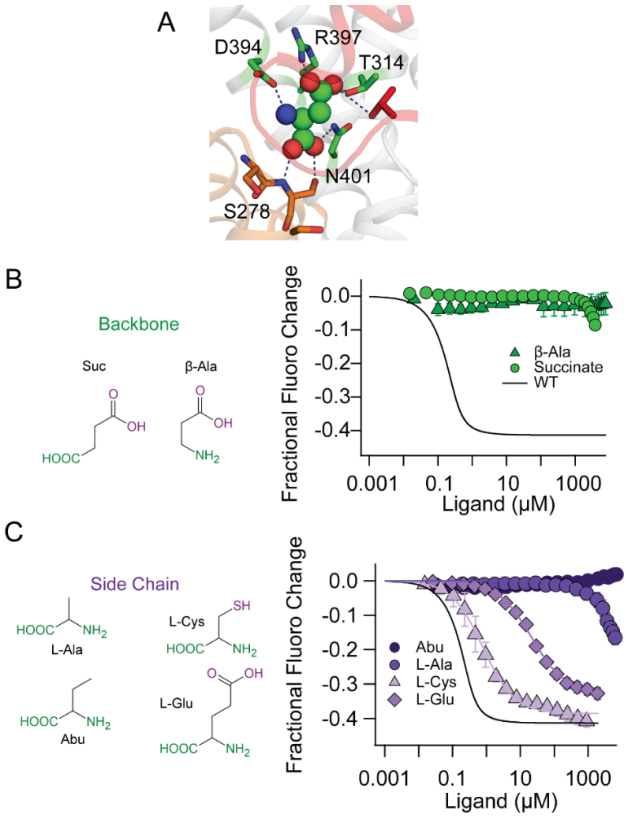

Figure C.4. Alternative substrates demonstrate the need for backbone coordination with varying impact from sidechain modifications. **A)** Substrate binding site of Glt_{Ph} using Glt_{Tk} structure pdb 5E9S to highlight where the backbone and sidechain of the substrate are oriented **B)** Chemical structure of alternative substrates which lack one of the backbone functional groups and the HP2 closure titrations with the respective substrates in 200 mM Na^+, black line is WT with Asp. There is barely any signal change to determine $K_{0.5}$ (>1500 μM) **C)** Chemical structure of alternative substrates which alter the substrate side chain properties and the HP2 closure titrations with the respective substrates in 200 mM Na^+, black line is WT with Asp ($K_{0.5}$: L-Glu 22 ± 1.1 μM, L-Cys 0.78 ± 0.06 μM, L-Ala >4000 μM, Abu no binding). All error bars are S.E.M. from an N ≥ 3.

Discussion:

In this body of experiments, we were able to test the importance of individual protein-substrate interactions in HP2 closure. We made substitutions to substrate coordinating residues and tested a substrate analogue series with our HP2 movement assay. Although there are confounding factors when looking at HP2 closure with protein mutants, especially when they effect HP2 opening, the analogue series allowed for conclusions to be drawn. All coordinating residues are essential for both high affinity substrate binding and proper HP2 closure. Substrate backbone coordination is essential

while there is a variety of effects from perturbation of side chain coordinators. Selectivity may therefore stem from the interactions of the sidechain of substrate with the binding site and HP2. Side chain modification directly modulates the ability to close HP2. We have identified that the substrate also needs a polar moiety at the side chain as well as small enough to fit in coordination sphere to support HP2 closure.

The next set of experiments would be to further probe the alternative substrate series with other Asp binding assays, like L130W, as well as test within each of the coordinating residue mutants. The alternative analogue series allows for further investigation into protein-substrate interactions using the protein coordinator substitutions. Moving forward in elucidating the molecular closure mechanism, we want to make substitutions to HP2 and HP1 residues that help define the binding site. We have preliminary data for HP1 residue S278 being involved in substate coordination and a previous paper has demonstrated that certain HP2 residues can alter substrate selectivity and transport rates(238). When all substrate-protein interactions are explored in conjunction with the alternative substrate series, we will have a structure activity relationship for substrate binding and HP2 closure. Kinetics measurements also provide avenue for gaining deeper mechanistic insight into how HP2 is closed upon substrate binding.

A key component in HP2 closure is the final Na^+ ion binding to the Na2 site which is mainly formed by HP2 residues. Experiments using the HP2 movement assay can be used to explore the role of the Na2 site in both substrate binding and HP2 closure. Perturbing the Na2 site and monitoring the functional effects will help inform the last piece in sequential binding: the role of Na2 site. The HP2 movement assay can also be used to explore substrate release mechanism through studying Glt_{Ph} trapped in the inward facing state, kinetics measurements, and mutagenesis.

Methods:

Protein Expression Same methods were used to express and create L130W proteins as outlined in Chapter 2 Methods and proteins in the HP2 movement assay background were created and purified as outlined in Chapter 2 Methods.

Asp binding using L130W The assays were carried out as outlined in Chapter 2 Methods using the same assay buffer.

HP2 movement Assay Closure titrations were performed with ~100 µgs of Glt_{Ph}(V355W/S279Phe_{CN}) protein. The protein was equilibrated in the Na^+ containing assay buffer solution for at least 30 min before monitoring the fluorescence change upon Asp addition (emission at 345 nm with excitation at 295 nm). The assays were carried out at 30 °C and the assay buffer was composed of 20 mM HEPES/Tris pH 7.5, X mM of Na^+ and the corresponding amount of choline chloride to maintain ionic strength at 200 mM, except for 500 mM Na^+ assays. Each titration point was collected following a 1 min equilibration step. The resulting titrations were fit to equation 1 or equation 2 if the protein concentration was similar to or greater than the affinity for Asp just as in Chapter 3 Methods.

$$F = ymax \frac{Asp^n}{Asp^n + K_D^n}$$ Equation 1

$$F = \text{ymax} \frac{\left(K_{0.5}^{Asp} + [P] + [Asp]\right) - \sqrt{\left(K_{0.5}^{Asp} + [P] + [Asp]\right)^2 - (4\ [P]\ [Asp])}}{2[P]}$$ Equation 2

The alternative substrates and substrate binding mutants were titrated in the presence of 200 mM Na^+ following the same procedure as outlined above and conditions of Chapter 2. Fractional fluorescence changes were also fit in the same manner using either equation 1 or 2 depending on the affinity vs protein concentration.

Chapter 4: A Facile Approach for the *In Vitro* Assembly of Multimeric Membrane Transport Proteins

This chapter was published in elife in 2018 as:

Riederer E. A.*, Focke P.J.*, Georgieva E.R., Akyuz N., Matulef K., Borbat P.P., Freed J.H., Blanchard S.C., Boudker O., Valiyaveetil, F.I. (2018). A facile approach for the in vitro assembly of multimeric membrane transport proteins. Elife. 2018 Jun 11;7. pii: e36478. doi: 10.7554/eLife.36478.

P.J.F and F.I.V established the reassociation methodology and assessed the applicability to other transporters. E.A.R generated the proteins and performed the experiments for the Glt_{Ph} flux assays and fluorescence binding data (Figure 4.1, Figure 4.3, and Figure S4.1-3) as well as the in vitro assembly of Glt_{Sm} (Figure 4.5) and fluorescence experiments for CLC-ec1 (Figure 4.7C). The remaining data was generated by the fellow authors. F.I.V wrote the manuscript.

Abstract:

Membrane proteins such as ion channels and transporters are frequently homomeric. The homomeric nature raises important questions regarding coupling between subunits and complicates the application of techniques such as FRET or DEER spectroscopy. These challenges can be overcome if the subunits of a homomeric protein can be independently modified for functional or spectroscopic studies. Here, we describe a general approach for *in vitro* assembly that can be used for the generation of heteromeric variants of homomeric membrane proteins. We establish the approach using Glt_{Ph}, a glutamate transporter homolog that is trimeric in the native state. We use heteromeric Glt_{Ph} transporters to directly demonstrate the lack of coupling in substrate binding and demonstrate how heteromeric transporters considerably simplify the application of DEER spectroscopy. Further, we demonstrate the general applicability of this approach by carrying out the *in vitro* assembly of VcINDY, a Na^+-coupled succinate transporter and CLC-ec1, a Cl^-/H^+ antiporter.

Introduction:

Movement of ions and small molecules across cellular membranes takes place through transport proteins such as ion channels and transporters. A frequently observed feature of transport proteins is that they form multimeric assemblies of identical subunits in their native state (239, 240). There are challenges in spectroscopic investigations of homo-multimeric (or homomeric) proteins that arise due to the presence of multiple identical subunits. One such example is in using Double Electron-Electron Resonance, DEER or Fluorescence Resonance Energy Transfer, FRET, spectroscopy with homomeric proteins. These spectroscopic techniques, which are commonly used for detecting structural changes accompanying function, rely on site-specific labeling with appropriate spectroscopic probes, typically at introduced cysteine residues. In homomeric proteins, such efforts result in the labeling of each of the individual subunits and therefore the presence of multiple probes in the protein, which can complicate the spectroscopic measurements. It is also not feasible to label a single subunit in a homomeric protein, which hinders the use of these spectroscopic approaches for investigating the structural changes that take place within individual subunits. The presence of multiple identical subunits in transport proteins also raises the pertinent question of whether there is a functional coupling or “crosstalk” between the subunits. These challenges in investigating homomeric proteins can be overcome if we generate heteromeric variants in which a single subunit (or a set of subunits) can be selectively modified. Labeling a single subunit with spectroscopic probes will facilitate the investigations of the intra-subunit structural changes, while functional perturbation of a subset of subunits in the assembly will enable investigations of the functional coupling between protomers. Thus, the ability to generate a heteromeric variant of a homomeric protein will be a great asset.

Cellular expression of heteromeric proteins containing wild type and mutant subunits has been carried out using either concatenation or co-expression approaches. In the concatenation approach, protein expression is carried out using a DNA construct in which the genes for the wild type and mutant subunits are concatenated into a single reading frame. Expression of this concatenated construct yields a heteromeric membrane protein in which the subunits are linked together. This approach has been widely used for the expression of heteromeric ion channels in *Xenopus* oocytes for functional studies (241, 242). There are only a few examples where multimeric membrane proteins encoded in a single polypeptide have been purified for functional and spectroscopic studies (243-246). In the co-expression approach, the wild type and the mutant subunits are co-expressed in the same cell (247, 248), wherein the random mixing of the subunits during assembly results in the generation of heteromeric and homomeric proteins. Placing different purification tags on the wild type and the mutant subunits allows the purification of the desired heteromeric protein. Both of these approaches frequently suffer from very low yields.

The alternate approach is to assemble the heteromeric proteins *in vitro* by using a mixture of wild type and mutant subunits. In this manner, a mixture of heteromeric and homomeric proteins is produced from which the desired heteromeric complex can be purified. The advantage of the *in vitro* approach is that the ratio of the wild type and the mutant subunits can be adjusted to ensure formation of the desired heteromeric protein in good yields. The heteromeric assembly can be carried out through a coupled folding and oligomerization process starting with fully unfolded subunits. However, refolding of membrane proteins is very challenging, and there are only few reports in the literature (249, 250). In lieu of complete refolding, we envisioned an approach in which we dissociate the native wild type and mutant multimeric proteins into subunits and then use a mixture of the dissociated subunits for assembly of the hetero-oligomers. We

anticipated that this dissociation/reassociation approach should be generally applicable and also provide higher yields compared to complete refolding.

Here we describe a simple methodology for the *in vitro* reassembly of functional multimeric membrane proteins from dissociated subunits. We develop the methodology using the archaeal glutamate transporter homolog Glt_{Ph}. We demonstrate the utility of the approach by assembling heteromeric Glt_{Ph} transporters that we use to investigate the cross-talk between the substrate binding sites and to evaluate the intra-subunit structural changes in Glt_{Ph} using DEER spectroscopy. Further, we establish the general applicability of the methodology by carrying out the *in vitro* reassembly of the archaeal transporter Glt_{Sm} and the bacterial transporters VcINDY and CLC-ec1.

Results:

In vitro reassembly of Glt_{Ph}

To develop a protocol for the *in vitro* reassembly of multimeric membrane proteins, we initially focused on Glt_{Ph}, a homo-trimeric sodium coupled aspartate transporter (Figure 4.1A)(149, 150). Each subunit of Glt_{Ph} has a complex topology with eight transmembrane and two reentrant hairpin segments. Remarkably, we have previously successfully refolded Glt_{Ph} from a completely unfolded state by using lipid vesicles to obtain an active native-like protein (155). Here, we investigated whether Glt_{Ph} can be reassembled *in vitro* from dissociated subunits using lipid vesicles (Figure 4.1B).

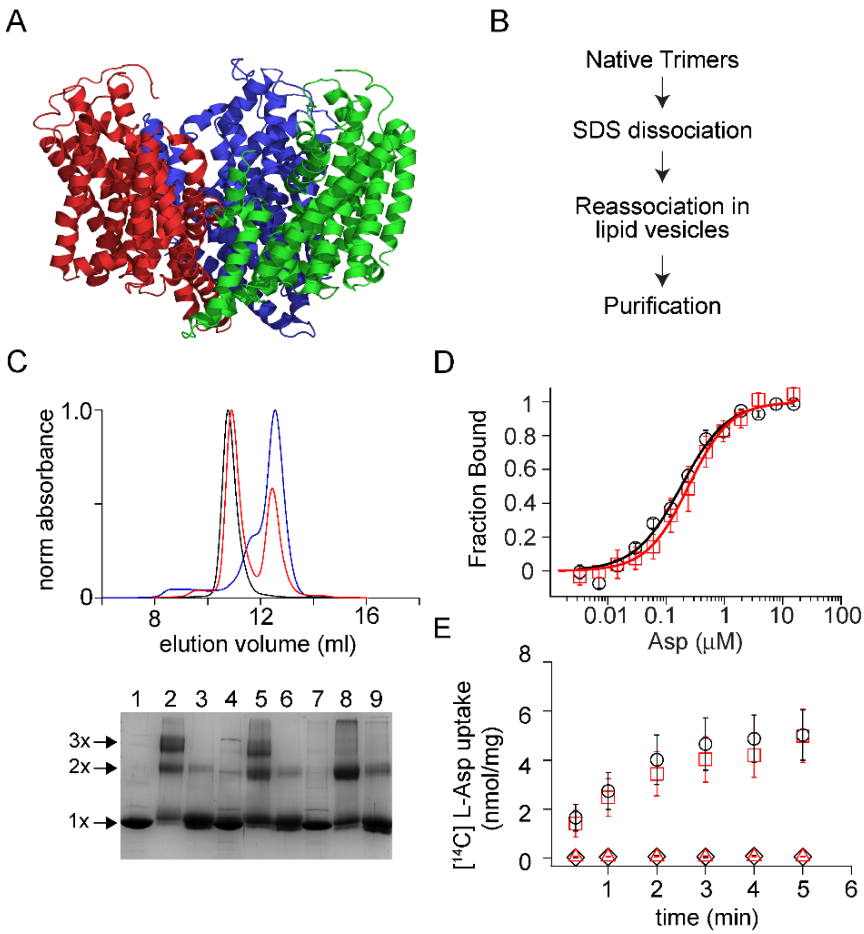

Figure 4.1. Dissociation and reassociation of Glt_{Ph}. **A**) Structure of the Glt_{Ph} trimer, pdb: 2nwx, is shown in ribbon representation. **B**) Flow chart outlining the strategy used for the dissociation and reassociation of the Glt_{Ph} trimer. **C**) Size exclusion chromatography of the native Glt_{Ph} (black) and the SDS dissociated Glt_{Ph} following dilution into lipid vesicles (red) and into DDM (blue). Reassembly of Glt_{Ph} takes place in lipid vesicles. Inset, SDS-PAGE gel showing the glutaraldehyde crosslinking of the native Glt_{Ph} (lanes 1-3), reassociated Glt_{Ph} (r-Glt_{Ph}, lanes 4-6) and the SDS dissociated Glt_{Ph} subunits (lanes 7-9). Lanes 1, 4, and 7, without glutaraldehyde crosslinking, lanes 2, 4, and 8, with glutaraldehyde crosslinking and lanes 3, 6, and 9, with glutaraldehyde crosslinking in the presence of 1% SDS. The oligomeric nature of the protein band (1x, 2x, and 3x) is indicated. **D**) Asp binding by native and r-Glt_{Ph}. Asp binding was monitored by changes in fluorescence of the native (black circles) or r-Glt_{Ph} (red squares) with the L130W substitution. The fraction of the protein bound (F_{bound}) is determined by dividing the change in fluorescence upon addition of Asp by the total change at the end of the titration. Solid lines are fits to the data using the equation described in methods with K_D values of 183 ± 16 nM for native Glt_{Ph} and 216 ± 15 nM for r-Glt_{Ph}. The binding assays were conducted in 10 mM Na^+. **E**) Asp uptake assay. The time course of [^{14}C]-Asp uptake for native Glt_{Ph} (black circles) and r-Glt_{Ph} (red squares) in the presence of a Na^+ gradient. No uptake is observed for native Glt_{Ph} (black diamonds) and r-Glt_{Ph} (red triangles) in the absence of a Na^+ gradient. For panels D and E, error bars indicate standard error of mean (S.E.M.) for $N \geq 3$.

Glt_{Ph} migrates as a monomer on SDS-PAGE, suggesting that SDS dissociates Glt_{Ph} into subunits (149). Glutaraldehyde cross-linking confirmed complete dissociation of the trimeric species by SDS (155). While crosslinking of the native Glt_{Ph} gives a protein band on SDS-PAGE corresponding to the trimer, crosslinking following SDS treatment only yields monomers. For reassembly, we diluted the protein after SDS treatment into buffer supplemented with lipid vesicles achieving SDS concentrations below the critical micellar concentration (155). Consequent glutaraldehyde crosslinking showed the presence of a trimeric band indicating subunit reassociation. We solubilized the reassembled Glt_{Ph} (r-Glt_{Ph}) from the lipid vesicles using dodecyl-β-D-maltopyranoside (DDM) detergent and purified it by affinity and size exclusion chromatography (SEC). The SEC elution profile for r-Glt_{Ph} was similar to that of native Glt_{Ph} and crosslinking confirmed the trimeric state of r-Glt_{Ph} (Figure 4.1C). Lipid vesicles were required for the reassociation process, and dilution of the SDS-dissociated Glt_{Ph} subunits directly into DDM did not yield a trimeric species, as indicted by both SEC and cross-linking (Figure 4.1C).

To establish the functionality of r-Glt_{Ph}, we examined its ability to bind and transport substrate L-aspartate (Asp). Substrate binding was assayed by monitoring changes in the intrinsic fluorescence of the L130W mutant of Glt_{Ph} upon titration with Asp (150, 210). The Asp dissociation constant (K_D) of the reassembled L130W mutant of Glt_{Ph} was similar to that of the transporter prior to the dissociation/reassociation procedure (Figure 4.1D). We reconstituted r-Glt_{Ph} into lipid vesicles to measure transport activity and observed uptake of [^{14}C]Asp into proteoliposomes in the presence of an inwardly directed Na^+ gradient (Figure 4.1E). The specific transport activity observed for r-Glt_{Ph} was similar to that of the native transporter.

The key conformational transition of Glt_{Ph} that underlies substrate translocation across the membrane is an elevator-like movement of the peripherally located transport

domain within each protomer relative to the central trimerization domain (158). Previously, single-molecule FRET (smFRET) was used to visualize these movements in real time (181, 182, 251). These experiments further suggested that the transition frequency determined the overall rate of substrate transport. We used smFRET to compare the dynamics of the r-Glt_{Ph} to the native protein. For these experiments, N378C mutant of Glt_{Ph} was derivatized with Cy3 and Cy5 fluorophores and with a PEG-biotin linker either before or after the reassembly procedure. As previously described (182), the labeled proteins were immobilized on passivated streptavidin-coated microscope slides and imaged using total internal reflection fluorescence (TIRF) to obtain smFRET recordings (Figure 4.2A). In these experiments, movements of two transport domains within the trimers relative to each other are detected. We found that r-Glt_{Ph} in the presence of 200 mM Na^+ and 100 μM Asp, sampled three FRET efficiency states, low-, intermediate- and high-FRET centered at ~0.35, ~0.55 and ~0.8, respectively (Figure 4.2B). Similar FRET efficiency states were observed for the native protein, where the low-FRET state was attributed largely to the outward facing state of the transporter. Excursions into the higher-FRET states reflect sampling of the inward-facing conformations (182). The populations of the low-, intermediate-, and high-FRET states for the r-Glt_{Ph} were 76%, 17% and 7%, respectively, in good agreement with the values observed for the native transporter (71%, 16% and 13%, respectively). Transition density plots showed that the r-Glt_{Ph} exhibit conformational transitions at a rate of ~0.03/sec, also in good agreement with the transition frequency of the native transporter (Figure 2C). In line with these findings, the FRET-state lifetimes were similar in the native and reassembled transporters (Figure 4.2D). These smFRET measurements suggest that the reassembled transporter samples the outward- and inward-facing state with probabilities and frequency similar to the native protein. Collectively, these results show that r-Glt_{Ph} is structurally, functionally and dynamically similar to the native transporter.

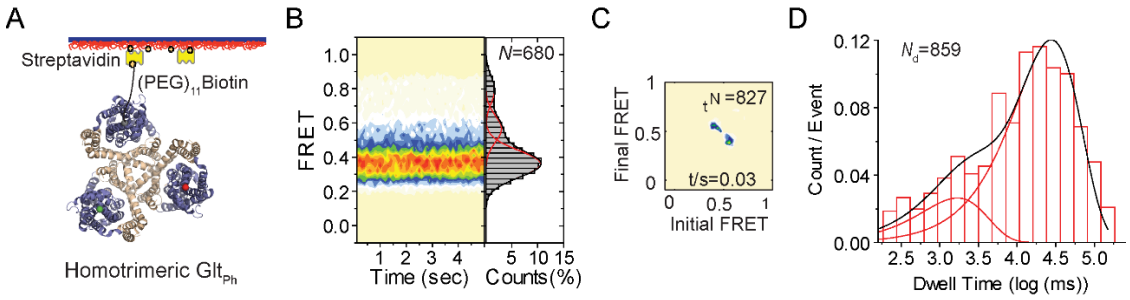

Figure 4.2. smFRET experiments on reassociated Glt_{Ph} molecules. A) Labeling and surface-immobilization strategy for smFRET experiments. **B)** Population distributions FRET efficiency population contour plots (left) and cumulative population histograms (right) are shown for r-Glt_{Ph}. The contour plots are color-coded from tan (lowest) to red (highest population) with the color scale from 0-12%. The population histograms display the time-averaged values and standard deviations. The solid black lines are fits to the sums of individual Gaussian functions (red lines). The number of molecules analyzed (*N*) is shown. **C)** Transition density plots show that transitions occur at a frequency of ~0.03 /s. The number of transitions in the dataset (N_t) is shown. **D)** Dwell time distribution for the low-FRET state obtained for r-Glt_{Ph} shows biphasic behavior and was fitted to a probability density function. The number of dwells in the analysis (N_d) is shown.

Using heteromeric transporters to evaluate cooperativity in Asp binding to Glt_{Ph}

A key question in multimeric transporters is whether the protomers function entirely independently or are coupled or coordinated in some manner. In glutamate transporters, several lines of evidence suggest that subunits in the trimer are independent of each other (120, 181, 185, 252). However, addressing directly whether one subunit senses substrate binding to its neighbor has not been possible. Our methodology allows assembly of heteromeric Glt_{Ph} transporters in which the ability of individual subunits to bind substrate can be independently manipulated. Thus, we assembled Glt_{Ph} heteromers containing one reporter and two test subunits (Figure 4.3A). The reporter subunit carried the L130W substitution, which provides a spectroscopic probe for Asp binding (Figure S4.1). The test subunits were either wild type or carried the R397A mutation, which lowers Asp affinity by approximately a thousand fold (Figure S4.2)(154). A comparison of Asp binding to the reporter subunit of Glt_{Ph} heteromers

containing either wild type or mutant test subunits should reveal whether the reporter subunit senses substrate binding to its neighboring subunits.

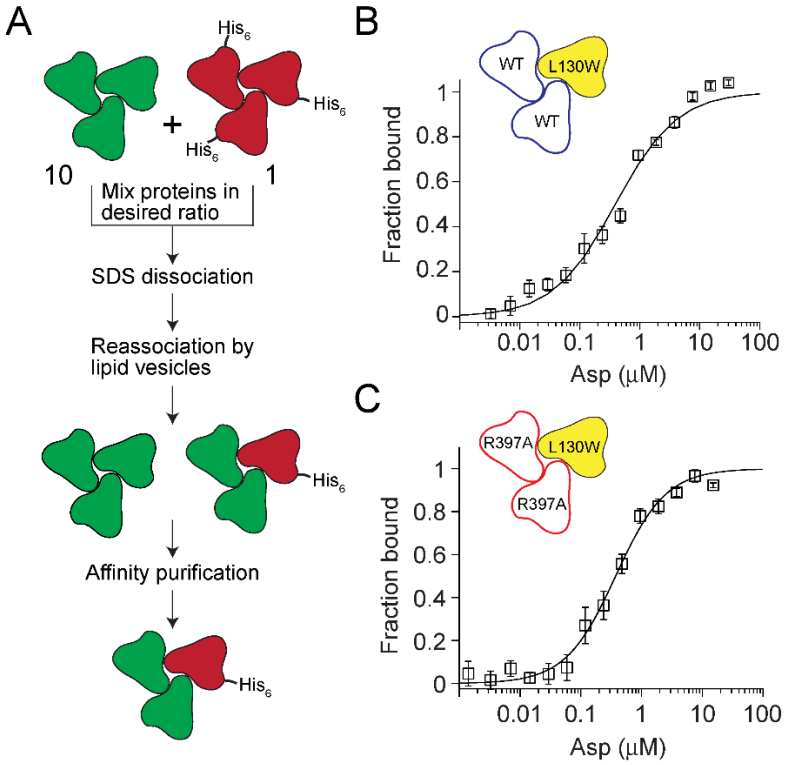

Figure 4.3. **Testing crosstalk between Glt_{Ph} subunits in Asp binding**. **A**) Flowchart outlining the strategy used for assem.bling heterotrimers of Glt_{Ph}. The test subunits are depicted in green and the reporter subunits are in red. A 10: 1 ratio of test to reporter subunits is used to ensure that the probability of assembling heterotrimers with more than one reporter subunit is very low. The presence of a polyhistidine tag on the reporter subunit enables purification of the heterotrimers that contain a reporter subuit. **B** and **C**) Asp binding to heterotrimeric Glt_{Ph} with test subunits containing the wild type Asp binding site (blue, **B**) or with a R397A substitution in the Asp binding site (red, **C**). The reporter subunit (yellow) contains the L130W substitution for monitoring Asp binding to the subunit. Asp binding assays as described in Figure 1D. The solid lines indicate fits to the data using a Hill equation with K_D = 455 $\pm$ 61 nM, Hill coefficient = 0.84 $\pm$ 0.08 for the heterotrimer with the wild type test subunits and with K_D = 356 $\pm$ 36 nM, Hill coefficient = 1.05 $\pm$ 0.07 for the heterotrimer with test subunits carrying the R397A substitution. Error bars indicate S.E.M. for N $\geq$ 3.

We reassembled heteromeric Glt_{Ph} transporters using a 10:1 mixture of the test to the reporter subunits. At this ratio, a random mixing of the subunits ensures that the majority of the transporters assembled will contain either no reporter subunits (73%) or only one reporter subunit (24%), while the fraction with two or three reporter subunits will

be negligibly small (3% and 0.1% respectively). The reporter subunits carried a His_8 tag while the test subunits carried no purification tags. The presence of the His_8 tag on the reporter subunit allowed us to purify only the heteromers containing a reporter subunit (Figure S4.3). We measured Asp binding affinity to the reporter subunit of heteromeric Glt_{Ph} transporters in the context of either the wild type or the R397A test subunits (Figure 4.3B/C). The binding isotherms were obtained in the presence of 10 mM Na^+ ions and fitted to the Hill equation. The K_D values for Asp were 455 ± 61 nM and 356 ± 36 nM for the heteromers with wild type and R397A test subunits, respectively. The Hill coefficients were also similar. Notably, the expected affinity of the R397A mutant in the presence of 10 mM Na^+ ions is approximately 238 μM (Figure S4.2), suggesting that the R397A mutant test subunits remain largely unbound to Asp throughout the titration. This result indicates that Asp binding to the test subunits does not affect Asp binding to the reporter subunit. Therefore, for the first time, we directly demonstrate the lack of coupling in substrate binding to the trimeric transporter Glt_{Ph}.

Using heteromeric transporters to evaluate intra-subunit structural changes using DEER spectroscopy.

Understanding the transport mechanism requires determination of the structural changes that take place during function. In recent years, pulse dipolar ESR spectroscopy (PDS), in particular the double electron-electron resonance method, utilizing spin labeling has become the method of choice for monitoring structural transitions in biological macromolecules and complexes by reporting on distances in the range from about 10 Å (253, 254) to as large as 80 Å (254-257) or even longer (258) in some cases. It has been widely applied to follow conformational changes in membrane transporters. (183, 184, 259-261) In these experiments, the transporters are site-specifically spin-labeled at introduced cysteine residues and dipolar coupling between pairs of spin-label unpaired electron spins is measured. The dipolar coupling depends on

the inter-spin distance r, as $1/r^3$, making the method quite an accurate tool for accessing minute distance variations.

The use of DEER spectroscopy for distance measurements in transporters comprised of more than two subunits is problematic, however, as these proteins present multi-spin systems if spin-labeled using standard approaches (183, 184, 262, 263). It is especially challenging to use DEER to probe the structural changes taking place within a single subunit, because dipolar coupling is present not only between the spin labels within this subunit, but also between those in different subunits. In Glt_{Ph}, the key transition involves the movement of the transport domain relative to the scaffold domain by as much as 15 Å. Probing this movement requires spin labels in both of these domains. However, the introduction of Cys mutations into each domain and subsequent labeling of Glt_{Ph} yields six spin labels per the trimeric protein (Figure 4.4A). In the simplest case, with all subunits being in the outward-facing state, we expect up to five unique distances between spin labels, depending on symmetry. Consequently, the distance distributions, generated from DEER signals, are very broad and difficult to extract, being further complicated by non-linear effects (264) and less than ideal spin-labelling efficiency. The use of heteromeric Glt_{Ph} transporters, in which only a single subunit is labeled (Figure 4.4A), would be a great simplification directly yielding, for example, the distance distributions between the probes in the scaffold and transport domains of a single protomer.

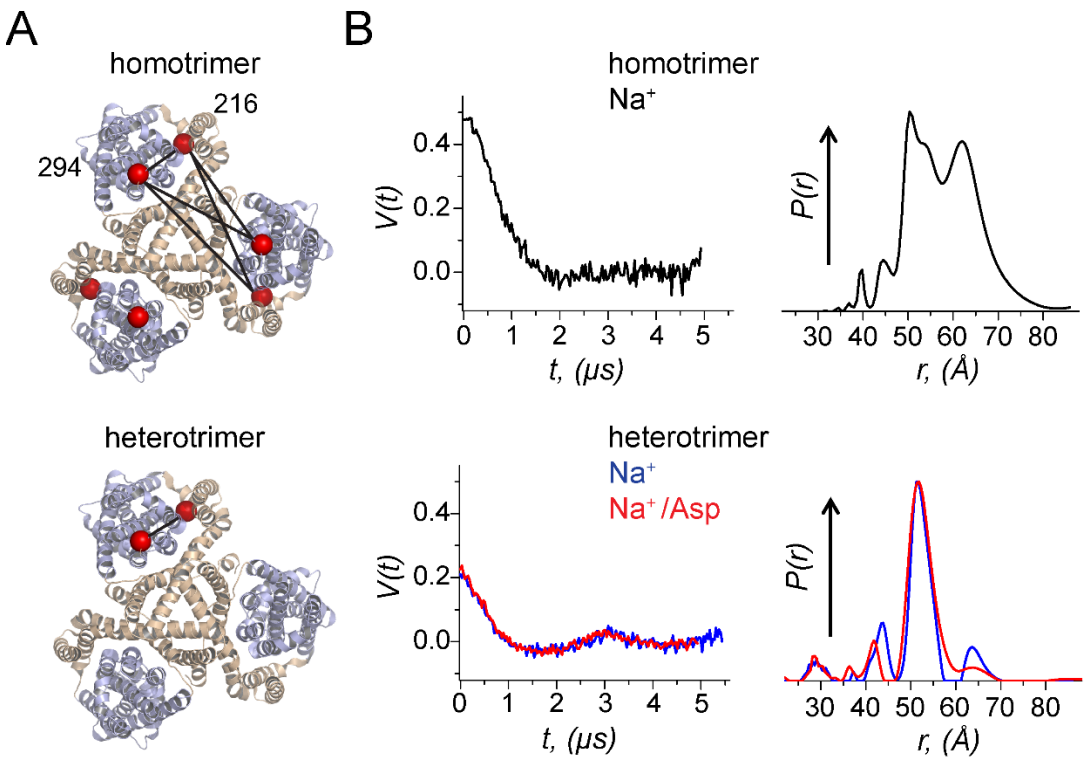

Figure 4.4. **Using a heterotrimeric Glt_{Ph} to probe movements of the transport domain using DEER A**) A homomeric and a heteromeric Glt_{Ph} transporter are shown in ribbon representation. The scaffold domain is colored in wheat while the transport domain is colored in light blue. The C_α atoms of the Cys residues at 216 and 294 labelled with spin probes are shown as red spheres. All subunits in the homomeric Glt_{Ph} carry the Cys substitutions while only one subunit in the heteromeric Glt_{Ph} carries the Cys substitutions. The distances monitored in the DEER experiment are indicated by solid lines. **B**) Background-corrected DEER amplitude, $V(t)$ vs. evolution time t (left). The data are shown for: Glt_{Ph} homotrimers with spin labels at both positions in each of the protomers prepared with 200 mM NaCl (black); Glt_{Ph} heterotrimer with spin-labels just in one of the protomers prepared with either 200 mM NaCl (blue) or 200 mM NaCl/300 μM aspartate (red). The data are plotted to have the "DEER modulation depth" at t = 0 and decay to zero value asymptotically (see Materials and Methods). Larger modulation depth, i.e. $V(0)$ indicates larger number of coupled spins. Inter-spin distance distributions, $P(r)$, reconstructed from the above DEER data, are plotted in respective colors (right). All $P(r)$'s were normalized to common value at the maxima. Glt_{Ph} heterotrimers show much simpler $P(r)$ as compared to convoluted result for homotrimers.

To demonstrate the utility of heteromeric Glt_{Ph} for DEER spectroscopy, we assembled a Glt_{Ph} trimer from a 10:1 mixture of wild-type (i.e., cysteine-less) subunits and V216C/I294C mutant subunits bearing cysteine mutations in the scaffold and transport domains. The heterotrimers were purified using the His_8-tag on the

V216C/I294C subunit and labeled with the MTSL nitroxide [(1-oxyl-2,2,5,5-tetramethylpyrrolidin-3-yl) methyl methanethiosulfonate] spin label. As a control, we also prepared a homomeric V216C/I294C spin-labeled trimer Glt_{Ph}. In the presence of Na^+ ions and Asp, homomeric V216C/I294C mutant yielded, as expected, broad weakly-structured distance distributions, spanning the distance range from ca. 40 to 70 Å (Figure 4.4B). In contrast, the heteromeric protein exhibited a single narrow peak at 52 Å. Remarkably, these measurements suggest that under our experimental conditions the V216C/I294C mutant subunit predominantly populates the inward facing state. In this conformational state, the C_α-C_α distance between residues 216 and 294 is 48 Å based on the crystallographic model, in good agreement with the DEER measurement. The corresponding distance in the outward facing state is 34 Å. In conclusion, using a heteromeric trimer greatly simplified the experimentally obtained distance distributions and allowed for straightforward determination of the conformational state of the labeled protomer.

General applicability of in vitro reassembly.

To investigate whether our *in vitro* subunit reassembly procedure is applicable to other multimeric transporters, we initially tested the procedure on Glt_{Sm}, a glutamate transporter homolog from *Staphylothermus marinus* that shares 58% sequence identity to Glt_{Ph} (Figure 4.5A)(265). We observed that SDS dissociated the Glt_{Sm} transporter and that the dissociated subunits can be reassembled back to the trimeric state upon dilution of SDS coupled with protein incorporation into lipid vesicles (Figure 4.5B). The reassembled Glt_{Sm} transporter was functionally similar to the native protein, suggesting that the disassembly/reassembly procedure was well tolerated by Glt_{Sm}, similar to Glt_{Ph} (Figure 4.5C).

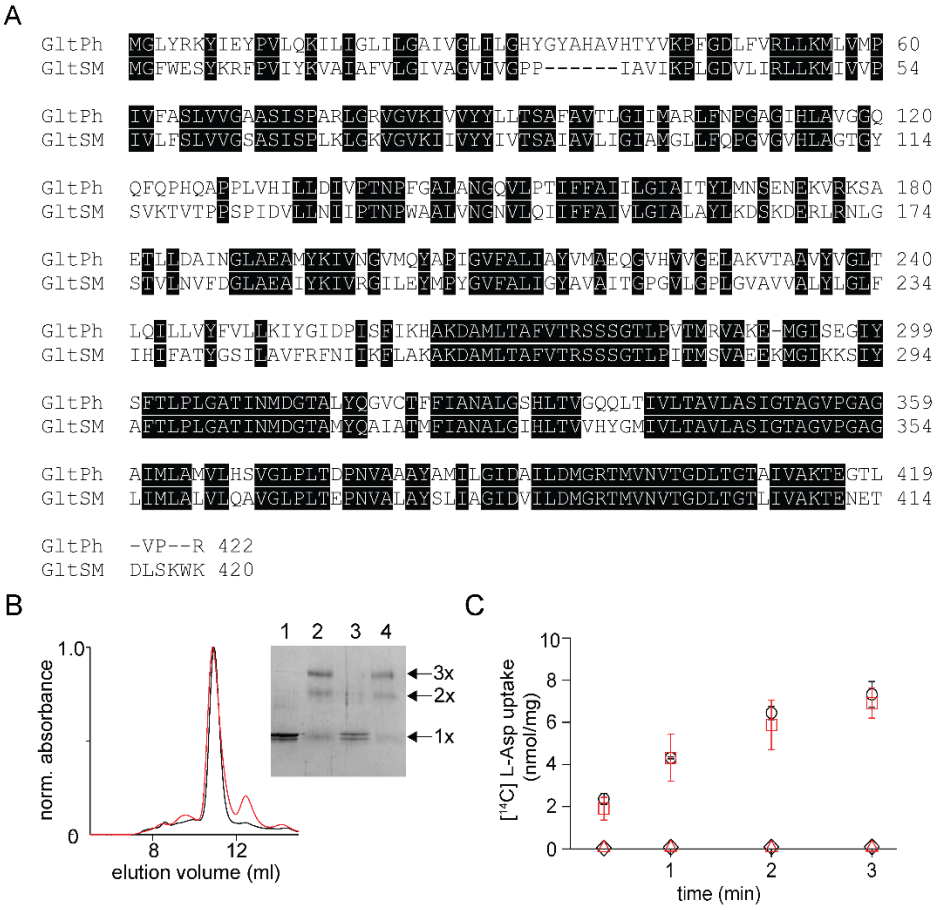

Figure 4.5. ***In vitro*** **assembly of Glt_{Sm}. A)** Sequence alignment of Glt_{Sm} with Glt_{Ph} with identical residues highlighted. **B)** Size exclusion chromatography of the native (black) and the reassociated Glt_{Sm} (r-Glt_{Sm}, red). Inset, SDS-PAGE gel shows the glutaraldehyde cross-linking of the native and r-Glt_{Sm}. Native Glt_{Sm} without (lane 1) and with glutaraldehyde crosslinking (lane 2) and r-Glt_{Sm} without (Lane 3) and with glutaraldehyde crosslinking (Lane 4) are shown. The oligomeric nature of the protein band (1x, 2x, and 3x) is indicated. **C)** Aspartate uptake assay. The time course of [^{14}C]-Asp uptake by native Glt_{Sm} (black circles) and r-Glt_{Sm} (red squares) in the presence of a Na^+ gradient. No uptake is observed for native Glt_{Sm} (black diamonds) and r-Glt_{Sm} (red triangles) in the absence of a Na^+ gradient. Error bars indicate S.E.M. for N≥ 3.

We further tested the procedure on the VcINDY and CLC-ec1 transporters. VcINDY is a homo-dimeric Na^+- coupled succinate transporter (Figure 4.6A)(266). Each subunit of VcINDY consists of 11 transmembrane helices that are arranged in two domains, a scaffold dimerization domain and a peripheral transport domain. The transport mechanism in VcINDY involves an elevator-like movement of the transport domain with respect to the scaffold domain (160). While the elevator mechanism of

VcINDY is reminiscent of the mechanism in Glt_{Ph}, the topology and fold of the VcINDY transporter is very distinct (157). The VcINDY transporter is dimeric in the native state but migrates as a monomer on SDS-PAGE, indicating that SDS dissociates the transporter into monomers (Figure 4.6B). We used glutaraldehyde crosslinking to confirm complete dissociation of the VcINDY dimer by SDS. Crosslinked native VcINDY runs as a dimer on SDS-PAGE while VcINDY crosslinked after dissociation by SDS runs as a monomer. As anticipated, crosslinking following reassembly in lipid vesicles yielded a dimeric species (Figure 4.6B). We solubilized the reassembled (r-)VcINDY protein in DDM detergent and purified it using a His-tag. Analysis by SEC showed that r-VcINDY had a similar elution profile to the native transporter (Figure 4.6C). The r-VcINDY transporter reconstituted into lipid vesicles mediated succinate uptake in the presence of a Na^+ ion gradient with a rate similar to the native transporter (Figure 4.6D).

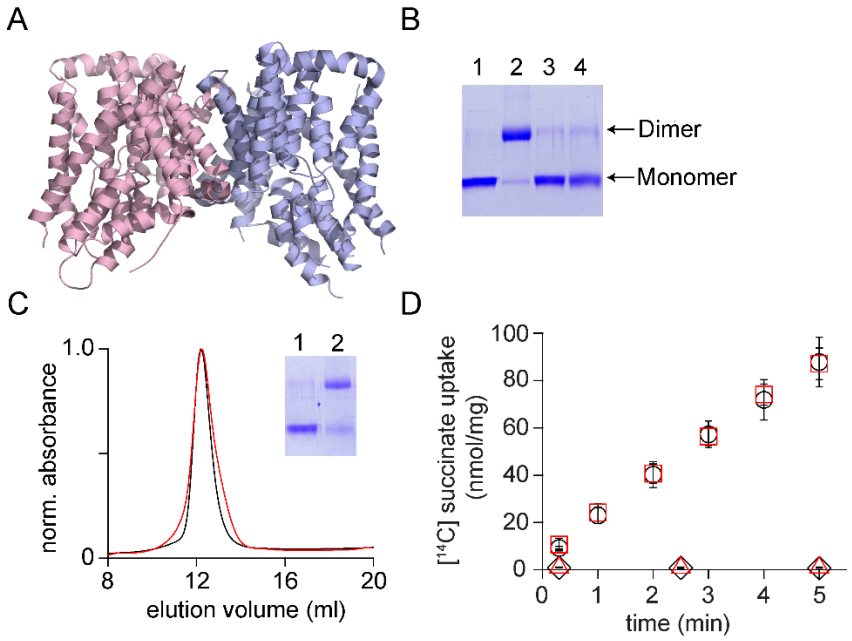

Figure 4.6. *In vitro* assembly of VcINDY. A) Structure of VcINDY (pdb: 4f35) is shown in ribbon representation. **B**) Dissociation of the VcINDY dimer by SDS. SDS-PAGE gel showing the native VcINDY without (lane 1), with glutaraldehyde crosslinking (lane 2) and the SDS dissociated VcINDY without (lane 3) and with glutaraldehyde crosslinking (lane 4). **C**) Size exclusion chromatography of the native (black) and the reassociated VcINDY (r-VcINDY, red). Inset, SDS-PAGE gel showing the glutaraldehyde cross-linking of the peak fraction of r-VcINDY without (lane 1) and with glutaraldehyde crosslinking (lane 2).

D) Succinate uptake assay. The time course of [^{14}C]-succinate uptake by native VcINDY (black circles) and r-VcINDY (red squares) in the presence of a Na^+ gradient. No uptake is observed for native VcINDY (black diamonds) and r-VcINDY (red triangles) in the absence of a Na^+ gradient. Error bars indicate S.E.M. for N $\geq$ 3.

CLC-ec1 is a Cl^-/H^+ antiporter; it is a homodimeric protein in which each subunit consists of 18 helical segments (Figure 4.7A)(267, 268). The CLC-ec1 fold has an internal antiparallel structural repeat with the N-terminal nine helical segments structurally related to the C-terminal segments. The CLC-ec1 fold is very complex and thereby provides an excellent test for the general applicability of the *in vitro* reassembly protocol. Studies on the dimerization of CLC-ec1 have shown that it is one of the strongest membrane protein complexes known (269). Thus, we used a more stringent protocol to ensure complete dissociation of the dimers. Specifically, the protein was precipitated with trichloroacetic acid and acetone, dissolved in trifluoroethanol: buffer A [H_2O and 0.1% (v/v) trifluoroacetic acid] and lyophilized (270). When the lyophilized protein was solubilized in 1% SDS, it migrated as a homogeneous monomer on SDS PAGE (Figure 4.7B).

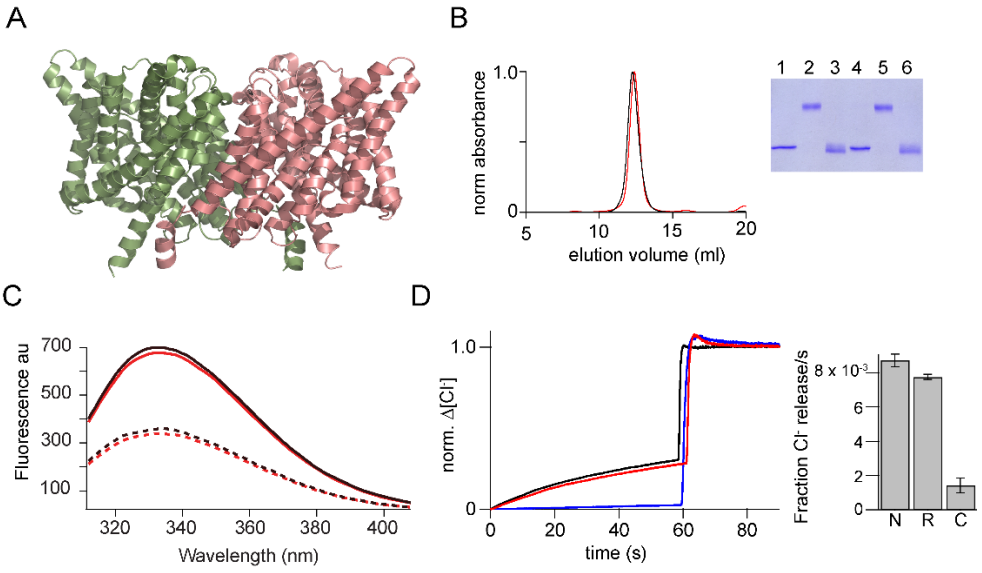

Figure 4.7. *In vitro* assembly of CLC-ec1. A) Structure of CLC-ec1 (pdb: 1kpl) shown in ribbon representation. **B**) Size exclusion chromatography of the native (black) and the *in vitro* assembled CLC-ec1 (r-CLC-ec1, red). Inset, SDS-PAGE gel showing the glutaraldehyde cross-linking of the peak fraction of native and r-CLC-ec1. Native CLC-ec1

without glutaraldehyde crosslinking (lane 1), with glutaraldehyde crosslinking before (lane 2) and after (Lane 3) treatment with 1% SDS. r-CLC-ec1 without glutaraldehyde crosslinking (lane 4), with glutaraldehyde crosslinking before (lane 5) and after (Lane 6) treatment with 1% SDS. **C**) Fluorescence spectra of the native and r-CLC-ec1. Intrinsic fluorescence spectra (excitation at 295 nm) for the native (solid black) and r-CLC-ec1 (solid red) in 50 mMTris-HCl, pH 7.5, 200 mM NaCl, 0.25% DM. Dashed lines show the fluorescence spectra for the native (dashed black) and r-CLC-ec1 (dashed red) after the addition of 1% SDS. **D**) Chloride transport assays. Left: Chloride efflux from liposomes containing native CLC-ec1 (Black), r-CLC-ec1 (red), and no protein control (blue). Bulk efflux was initiated at time zero by the addition of valinomycin. Triton X-100 was added after 60 sec to release all of the intra-vesicular chloride. Chloride efflux was normalized to the total chloride concentration upon addition of Triton X-100. Right: Bar graph showing the normalized rate of chloride movement through liposomes containing native CLC-ec1 (N), r-CLC-ec1 (R), and no protein control (C). Normalized rates were calculated from the initial slope after addition of valinomycin from graphs such as those shown on the left. Error bars represent the S.E.M. from 6 independent flux assays.

To reassemble the dimer, we diluted the SDS solubilized CLC-ec1 subunits into lipid vesicles. Following incorporation into lipid vesicles, glutaraldehyde cross-linking indicated the formation of dimers, suggesting the successful reassembly of CLC-ec1. The reassembled (r-) CLC-ec1 was solubilized in decyl-β-D-maltopyranoside (DM) detergent and purified from lipid vesicles using His_6 tag. SEC of r-CLC-ec1 produced an elution profile that was similar to the native CLC-ec1 (Figure 4.7B). The intrinsic fluorescence spectra of the native CLC-ec1 shows an emission maxima at 333 nm (Figure 4.7C). Addition of SDS results in a 46% decrease in fluorescence intensity. The fluorescence spectra of the r-CLC-ec1 was similar to the native protein and showed a similar decrease in fluorescence intensity on the addition of SDS. The r-CLC-ec1 transporter reconstituted into lipid vesicles mediated chloride flux activity similar to the native protein (Figure 4.7D) suggesting that a fully functional transporter has been reassembled.

Discussion:

Here, we present a facile approach for the *in vitro* reassembly of heteromeric variants of homomeric membrane proteins. The method involves the assembly of the multimeric proteins from dissociated subunits in the context of lipid vesicles. Heteromeric

proteins are obtained simply by mixing wild type and mutant subunits. We established the approach using the Glt_{Ph} transporter and then demonstrated its applicability to a number of other systems including Glt_{Sm}, VcINDY and CLC-ec1 transporters. Using biochemical, functional and single molecule approaches, we show that the reassembled transporters are indistinguishable from native proteins.

Heteromeric Glt_{Ph} transporters allowed us to probe the communication between the Asp binding sites. In typical binding experiments, the presence or absence of coupling between multiple binding sites in multimeric transporters is deduced from the shape of the binding isotherms and corresponding Hill coefficients (271). The Hill coefficients that are greater or less than unity suggest, respectively, positive or negative cooperativity between the binding sites. However, Hill coefficients are relatively poorly determined and can be affected by baseline drifts and noise in the data. Furthermore, the existence of multiple coupled substrate binding sites within single subunits, as for example in BetP (272), may obscure the extent of inter-subunit coupling. The approach that we develop here allows us to circumvent these complications by assembling the reporter subunit together with test subunits that either can or cannot bind substrate with relevant affinity. Using this approach we show that binding to the adjacent test subunits does not affect Asp binding to the reporter subunit thereby establishing unambiguously that the substrate binding sites in Glt_{Ph} are uncoupled.

Whether independent binding sites are a general feature of the multimeric transporters is not fully known, and our approach can provide a facile means of probing for such long-distance interactions between subunits. Interestingly, some transporters are assembled from multiple subunits with substrate-binding sites located at the interfaces, for example, the EmrE and the semi-SWEET transporters (273, 274). The ability to break the intrinsic symmetry of these systems by assembling them from distinct subunits may open novel approaches to probe their mechanisms.

A multitude of spectroscopic approaches to probe the dynamics of transporters and channels has been developed in recent years. Most of them rely on site-specific labeling of introduced cysteine residues. DEER spectroscopy and smFRET microscopy specifically have been applied to study conformational flexibility and dynamics of diverse systems (275, 276). A major challenge in the experimental design is identification of informative labeling sites. Because these approaches are based on distance measurements, an ideal labeling strategy would incorporate two labels at sites that show conformation-dependent distance changes. However, in multimeric proteins this effort is compounded by the presence of multiple subunits, each of which would carry cysteine substitutions. Thus, many of the successful experiments relied on measurements of inter-subunit distance changes (183, 184, 259, 260, 277). Clearly, these approaches have severe limitations when the structural transitions of interest occur within individual subunits. The ability to assemble a multimeric system of interest with single reporter subunits bearing cysteine mutations would significantly expand the repertoire of useful experiments and also facilitate and simplify analysis. We demonstrate the advantage of the reassembled heteromeric proteins by using DEER spectroscopy to probe the conformational state of Glt_{Ph} transporter. Indeed, the distance distribution that was obtained for heteromeric Glt_{Ph} bearing a single labeled subunit is dramatically simplified compared to a homomeric labeled protein, and allows facile determination of the conformational state of the labeled subunit. Similarly, the heteromeric transporters will be useful in introducing fluorescent probes at appropriate sites for smFRET studies of multimeric membrane transporters and channels. For example, we expect significant simplification and increased resolution compared to approaches previously employed to study dynamics of Glt_{Ph} (181, 182).

Many ion channels are homomeric in nature. Ion channels transition between different conformational states during function. Determining the structural nature of these

conformational changes and how these changes are coupled among the individual ion channel subunits is important for understanding their mechanism. The approaches developed herein for the study of transporters can similarly be applied to homomeric ion channels to generate heteromeric variants. These heteromeric variants will provide the ability to alter the amino acid sequence of one or several of the subunits for functional or spectroscopic investigations and will potentially be very useful in probing the mechanism of action.

In our approach, SDS is used to dissociate the multimeric protein. SDS is not a strong denaturant for most membrane proteins and therefore we expect that the SDS-dissociated subunits are only partially unfolded (278). We also used a stringent dissociation process involving treatment with strong acids and organic solvents. Following this stringent dissociation protocol, we were able to observe successful reassembly for only two of the proteins in our test set, Glt_{Ph} and CLC-ec1 while VcINDY and Glt_{Sm} could not be reassembled. This observation suggests that the success of the disassembly/reassembly depends on the gentle dissociation of the multimeric proteins without extensive unfolding of the subunits. Further, lipid bilayers were required for the reassociation process, and a mere dilution of the SDS in the presence of mild detergents did not result in successful reassembly. We speculate that incorporation of the dissociated subunits into lipid bilayers concentrates and orients the subunits to facilitate the assembly.

The overall mechanism of coupled refolding and assembly that takes place in the lipid bilayers is not clear. For CLC-ec1 it was shown that monomers are stable (279) and thus, it is possible that these transporters first assume a native-like fold and then assemble into dimers. The trimeric Glt_{Ph} forms a bowl-like structure in the outward facing state (149). The bowl extends approximately half way across the bilayer; it is lined with polar residues and is most certainly filled with water. It seems unlikely that the

conformation of dissociated Glt_{Ph} monomers is entirely native-like because it would lead to the exposure of the polar regions of the bowl to the hydrophobic milieu of the membrane. Thus, it seems likely that reaching the native conformation is coupled with the trimer assembly in this protein. Our reassembly protocols will be useful to probe the mechanisms of multimeric membrane protein assembly. For example, these processes have been shown to have specific lipid requirements (280). The ability to assemble multimeric membrane proteins in defined lipid environments will facilitate an investigation of how lipid molecules participate in the multimerization process.

While our experiments have only focused on bacterial and archaeal transporters, it will be of great interest to determine whether this simple protocol is applicable also to eukaryotic proteins. Using this procedure for multimeric eukaryotic proteins will involve identifying appropriate detergents for mild dissociation and appropriate compositions of lipid bilayers for reassociation.

Acknowledgements: This research was supported by the grants from the NIH: R01 GM087546 (FV), R37NS085318 (OB, SB and FV), P41GM103521 (JHF, ACERT) and R01 GM123779 (JHF and ERG). PJF was supported by a postdoctoral fellowship from the American Heart Association (12POST11910068).

Methods:

Table 4.1 Key Resources

Reagent type (species) or resource	Designation	Source or reference	Identifiers	Additional information
gene (Pyrococcus horikoshii)	GltPh	10.1038/nature03018	Uniprot ID: O59010	
gene (Vibrio cholerae)	VcINDY	10.1038/nature11542	Uniprot ID: Q9KNE0	
gene (Escherichia coli)	CLC-ec1	10.1085/jgp.200308935	Uniprot ID: P37019	
gene (Staphylothermus marinus)	GltSm	10.1111/febs.12105	Uniprot ID: A3DPQ3	
recombinant DNA reagent	pBCH/G4-GltPh	10.1038/nature03018		
recombinant DNA reagent	pET-VcINDY	10.1038/nature11542		
recombinant DNA reagent	pASK-CLC-ec1	10.1085/jgp.200308935		
recombinant DNA reagent	pBAD-GltSm	This study		GltSm from the GltSm-GFP fusion gene (ref: 10.1111/febs.12105) was cloned into a pBAD-HisA vector (Fisher Scientific)
chemical compound, drug	Asolectin	Avanti Polar Lipids	Cat # 541601G	
Software, algorithm	Pymol	PyMOL Molecular Graphics System, Schröding er, LLC	RRID:SCR_000305	www.pymol.org
Software, algorithm	Matlab	Mathworks	RRID:SCR_001622	www.mathworks.com
Software, algorithm	Origin	Originlab	RRID:SCR_014212	www.originlab.com

Glt_{Ph}

Native Expression. Glt_{Ph} constructs used in this study were expressed from the pBCH/G4 vector (kindly provided by Dr. Eric Gouaux) in *Escherichia coli* TOP10 cells (Fisher Scientific)(149). Protein expression and membrane preparation was carried out as described (155). The membrane vesicles were solubilized using dodecyl-β-D-maltopyranoside [DDM, 2% (w/v)] and Glt_{Ph} was purified by metal affinity chromatography (Ni NTA resin, Qiagen) and size exclusion chromatography (SEC) as described (155). SEC was carried out on a Superdex S-200 column (GE Biosciences) using 20 mM HEPES-NaOH pH 7.5, 200 mM NaCl, and 0.1% (w/v) DDM as the column buffer.

Dissociation and reassociation of Glt_{Ph}. Dissociation of Glt_{Ph} into subunits was carried out by the addition of 1% (w/v) SDS, 0.1 M DTT, 1 mM EDTA and incubation at 45 ^{o}C for 1 hour. Reassociation was carried out by a 10-fold dilution of the SDS-dissociated subunits into 20 mg/ml Asolectin vesicles in lipid buffer (20 mM HEPES-NaOH pH 7.5, 200 mM NaCl, 10 mM DTT, 1 mM Asp) and incubated at room temperature for 5 hours. For purification of the reassociated Glt_{Ph} (r- Glt_{Ph}), the lipid vesicles were dialyzed against 20 mM HEPES-NaOH pH 7.5, 200 mM NaCl for the removal of DTT and EDTA. r-Glt_{Ph} was purified from the lipid vesicles as described for the native protein. For the detergent control, the SDS dissociated Glt_{Ph} was diluted 10-fold into 2% (w/v) DDM in lipid buffer. Following incubation at room temperature for 5 hours, the solution was dialyzed against 20 mM HEPES-NaOH pH 7.5, 200 mM NaCl, 0.1% (w/v) DDM and the protein was purified as described.

Glutaraldehyde crosslinking. The oligomeric state of the proteins was assessed using chemical crosslinking with 0.1 % (w/v) glutaraldehyde for 15 minutes at room temperature. Crosslinking reaction was quenched by the addition of 100 mM Tris. The

samples were electrophoresed on a 12% SDS-PAGE gel and the proteins were visualized by staining with Coomassie Blue.

Aspartate binding assays. Aspartate binding assays were carried out on Glt_{Ph} with a L130W substitution (150). Prior to the binding assay, the Glt_{Ph} sample was extensively dialyzed against the assay buffer [20 mM Tris-HEPES pH 7.4, 200 mM Choline Chloride, 0.1% (w/v) DDM] to remove any bound Asp. The binding assays were carried out using ~100 nM of Glt_{Ph} at 30 ºC in assay buffer containing 10 mM NaCl. Binding of Asp was monitored by the change in the fluorescence emission at 334 nm following excitation at 295 nm. The fraction bound was calculated by normalizing the change in fluorescence following Asp addition to the maximum change observed and K_D was determined by a fit to the equation: $\mathrm{F_b} = \frac{[\mathrm{Asp}]}{\mathrm{K_D}+[\mathrm{Asp}]}$

Aspartate transport assays. For Asp transport assays, the native and r-Glt_{Ph} was reconstituted at into lipid vesicles comprised of a 3: 1 ratio of *Escherichia coli* Polar lipids to 1-palmitoyl-2-oleoyl-glycero-3phosphatidylcholine (POPC) at 6 µg of protein/mg of lipid as previously described (151). The transport assays were carried out in 20 mM Tris-HEPES pH 7.5, 200 mM NaCl, 1 µM valinomycin and 100 nM ^{14}C Asp (Moravek Biochemicals) at room temperature as previously described (155). Background levels of Asp transport was determined in the absence of NaCl, with 100 mM KCl in the assay buffer.

Single Molecule Experiments. Native and r- Glt_{Ph} used for the smFRET experiments carried the N378C substitution. The native and r-Glt_{Ph} molecules were exchanged into Buffer A [20 mM Hepes/NaOH, pH 7.4, 200 mM NaCl, 0.1 mM L-aspartate, 0.1 mM Tris(2-carboxyethyl)phosphine and 40 mM DDM)] using SEC and the proteins were labeled at a concentration of 20 µM in Buffer A with a mixture of maleimide-activated Cy3, Cy5 and biotin-PEG_{11} at 50, 100 and 20 µM final concentrations, respectively

(molar ratio 1:2:0.4), as before(182). Single-molecule experiments were performed using a home-built, prism-based total internal reflection fluorescence instrument constructed around a Nikon TE2000 Eclipse inverted microscope body. Individual molecules were surface immobilized within a streptavidin-coated, passivated microfluidic via the biotin-PEG_{11} moiety (182, 281). All imaging experiments were performed in a buffer containing: 200 mM NaCl and 0.1 mM aspartate, 20 mM Tris-HEPES pH 7.4, 1 mM DDM, 5 mM β-mercaptoethanol, 1 mM cyclooctatetraene, an enzymatic oxygen scavenger system comprising 1 unit/ml glucose oxidase (Sigma), 8 units/ml catalase (Sigma) and 0.1% glucose (282).

Acquired Cy5 intensities (I_{Cy5}) from native and r-Glt_{Ph} molecules were analyzed in MATLAB (Mathworks) using the SPARTAN software package (283) (available at http://www.scottblanchardlab.com/software) and plotted in Origin (OriginLab). FRET trajectories obtained were calculated from the acquired intensities, I_{Cy3} and I_{Cy5}, using the formula FRET = $I_{Cy5}/(I_{Cy3} + I_{Cy5})$. Trajectories for further analysis were selected within the SPARTAN software environment according to the following criteria: a single catastrophic photobleaching event; over 8:1 signal-to-background noise ratio; a FRET lifetime of at least 5 seconds. Population contour plots were constructed by superimposing the FRET data from individual traces. Histograms of these population data were fit to Gaussian functions in Origin (OriginLab).

Assembly of heteromeric Glt_{Ph}. The wild type Glt_{Ph} construct or with the R397A substitution were expressed and purified as described. The His_6 tag present was removed by proteolysis with Thrombin overnight at room temperature. The complete removal of the His_6 tag was confirmed by SDS-PAGE and the protein was purified by SEC as described. Glt_{Ph} protein with the L130W substitution was similarly expressed and purified but in this case the His_6 tag was not removed.

Prior to the mixing experiment, the concentration of the proteins was determined by measuring the absorbance at 280 nm. Since accurate determination of the protein concentration is important, the protein concentrations were confirmed by running a serial dilution of the proteins on a SDS-PAGE gel and comparing the intensity of the protein bands after Coomassie Blue staining. The wild type and the R397A Glt_{Ph} proteins were mixed with the L130W Glt_{Ph} protein in a 10:1 ratio. The protein was then dissociated and reassociated as described. The presence of a His_6 tag on the L130W subunit allows the purification of the Glt_{Ph} heterotrimers with a L130W subunit. The Glt_{Ph} heterotrimers were further purified by SEC. Asp binding assays for the heterotrimeric Glt_{Ph} were carried out as described.

DEER experiments. The Glt_{Ph} construct with cysteine substitutions at 216 and 294 positions was expressed and purified as described above. Following purification, the protein in detergent solution was labelled with the MTSL spin label (1-oxyl-2,2,5,5-tetramethylpyrrolidin-3-yl) methyl methanethiosulfonate; Toronto Research Chemicals) at 20:1 spin label to channel molar ratio. Following overnight labeling at 4 ˚C, the excess label was removed using SEC as described (208). Heteromeric Glt_{Ph} transporters, in which only a single subunit carried the 216, 294 Cys substitutions, were assembled as previously described and spin labelled.

Prior to DEER measurements, the buffer was exchanged to 200 mM NaCl or 200 mM NaCl/300 μM aspartate, 2 mM DDM, 20 mM HEPES pH 7.4, and ca. 80-85% D_2O. (Stock solutions of buffer components in H_2O were mixed and diluted with D_2O to the final concentrations). Subsequently ca. 96 μM Glt_{Ph} monomer solution (i.e., about 32 μM trimer) was mixed with glycerol-d_8 to the final glycerol concentration of 20% (w/v). Sample volumes of about 20 μl were loaded into custom-sized glass capillary tubes (o.d. ~2.6 mm, Wilmad LabGlass, Inc.) and plunge-frozen in liquid N_2 for DEER measurements. All measurements were performed at 60 K using a home-built Ku-band

pulse EPR spectrometer (284) operating at 17.3 GHz as described previously (183, 285). The standard four-pulse DEER experiment (286) used for detection $\pi/2\text{-}t_1\text{-}\pi\text{-}t_2\text{-}\pi$ pulse sequence with respective pulse widths of 16 ns, 32 ns and 32 ns. A 32 ns pump π-pulse, applied at the center peak of nitroxide ESR spectrum, was used throughout all measurements. The frequency separation between detection and pump pulses was 70 MHz to position the detection pulses at the low-field edge of the nitroxide spectrum. Homogeneous (log-linear) signal background decay was removed from the raw DEER data and the background-subtracted DEER signals were normalized to read modulation depths at zero evolution time as described previously. (285) Interspin distances were reconstructed from the background-subtracted DEER data using the L-curve Tikhonov regularization method (287) and refined by the maximum entropy method (288).

Glt_{Sm}

Glt_{Sm} was amplified by PCR from a plasmid carrying the gene for a Glt_{Sm}-GFP fusion protein (265) and cloned into a pBAD-HisA vector (Fisher Scientific) with a N-terminal His_6 tag. The Glt_{Sm} vector was transformed into TOP10 cells (Fisher Scientific) for protein expression. Protein expression and purification of the Glt_{Sm} protein was carried out as described for Glt_{Ph}. Dissociation and reassociation of Glt_{Sm} was carried out using the same protocol used for Glt_{Ph}. The native and reassociated Glt_{Sm} was reconstituted into lipid vesicles comprised of a 3: 1 ratio of *Escherichia coli* polar lipids to POPC at 3 µg of protein/mg of lipid and transport assays were carried out in 20 mM Tris-HEPES pH 7.5, 200 mM NaCl, 1 µM valinomycin and 100 nM ^{14}C Asp at 30 ^{o}C as previously described for the Glt_{Ph} transporter .

VcINDY

Native Expression. VcINDY was expressed from a pET vector (kindly provided by Dr. Joseph Mindell) in *Escherichia coli* BL21-AI (Fisher Scientific) cells as described (2, 266). Following expression, cells were pelleted, suspended in 50 mM Tris-HCl pH 7.5,

200 mM NaCl, 0.25 M sucrose, 1 mM $MgCl_2$ and membranes were prepared as previously described (270). The membranes were solubilized in 2% (w/v) DDM and the VcINDY protein was purified using metal affinity chromatography (Talon, Clontech) followed by SEC. SEC was carried out on a Superdex S200 column (GE Biosciences) using 50 mM HEPES-NaOH (pH 7.5), 200 mM NaCl, 1 mM DTT, 0.1 mM EDTA and 0.1% (w/v) DDM as the column buffer.

Dissociation and Reassociation of VcINDY. Dissociation of VcINDY into subunits was carried out by the addition of SDS to 1% (w/v), 0.1 M DTT, 1 mM EDTA and incubation at 45 ^{o}C for 30 mins. Reassociation was carried out by a 10-fold dilution of the SDS-dissociated subunits into lipid vesicles (20 mg/ml Asolectin in 50 mM HEPES-NaOH, 50 mM Citrate, 100 mM NaCl, 10 mM DTT and incubated overnight at room temperature. For purification of the reassociated (r-) VcINDY, the lipid vesicles were dialyzed against 50 mM Tris-HCl, pH 7.5, 200 mM NaCl to remove the DTT. The lipid vesicles were solubilized and r-VcINDY was purified as described for the native protein.

Succinate transport Assays. The native and the r-VcINDY were reconstituted into liposomes consisting of a 3:1 ratio of *Escherichia coli* Polar lipids to POPC (2). The lipids obtained as chloroform solutions, were dried and re-suspended at a concentration of 10 mg/ml in 10 mM HEPES-KOH, pH 7.5, 100 mM KCl. The lipid solution was subjected to five freeze–thaw cycles with liquid N_2 and then extruded though a 400-nm filter. The lipid vesicles were partially solubilized by the addition of decyl-β-D-maltopyranoside [DM, 0.5% (w/v)]. Protein was added to the lipids at a ratio of 3 μg protein/mg lipid along with another aliquot of DM to bring the detergent concentration to 1.0% (w/v). The protein-lipid mixture was incubated at room temperature for 3-4 hours with gentle shaking and then the detergent was gradually removed, and proteoliposomes were formed by multiple additions of Biobeads (Bio-Rad Laboratories) over 24 hours. The

proteoliposomes were separated from the Biobeads, collected by centrifugation, frozen in aliquots using liquid N_2 and stored at −80°C.

For transport assays, the previously frozen proteoliposomes were thawed and centrifuged at 175,000g for 70 minutes at 4 °C. The pelleted proteoliposomes were re-suspended in the low Na^+ buffer [20 mM Tris-HEPES (pH 7.5), 199 mM KCl, 1 mM NaCl] at 10 mg/ml lipid, subjected to two freeze−thaw cycles with liquid N_2, and extruded through a 400-nm filter. The proteoliposomes were then centrifuged and re-suspended in the low Na^+ buffer at 100 mg/ml lipid. The uptake reaction was initiated by diluting the proteoliposomes 100-fold into the assay buffer [20 mM Tris-HEPES (pH 7.5), 100 mM KCl, 100 mM NaCl and 1 mM ^{14}C-Succinate (Moravek Biochemicals)] at room temperature. For each time point, a 200 µL aliquot was removed and diluted 10-fold into ice-cold quench buffer [20 mM Tris-HEPES (pH 7.5), 100 mM choline chloride] followed by filtration over nitrocellulose filters (0.22 µm, Millipore). Filters were washed thrice with 2 mL of ice-cold quench buffer and assayed for radioactivity. Background levels of ^{14}C-Succinate uptake were determined in the absence of a sodium gradient (1 mM Na^+ on both sides).

CLC-ec1

Dissociation of the CLC-ec1 dimer. CLC-ec1 containing a C-terminal polyhistidine tag was overexpressed in *Escherichia coli* BL21 (DE3) cells and purified as described (289). Dissociation of the CLC-ec1 was carried out as described for the K_vAP channel (270). Briefly, Triton X-100 was added to the CLC-ec1 solution to 2% (v/v), and the protein was precipitated by the addition of trichloroacetic acid to 15% (w/v) and incubated at 4 °C for 30 min. The protein precipitate was collected by centrifugation, washed twice with acetone and 0.1% TFA (trifluoroacetic acid), and then solubilized in 50% TFE (trifluoroethanol) and 0.1% TFA. The TFE solution was lyophilized to provide the dissociated CLC-ec1 that was used for *in vitro* assembly.

In vitro assembly of CLC-ec1. The lyophilized CLC-ec1 was dissolved in 50 mM HEPES-NaOH pH 7.4, 200 mM NaCl, 10 mM EDTA, 0.1 M DTT, 1% (w/v) SDS and diluted 10-fold into lipid vesicles (20 mg/ml asolectin in 50 mM HEPES-NaOH, 200 mM NaCl, 10 mM DTT) and incubated overnight at room temperature. For purification, the lipid vesicles were initially dialyzed against 50 mM Tris-HCl, pH 7.5, 200 mM NaCl to remove the DTT and EDTA. The lipid vesicles were then solubilized and the *in vitro* assembled CLC-ec1 (r-CLC-ec1) was purified as described for the native protein.

Chloride flux assays for CLC-ec1. The native and r-CLC-ec1 channels were reconstituted into liposomes and Cl^- flux assays were carried out similarly to that previously described (290) with some minor differences. Briefly, ClC-ec1 was reconstituted into *E. coli* polar lipids at a concentration of 0.4 µg of protein per mg lipid. Detergent was removed to form liposomes by dialysis against 300 mM KCl, 25 mM citrate pH 4.5. For flux assays, vesicles were freeze-thawed five times in dry ice/acetone and extruded through a 400 nm filter. Extra-vesicular solution was exchanged by centrifuging 60 µL of extruded vesicles through a 1.5 mL Sephadex G-50 column equilibrated in Flux Buffer (100 mM K_2SO_4, 0.05 mM KCl, 25 mM anhydrous citrate pH 4.5 with NaOH). The vesicles were then diluted into Flux buffer and extra-vesicular chloride concentration was monitored with an Ag/AgCl electrode. Chloride efflux was initiated with ~5.8 µM valinomycin, and after an additional 1 minute, vesicles were broken upon with addition of ~0.13% Triton X-100. Flux was normalized to the total amount of chloride release after addition of Triton X-100.

Appendix D: Supplementary Information

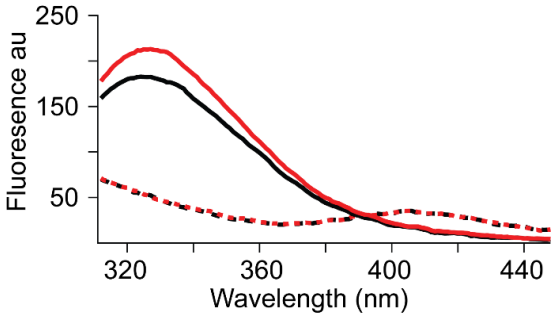

Figure S4.1. Spectral properties of wild type and L130W-Glt$_{Ph}$. Fluorescence emission spectra of the L130W-Glt$_{Ph}$ in 10 mM NaCl (solid black) and after addition of 100 µM Asp (solid red) with excitation at 295 nm. Spectra of the wild type Glt$_{Ph}$ before (dashed black) and after the addition of 100 µM Asp (dashed red). Equal amounts (50 nM) of the wild type and the L130W-Glt$_{Ph}$ protein was used for measuring the spectra. An increase in fluorescence at 334 nm is observed on Asp binding by L130W-Glt$_{Ph}$. No corresponding fluorescence change is observed for the wild type Glt$_{Ph}$.

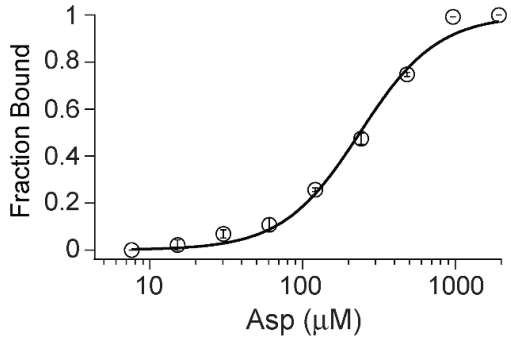

Figure S4.2. Asp binding by R397A-Glt$_{Ph}$. Asp binding by R397A-Glt$_{Ph}$ with the L130W substitution in 10 mM Na^+ was carried out as described in legend to figure 1. The R397A substitution (K_D = 238 µM) causes a ~ 1300 fold decrease in affinity for Asp binding compared to the wild type Glt$_{Ph}$ (K_D = 0. 183 µM). Error bars indicate S.E.M. for n $\geq$ 3.

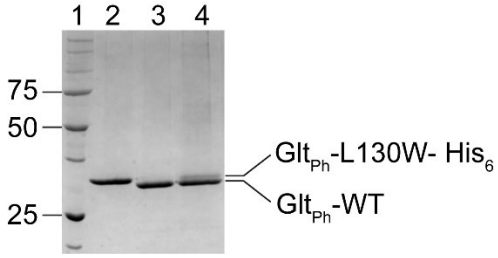

Figure S4.3. Assembly of heteromeric Glt$_{Ph}$. A heteromeric Glt$_{Ph}$ with two wild type subunits and one subunit with the L130W substitution was assembled using the protocol diagrammed in figure 3A. SDS-PAGE gel showing molecular weight markers (Lane 1), the L130W-Glt$_{Ph}$ His$_6$ (lane 2), wild type Glt$_{Ph}$ (Lane 3) and heterotrimeric Glt$_{Ph}$ (Lane 4). The presence of both the subunits in the heterotrimeric Glt$_{Ph}$ is shown.

Chapter 5: Concluding Remarks

At the start of my thesis research, there was a wealth of functional and biochemical data on the overall transport cycle of EAATs with only a few structures available to describe rearrangements of glutamate transporters along the transport cycle. The stoichiometry and basic steps in the transport cycle were determined for EAATs as well as the prokaryotic homolog, Glt_{Ph}. Both EAATs and Glt_{Ph} couple three Na^+ ions to the translocation of one molecule of substrate and isomerize the transport domain between OFS and IFS through an elevator mechanism. Our knowledge of the transport mechanism has been greatly enhanced by the use of the archaeal homolog, Glt_{Ph}, including the structural basis for the elevator mechanism and the sequential binding events necessary for transport. The allosteric coupling mechanism necessary to regulate both binding site rearrangements and extracellular gate movement to accomplish substrate translocation was unknown. My thesis work has focused on filling the gap in understanding of the molecular mechanism underlying the coupling mechanism in glutamate transporters. During the course of this thesis research, several structural studies were able to populate steps of the transport cycle and resolve distinct conformations of the binding site in different ligand states (for example OFS: Apo, Na^+ only, Na^+/TBOA, Na^+/Asp). I was able to exploit these structural data to use in conjunction with novel functional assays and mutagenesis studies to elucidate the coupling mechanism at a molecular resolution.

Extracellular gate movement is one of the main components which determines the ability of the transporter to bind and translocate substrate. In the coupling mechanism, Na^+ binding at the Na1 and Na3 sites causes both rearrangements in the binding site and the extracellular gate. Both structural and spectroscopic studies confirm that in the presence of Na^+, the extracellular gate is open(203, 208). Therefore, HP2 opening can take place through two different mechanisms: Na^+ binding induces HP2

opening through an allosteric mechanism (induced fit) or Na^+ binding traps the protein in the HP2 open state (conformational selection). The first step in investigating the coupling mechanism was to determine how Na^+ binding accomplishes HP2 opening. One of the main limitations to addressing this essential process was a lack of tools to monitor protein dynamics. As presented in Chapter 2, I was able to develop a fluorescence-based assay to monitor HP2 movement using dual probe incorporation. By collecting the rates of opening at different Na^+ concentrations, I was able to establish that HP2 opens in an induced fit mechanism, meaning the allosteric changes which occur upon Na^+ binding are responsible for opening HP2. This was further supported by kinetics experiments of Na^+ binding in Chapter 3.

Several binding site residues which undergo Na^+ based conformational changes were identified through structural analysis(154, 164). Candidate residues were screened for a role in the coupling process before assessing their potential role in Na^+ induced HP2 opening. Through steady state and kinetic studies of residue substitutions in the HP2 movement assay, I was able to propose a mechanism for how HP2 is opened. Briefly, Na^+ binds to Na1/3 sites which causes rearrangements in the NMDGT, specifically M311 and T314. Na^+ binding causes M311 to flip toward the binding site where it serves as a wedge to break HP1-HP2 interactions and keep HP2 open. T314 moves toward the binding site to push R397 out of the binding site into the flipped conformation. T314 is further stabilized in the Na^+ bound conformation through side chain interactions with N401. The movement of R397 out of the binding site disrupts HP2 interactions to allow for full opening and stabilization of the flipped R397 conformation which is essential for efficient, coupled HP2 opening. Once HP2 is open, substrate can bind and partially close HP2. Na2 binding is then needed to overcome the M311 wedge for full HP2 closure so the transporter can translocate substrate. This mechanism explains why substrate cannot bind without Na^+ since Na^+ is responsible for

rearrangements of substrate coordination residues and HP2 opening necessary to bind substrate.

The determined pathway between Na^+ binding and HP2 opening is comprised of various binding site rearrangements, but the specific molecular consequence of Na^+ binding to the Na1 and Na3 sites individually was initially undetermined. To probe the beginning steps of the coupling process involving Na^+ binding, I developed two additional fluorescence-based assays to monitor the initial Na^+ binding event and the intrinsically linked Na^+ induced NMDGT rearrangements. These assays along with the HP2 movement assay permitted full coverage of key events in the coupling mechanism. These assays, when paired with Na^+ site perturbations, allowed for specific roles of the Na1 and Na3 sites to be elucidated. Through individually perturbing the Na^+ sites, I found that Na1 binding causes partial HP2 opening which supports low affinity substrate binding, Na3 binding is predominately responsible for NMDGT rearrangements, and both Na1 and Na3 binding are needed for efficient HP2 opening and high affinity substrate binding. From previous studies and my new data on the consequences of binding at Na1 and Na3 sites, I was able to further refine my proposed coupling mechanism for HP2 opening. Briefly, Na1 binds first to the Apo transporter, breaking the hydrogen bond network which keeps the binding site and HP2 locked in Apo conformation. Na1 binding allows for HP2 to partially open and support low affinity substrate binding. The second Na^+ ion then binds to the Na3 site by way of the Na1 site or through an alternative path revealed in the partially open HP2 state and causes the necessary rearrangements in the NMDGT. With both Na1 and Na3 bound, the binding site is fully rearranged to support full HP2 opening and high affinity substrate binding. This mechanism explains two features of transport: substrate binding at low Na^+ and the ability of substrate to improve the affinity of Na^+. The Na1 bound state is responsible for the ability to bind substrate at low Na^+ even when HP2 is not fully open and how substrate can improve

Na^+ affinity. Therefore, substrate binds in a mix of two modes: the Na1 bound and Na1/3 bound states dependent on Na^+ concentration.

With the studies presented in Chapter 2 and 3, the HP2 opening arm of the coupling mechanism is resolved for Glt_{Ph}. The same key residues which have been identified in the Na^+ induced conformational wave are conserved in EAATs and therefore our newfound understanding of the coupling process in Glt_{Ph} can be applied to EAATs. Another indication that our findings are applicable is the fact that these key conserved players have similar secondary structure placement in EAATs. By comparing the differences between Glt_{Ph} and EAATs in transport, we can also gain insight into the transport mechanism. For example, the single side chain residue for Na1 site, D405, has been studied extensively both in Glt_{Ph} and in EAATs with varying effects. In Glt_{Ph}, there is a loss of Na^+ affinity with D405N and a loss of Na^+ dependence for substate binding while different studies in EAATs report a wide variety of effects on Na^+ affinity, substrate affinity and translocation, and K^+ countertransport(133, 166, 167). In my proposed mechanism Na1 binding partially opens HP2 and disrupts Apo-R397 positioning in Glt_{Ph}. Recently solved EAAT3 structures show that in the Apo-IFS, HP2 is already slightly open and the analogous R397 residue has an altered position partially out of the binding site and interacts with E374 instead of HP2 (protonation site)(197). The role for D405 to coordinate Na^+ at the Na1 site therefore may be masked by the additional Apo state position of R397 and HP2 in EAATs. Differences with the D405N mutation also alludes to the role of H^+ in the coupled binding process for EAATs involving R397 which would explain why D405 substitutions have less impact on the overall transport process when compared to Glt_{Ph}. Both differences and similarities between transport in EAATs and Glt_{Ph} can reveal insights into the transport mechanism.

In addition to the fluorescence assays, I also helped to validate and apply a new methodology to generate of heteromeric variants of homomeric membrane proteins in

Chapter 4. The methodology helps to address challenges in investigations of transporters which are homomeric. In spectroscopic studies such as DEER and smFRET, it is preferential to label one subunit to limit the number of probes reporting on conformational changes in order to make spectroscopic measurements easier. Heteromeric variants of monomeric proteins can be generated through alternative methods, but there is usually a large hit in protein yield. The dissociation and reassociation of oligomers presented in Chapter 4 utilizes recombinantly expressed proteins (increased protein yield) which can be mixed in defined ratios to get the desired heteromeric proteins. Most of my thesis research was focused on assay development and studying the coupling mechanism within a glutamate transporter protomer. With the *in vitro* reassembly methodology, I was able to probe coupled binding between protomers. It was previously established that each protomer can translocate independently, but I was able to assess if there is cross talk between subunits in substrate binding. As expected, coupled binding of substrate is independent from other subunits in the trimer.

The second arm of the coupling mechanism involves HP2 closure in the OFS. As presented in Appendix C, I have preliminary data exploring protein-substrate interactions which are necessary for HP2 closure. These data are consistent with a substrate assisted closure mechanism since different chemical moieties on the substrate affect the extent of HP2 closure differentially. Substrate backbone interactions are essential for substrate binding while the side chain moiety and size determine the extent of HP2 closure. More experiments are necessary to flesh out a mechanism for coupled HP2 closure such as further testing the effects of the analogue substrate series, HP mutant's effect on substrate binding, and kinetics experiment of HP2 closure to define a kinetic mechanism. Experiments using the HP2 movement assay can be used to explore the role of the Na2 site in both substrate binding and HP2 closure. Na^+ ion binding to the

Na2 site which is mainly formed from HP2 residues follows substrate binding. Perturbing the Na2 site and monitoring the functional effects will help inform the last piece in sequential binding: the role of Na2 site. It is then possible to differentiate if the Na2 site is necessary for HP2 closure or mainly a stabilizing binding event which follows both substrate binding and HP2 closure. With additional experiments using a combination of HP2 movement data, mutagenesis, alternative substrate series and kinetics, the second arm of the coupling mechanism in OFS can be determined.

A related area of research which can be addressed with HP2 closure experiments would be to test the substrate analogues along with proposed cancer drugs in a Glt_{Ph} modeled after ASCT1 and ASCT2. The experiments on altered Glt_{Ph} could inform on potential selectivity difference between the two isoforms. ASCT1 and ASCT2 differ in three key residues compared to Glt_{Ph} (T314 to Ala, R397, and T352 to Ala) which can be altered to confer different substrate selectivity in ASCT (291). At the corresponding Glt_{Ph} R397 position, the two isoforms differ where ASCT1 has a Thr while ASCT2 has a Cys. In previous studies with Glt_{Ph}, a Cys substitution at R397 resulted in altered selectivity for neutral amino acids and mimics ASCT2(153). It is an objective, when developing cancer therapeutics, to create selective molecules that will only inhibit one subtype of neutral amino acid transporters. By exploiting my Glt_{Ph} assays, the potential differences between ASCT isoforms can be characterized to inform selective inhibitor design.

An additional avenue of research would be to further develop the HP2 movement assay. This would consist of additional experiments to determine the mechanism for fluorescence changes, characterize HP2 motions in a lipid environment, and adapt the assay for other proteins. Lifetime measurements monitoring the Trp in the HP2 movement assay will determine the mechanism for Trp quenching by Phe_{CN}. By looking at the change in decay times and intensities, one can conclude if the quenching is

dynamic or static(233, 292). This data will also help define limitations to the probe pair's placement within a protein. Another area of enhancement of the HP2 movement assay is to test the fluorescence changes for both steady state and kinetics measurements in a lipid environment. Recombinant UAA containing Glt_{Ph} would be reconstituted into defined lipid environments to create protein containing nanodiscs. The use of polarized light and nanodiscs instead of liposomes will help to overcome lipid scattering in fluorescence measurements and maximize the signal change. The effects of different lipid composition on binding events and the coupling process would be explored as well as the potential role of specific lipids identified in new cryo-EM structures.

The final developmental stage for the HP2 movement assay would be to apply the dual probe incorporation to monitor protein dynamics in another transporter or another protein. The applicability of the dual-probe pair (Phe_{CN}/W) involves two key factors: what system the protein of interest is expressed in (pertaining to ability to incorporate UAA) and how many native Trps the protein contains (magnitude and specificity of signal change). Since one component of the probe pair is the unnatural amino acid Phe_{CN}, whatever system the protein of interest is expressed in must have a biorthogonal tRNA/tRNA synthetase pair available to accomplish nonsense-suppression UAA incorporation or be amenable to semisynthetic strategies for UAA incorporation. The other component of the probe pair is Trp which is the source of the fluorescence emission monitored for the movement assay. Most proteins have multiple Trp residues and to use the Phe_{CN}/Trp pair, the other Trps must be silenced to ensure monitoring of a specific event and the maximal fluorescence signal change. In Glt_{Ph}, the magnitude of fluorescence change is enough to tolerate the presence of an additional Trp and therefore silencing all Trps may not be necessary in other proteins. EAATs are next logical protein target to adapt the probe pair to monitor HP2 movement. The applicability of the HP2 movement assay to EAATs relies on the ability to produce enough UAA

incorporated eukaryotic protein to purify and perform experiments and the ability to silence the three to four native Trp residues. To circumvent the need for eukaryotic protein purification, the HP2 movement assay could be adapted into a cell-based plate reading assay. A cell-based assay would require a Trp analogue with unique fluorescence emission to ensure Trp residues in the cell do not contribute to the fluorescence monitored. But to incorporate a useful Trp analogue such as 4-cyanoTrp(293), the orthogonal tRNA/tRNA synthetase pair would have to be developed. Besides eukaryotic EAATs, a prime candidate for adapting the dual probe distance dependent quenching assay would be other transporters with similar topology and gates such as CNT_{NW}. CNT_{NW} is a nucleoside transporter which utilizes an elevator mechanism to isomerize between OFS and IFS and has two hairpin loops which help form the binding site(294). CNT_{NW} only has four native Trp residues to be silenced for maximal signal change and is readily expressed recombinantly in *E.coli*. A similar mechanistic understanding of gate movement could be explored in CNT_{NW} through a similar movement assay as well as demonstrate if the gating mechanism found in Glt_{Ph} is broadly applicable.

To fully complete our understanding of the allosteric coupled binding process, findings for Glt_{Ph} need to be validated in EAATs and expanded to incorporate the additional ions EAATs require for the transport cycle. EAATs can be readily expressed in *Xenopus* oocytes for functional experiments and this system is also amenable to unnatural amino acid incorporation. The lab has expertise in UAA incorporation to allow for an expansion of chemical modification which can be made to explore different facets of chemical properties. One application would be the perturbation of the Na^+ sites through altering the backbone chemistry from amide to ester instead of side chain substitutions. In addition to investigating forward transport to corroborate the mechanism determined in Glt_{Ph}, the role of H^+ in EAATs can be explored for forward transport. One

of the main areas of unknowns for glutamate transporters is how the additional ions, H^+ and K^+, factor into the molecular coupling mechanism as well as where the K^+ site is located.

Using the assays I have developed along with mutagenesis and complementary techniques, the molecular mechanism for coupled binding necessary for extracellular gate opening in Glt_{Ph} has been resolved. These same assays can be used to elucidate the second arm in the coupling mechanism involving HP2 closure. The HP2 movement assay can also be adapted for other proteins to study their respective transport mechanisms and/or conformational dynamics. Future studies on the transport cycle should focus on understanding how a H^+ is incorporated into fully loading the transporter and how K^+ binding is coupled to the IFS to OFS transition. The second large remaining unknown in the field is the mechanism of substrate release. This process can be partially addressed through studies in Glt_{Ph} using the HP2 movement assay, trapped OFS/IFS, and mutagenesis studies.

References

1. Wright EM, Loo DD, Hirayama BA. Biology of human sodium glucose transporters. Physiol Rev. 2011;91(2):733-94.

2. Mulligan C, Fitzgerald GA, Wang DN, Mindell JA. Functional characterization of a Na+-dependent dicarboxylate transporter from Vibrio cholerae. J Gen Physiol. 2014;143(6):745-59.

3. Godoy A, Ormazabal V, Moraga-Cid G, Zuniga FA, Sotomayor P, Barra V, et al. Mechanistic insights and functional determinants of the transport cycle of the ascorbic acid transporter SVCT2. Activation by sodium and absolute dependence on bivalent cations. J Biol Chem. 2007;282(1):615-24.

4. Shafqat S, Tamarappoo BK, Kilberg MS, Puranam RS, McNamara JO, Guadano-Ferraz A, et al. Cloning and expression of a novel Na(+)-dependent neutral amino acid transporter structurally related to mammalian Na+/glutamate cotransporters. J Biol Chem. 1993;268(21):15351-5.

5. Storck T, Schulte S, Hofmann K, Stoffel W. Structure, expression, and functional analysis of a Na(+)-dependent glutamate/aspartate transporter from rat brain. Proc Natl Acad Sci U S A. 1992;89(22):10955-9.

6. Carland JE, Thomas M, Mostyn SN, Subramanian N, O'Mara ML, Ryan RM, et al. Molecular Determinants for Substrate Interactions with the Glycine Transporter GlyT2. ACS Chem Neurosci. 2018;9(3):603-14.

7. Rudnick G, Sandtner W. Serotonin transport in the 21st century. J Gen Physiol. 2019;151(11):1248-64.

8. Arriza JL, Eliasof S, Kavanaugh MP, Amara SG. Excitatory amino acid transporter 5, a retinal glutamate transporter coupled to a chloride conductance. Proc Natl Acad Sci U S A. 1997;94(8):4155-60.

9. Fairman WA, Vandenberg RJ, Arriza JL, Kavanaugh MP, Amara SG. An excitatory amino-acid transporter with properties of a ligand-gated chloride channel. Nature. 1995;375(6532):599-603.

10. Arriza JL, Fairman WA, Wadiche JI, Murdoch GH, Kavanaugh MP, Amara SG. Functional comparisons of three glutamate transporter subtypes cloned from human motor cortex. J Neurosci. 1994;14(9):5559-69.

11. Utsunomiya-Tate N, Endou H, Kanai Y. Cloning and functional characterization of a system ASC-like Na+-dependent neutral amino acid transporter. J Biol Chem. 1996;271(25):14883-90.

12. Pines G, Danbolt NC, Bjoras M, Zhang Y, Bendahan A, Eide L, et al. Cloning and expression of a rat brain L-glutamate transporter. Nature. 1992;360(6403):464-7.

13. Kanai Y, Hediger MA. Primary structure and functional characterization of a high-affinity glutamate transporter. Nature. 1992;360(6403):467-71.

14. Danbolt NC. Glutamate uptake. Prog Neurobiol. 2001;65(1):1-105.

15. Rothstein JD, Dykes-Hoberg M, Pardo CA, Bristol LA, Jin L, Kuncl RW, et al. Knockout of glutamate transporters reveals a major role for astroglial transport in excitotoxicity and clearance of glutamate. Neuron. 1996;16(3):675-86.

16. Lehre KP, Danbolt NC. The number of glutamate transporter subtype molecules at glutamatergic synapses: chemical and stereological quantification in young adult rat brain. J Neurosci. 1998;18(21):8751-7.

17. Furness DN, Lehre KP. Immunocytochemical localization of a high-affinity glutamate-aspartate transporter, GLAST, in the rat and guinea-pig cochlea. Eur J Neurosci. 1997;9(9):1961-9.

18. Rauen T, Rothstein JD, Wassle H. Differential expression of three glutamate transporter subtypes in the rat retina. Cell Tissue Res. 1996;286(3):325-36.

19. Berger UV, Hediger MA. Distribution of the glutamate transporters GLAST and GLT-1 in rat circumventricular organs, meninges, and dorsal root ganglia. J Comp Neurol. 2000;421(3):385-99.

20. Matthews JC, Beveridge MJ, Malandro MS, Rothstein JD, Campbell-Thompson M, Verlander JW, et al. Activity and protein localization of multiple glutamate transporters in gestation day 14 vs. day 20 rat placenta. Am J Physiol. 1998;274(3):C603-14.

21. Martinez-Lopez I, Garcia C, Barber T, Vina JR, Miralles VJ. The L-glutamate transporters GLAST (EAAT1) and GLT-1 (EAAT2): expression and regulation in rat lactating mammary gland. Mol Membr Biol. 1998;15(4):237-42.

22. King N, Lin H, McGivan JD, Suleiman MS. Aspartate transporter expression and activity in hypertrophic rat heart and ischaemia-reperfusion injury. J Physiol. 2004;556(Pt 3):849-58.

23. Martinov V, Dehnes Y, Holmseth S, Shimamoto K, Danbolt NC, Valen G. A novel glutamate transporter blocker, LL-TBOA, attenuates ischaemic injury in the isolated, perfused rat heart despite low transporter levels. Eur J Cardiothorac Surg. 2014;45(4):710-6.

24. Brakspear KS, Mason DJ. Glutamate signaling in bone. Front Endocrinol (Lausanne). 2012;3:97.

25. Huggett J, Vaughan-Thomas A, Mason D. The open reading frame of the Na(+)-dependent glutamate transporter GLAST-1 is expressed in bone and a splice variant of this molecule is expressed in bone and brain. FEBS Lett. 2000;485(1):13-8.

26. Furness DN, Dehnes Y, Akhtar AQ, Rossi DJ, Hamann M, Grutle NJ, et al. A quantitative assessment of glutamate uptake into hippocampal synaptic terminals and astrocytes: new insights into a neuronal role for excitatory amino acid transporter 2 (EAAT2). Neuroscience. 2008;157(1):80-94.

27. Furuta A, Rothstein JD, Martin LJ. Glutamate transporter protein subtypes are expressed differentially during rat CNS development. J Neurosci. 1997;17(21):8363-75.

28. Melone M, Bellesi M, Conti F. Synaptic localization of GLT-1a in the rat somatic sensory cortex. Glia. 2009;57(1):108-17.

29. Melone M, Bellesi M, Ducati A, Iacoangeli M, Conti F. Cellular and Synaptic Localization of EAAT2a in Human Cerebral Cortex. Front Neuroanat. 2011;4:151.

30. Tanaka K, Watase K, Manabe T, Yamada K, Watanabe M, Takahashi K, et al. Epilepsy and exacerbation of brain injury in mice lacking the glutamate transporter GLT-1. Science. 1997;276(5319):1699-702.

31. Hu QX, Ottestad-Hansen S, Holmseth S, Hassel B, Danbolt NC, Zhou Y. Expression of Glutamate Transporters in Mouse Liver, Kidney, and Intestine. J Histochem Cytochem. 2018;66(3):189-202.

32. Najimi M, Stephenne X, Sempoux C, Sokal E. Regulation of hepatic EAAT-2 glutamate transporter expression in human liver cholestasis. World J Gastroenterol. 2014;20(6):1554-64.

33. Noorlander CW, de Graan PN, Nikkels PG, Schrama LH, Visser GH. Distribution of glutamate transporters in the human placenta. Placenta. 2004;25(6):489-95.

34. Haugeto O, Ullensvang K, Levy LM, Chaudhry FA, Honore T, Nielsen M, et al. Brain glutamate transporter proteins form homomultimers. J Biol Chem. 1996;271(44):27715-22.

35. Conti F, DeBiasi S, Minelli A, Rothstein JD, Melone M. EAAC1, a high-affinity glutamate tranporter, is localized to astrocytes and gabaergic neurons besides pyramidal cells in the rat cerebral cortex. Cereb Cortex. 1998;8(2):108-16.

36. Holmseth S, Dehnes Y, Huang YH, Follin-Arbelet VV, Grutle NJ, Mylonakou MN, et al. The density of EAAC1 (EAAT3) glutamate transporters expressed by neurons in the mammalian CNS. J Neurosci. 2012;32(17):6000-13.

37. Kugler P, Schmitt A. Glutamate transporter EAAC1 is expressed in neurons and glial cells in the rat nervous system. Glia. 1999;27(2):129-42.

38. Rothstein JD, Martin L, Levey AI, Dykes-Hoberg M, Jin L, Wu D, et al. Localization of neuronal and glial glutamate transporters. Neuron. 1994;13(3):713-25.

39. Bjorn-Yoshimoto WE, Underhill SM. The importance of the excitatory amino acid transporter 3 (EAAT3). Neurochem Int. 2016;98:4-18.

40. Hediger MA. Glutamate transporters in kidney and brain. Am J Physiol. 1999;277(4):F487-92.

41. Burckhardt BC, Burckhardt G. Interaction of Excitatory Amino Acid Transporters 1 - 3 (EAAT1, EAAT2, EAAT3) with N-Carbamoylglutamate and N-Acetylglutamate. Cell Physiol Biochem. 2017;43(5):1907-16.

42. Bailey CG, Ryan RM, Thoeng AD, Ng C, King K, Vanslambrouck JM, et al. Loss-of-function mutations in the glutamate transporter SLC1A1 cause human dicarboxylic aminoaciduria. J Clin Invest. 2011;121(1):446-53.

43. Peghini P, Janzen J, Stoffel W. Glutamate transporter EAAC-1-deficient mice develop dicarboxylic aminoaciduria and behavioral abnormalities but no neurodegeneration. EMBO J. 1997;16(13):3822-32.

44. Dehnes Y, Chaudhry FA, Ullensvang K, Lehre KP, Storm-Mathisen J, Danbolt NC. The glutamate transporter EAAT4 in rat cerebellar Purkinje cells: a glutamate-gated chloride channel concentrated near the synapse in parts of the dendritic membrane facing astroglia. J Neurosci. 1998;18(10):3606-19.

45. Pow DV, Barnett NL. Developmental expression of excitatory amino acid transporter 5: a photoreceptor and bipolar cell glutamate transporter in rat retina. Neurosci Lett. 2000;280(1):21-4.

46. Wersinger E, Schwab Y, Sahel JA, Rendon A, Pow DV, Picaud S, et al. The glutamate transporter EAAT5 works as a presynaptic receptor in mouse rod bipolar cells. J Physiol. 2006;577(Pt 1):221-34.

47. Lee A, Anderson AR, Stevens M, Beasley S, Barnett NL, Pow DV. Excitatory amino acid transporter 5 is widely expressed in peripheral tissues. Eur J Histochem. 2013;57(1):e11.

48. Nothmann D, Leinenweber A, Torres-Salazar D, Kovermann P, Hotzy J, Gameiro A, et al. Hetero-oligomerization of neuronal glutamate transporters. J Biol Chem. 2011;286(5):3935-43.

49. Arriza JL, Kavanaugh MP, Fairman WA, Wu YN, Murdoch GH, North RA, et al. Cloning and expression of a human neutral amino acid transporter with structural similarity to the glutamate transporter gene family. J Biol Chem. 1993;268(21):15329-32.

50. Nalecz KA. Solute Carriers in the Blood-Brain Barier: Safety in Abundance. Neurochem Res. 2017;42(3):795-809.

51. Broer A, Brookes N, Ganapathy V, Dimmer KS, Wagner CA, Lang F, et al. The astroglial ASCT2 amino acid transporter as a mediator of glutamine efflux. J Neurochem. 1999;73(5):2184-94.

52. Dolinska M, Zablocka B, Sonnewald U, Albrecht J. Glutamine uptake and expression of mRNA's of glutamine transporting proteins in mouse cerebellar and cerebral cortical astrocytes and neurons. Neurochem Int. 2004;44(2):75-81.

53. Dun Y, Mysona B, Itagaki S, Martin-Studdard A, Ganapathy V, Smith SB. Functional and molecular analysis of D-serine transport in retinal Muller cells. Exp Eye Res. 2007;84(1):191-9.

54. Gliddon CM, Shao Z, LeMaistre JL, Anderson CM. Cellular distribution of the neutral amino acid transporter subtype ASCT2 in mouse brain. J Neurochem. 2009;108(2):372-83.

55. Foster AC, Farnsworth J, Lind GE, Li YX, Yang JY, Dang V, et al. D-Serine Is a Substrate for Neutral Amino Acid Transporters ASCT1/SLC1A4 and ASCT2/SLC1A5, and Is Transported by Both Subtypes in Rat Hippocampal Astrocyte Cultures. PLoS One. 2016;11(6):e0156551.

56. Rosenberg D, Artoul S, Segal AC, Kolodney G, Radzishevsky I, Dikopoltsev E, et al. Neuronal D-serine and glycine release via the Asc-1 transporter regulates NMDA receptor-dependent synaptic activity. J Neurosci. 2013;33(8):3533-44.

57. Martineau M, Parpura V, Mothet JP. Cell-type specific mechanisms of D-serine uptake and release in the brain. Front Synaptic Neurosci. 2014;6:12.

58. El-Hattab AW. Serine biosynthesis and transport defects. Mol Genet Metab. 2016;118(3):153-9.

59. Hashimoto Y, Sadamoto Y, Konno A, Kon Y, Iwanaga T. Distribution of neutral amino acid transporter ASCT 1 in the non-neuronal tissues of mice. Jpn J Vet Res. 2004;52(3):113-24.

60. Broer S, Fairweather SJ. Amino Acid Transport Across the Mammalian Intestine. Compr Physiol. 2018;9(1):343-73.

61. Vandenberg RJ, Ryan RM. Mechanisms of glutamate transport. Physiol Rev. 2013;93(4):1621-57.

62. Allen NJ, Karadottir R, Attwell D. Reversal or reduction of glutamate and GABA transport in CNS pathology and therapy. Pflugers Arch. 2004;449(2):132-42.

63. Rossi DJ, Oshima T, Attwell D. Glutamate release in severe brain ischaemia is mainly by reversed uptake. Nature. 2000;403(6767):316-21.

64. Ketheeswaranathan P, Turner NA, Spary EJ, Batten TF, McColl BW, Saha S. Changes in glutamate transporter expression in mouse forebrain areas following focal ischemia. Brain Res. 2011;1418:93-103.

65. Rao VL, Bowen KK, Dempsey RJ. Transient focal cerebral ischemia down-regulates glutamate transporters GLT-1 and EAAC1 expression in rat brain. Neurochem Res. 2001;26(5):497-502.

66. Rao VL, Dogan A, Todd KG, Bowen KK, Kim BT, Rothstein JD, et al. Antisense knockdown of the glial glutamate transporter GLT-1, but not the neuronal glutamate transporter EAAC1, exacerbates transient focal cerebral ischemia-induced neuronal damage in rat brain. J Neurosci. 2001;21(6):1876-83.

67. Rothstein JD. Excitotoxic mechanisms in the pathogenesis of amyotrophic lateral sclerosis. Adv Neurol. 1995;68:7-20; discussion 1-7.

68. Jacob CP, Koutsilieri E, Bartl J, Neuen-Jacob E, Arzberger T, Zander N, et al. Alterations in expression of glutamatergic transporters and receptors in sporadic Alzheimer's disease. J Alzheimers Dis. 2007;11(1):97-116.

69. Howland DS, Liu J, She Y, Goad B, Maragakis NJ, Kim B, et al. Focal loss of the glutamate transporter EAAT2 in a transgenic rat model of SOD1 mutant-mediated amyotrophic lateral sclerosis (ALS). Proc Natl Acad Sci U S A. 2002;99(3):1604-9.

70. Lin CL, Bristol LA, Jin L, Dykes-Hoberg M, Crawford T, Clawson L, et al. Aberrant RNA processing in a neurodegenerative disease: the cause for absent EAAT2, a glutamate transporter, in amyotrophic lateral sclerosis. Neuron. 1998;20(3):589-602.

71. Scott HA, Gebhardt FM, Mitrovic AD, Vandenberg RJ, Dodd PR. Glutamate transporter variants reduce glutamate uptake in Alzheimer's disease. Neurobiol Aging. 2011;32(3):553 e1-11.

72. Trotti D, Aoki M, Pasinelli P, Berger UV, Danbolt NC, Brown RH, Jr., et al. Amyotrophic lateral sclerosis-linked glutamate transporter mutant has impaired glutamate clearance capacity. J Biol Chem. 2001;276(1):576-82.

73. Auray-Blais C, Cyr D, Drouin R. Quebec neonatal mass urinary screening programme: from micromolecules to macromolecules. J Inherit Metab Dis. 2007;30(4):515-21.

74. Jen JC, Graves TD, Hess EJ, Hanna MG, Griggs RC, Baloh RW, et al. Primary episodic ataxias: diagnosis, pathogenesis and treatment. Brain. 2007;130(Pt 10):2484-93.

75. Winter N, Kovermann P, Fahlke C. A point mutation associated with episodic ataxia 6 increases glutamate transporter anion currents. Brain. 2012;135(Pt 11):3416-25.

76. de Groot JF, Liu TJ, Fuller G, Yung WK. The excitatory amino acid transporter-2 induces apoptosis and decreases glioma growth in vitro and in vivo. Cancer Res. 2005;65(5):1934-40.

77. Ye ZC, Rothstein JD, Sontheimer H. Compromised glutamate transport in human glioma cells: reduction-mislocalization of sodium-dependent glutamate transporters and enhanced activity of cystine-glutamate exchange. J Neurosci. 1999;19(24):10767-77.

78. Palos TP, Ramachandran B, Boado R, Howard BD. Rat C6 and human astrocytic tumor cells express a neuronal type of glutamate transporter. Brain Res Mol Brain Res. 1996;37(1-2):297-303.

79. Jimenez AL, Chou AH, Khadadadi O, Palos TP, Howard BD. Wnt-1 has multiple effects on the expression of glutamate transporters. Neurochem Int. 2003;42(4):345-51.

80. Lee SG, Kim K, Kegelman TP, Dash R, Das SK, Choi JK, et al. Oncogene AEG-1 promotes glioma-induced neurodegeneration by increasing glutamate excitotoxicity. Cancer Res. 2011;71(20):6514-23.

81. Bacci M, Lorito N, Ippolito L, Ramazzotti M, Luti S, Romagnoli S, et al. Reprogramming of Amino Acid Transporters to Support Aspartate and Glutamate

Dependency Sustains Endocrine Resistance in Breast Cancer. Cell Rep. 2019;28(1):104-18 e8.

82. Tao J, Deng NT, Ramnarayanan K, Huang B, Oh HK, Leong SH, et al. CD44-SLC1A2 gene fusions in gastric cancer. Sci Transl Med. 2011;3(77):77ra30.

83. Garcia-Bermudez J, Baudrier L, La K, Zhu XG, Fidelin J, Sviderskiy VO, et al. Aspartate is a limiting metabolite for cancer cell proliferation under hypoxia and in tumours. Nat Cell Biol. 2018;20(7):775-81.

84. Liu Y, Zhao T, Li Z, Wang L, Yuan S, Sun L. The role of ASCT2 in cancer: A review. Eur J Pharmacol. 2018;837:81-7.

85. Wahi K, Holst J. ASCT2: a potential cancer drug target. Expert Opin Ther Targets. 2019;23(7):555-8.

86. Scalise M, Pochini L, Console L, Losso MA, Indiveri C. The Human SLC1A5 (ASCT2) Amino Acid Transporter: From Function to Structure and Role in Cell Biology. Front Cell Dev Biol. 2018;6:96.

87. Kim S, Kim DH, Jung WH, Koo JS. Expression of glutamine metabolism-related proteins according to molecular subtype of breast cancer. Endocr Relat Cancer. 2013;20(3):339-48.

88. Lu J, Chen M, Tao Z, Gao S, Li Y, Cao Y, et al. Effects of targeting SLC1A5 on inhibiting gastric cancer growth and tumor development in vitro and in vivo. Oncotarget. 2017;8(44):76458-67.

89. Lin J, Yang T, Peng Z, Xiao H, Jiang N, Zhang L, et al. SLC1A5 Silencing Inhibits Esophageal Cancer Growth via Cell Cycle Arrest and Apoptosis. Cell Physiol Biochem. 2018;48(1):397.

90. Wang Q, Hardie RA, Hoy AJ, van Geldermalsen M, Gao D, Fazli L, et al. Targeting ASCT2-mediated glutamine uptake blocks prostate cancer growth and tumour development. J Pathol. 2015;236(3):278-89.

91. Jin L, Alesi GN, Kang S. Glutaminolysis as a target for cancer therapy. Oncogene. 2016;35(28):3619-25.

92. Liberti MV, Locasale JW. The Warburg Effect: How Does it Benefit Cancer Cells? Trends Biochem Sci. 2016;41(3):211-8.

93. Zerangue N, Kavanaugh MP. Interaction of L-cysteine with a human excitatory amino acid transporter. J Physiol. 1996;493 (Pt 2):419-23.

94. Christensen HN, Liang M, Archer EG. A distinct Na+-requiring transport system for alanine, serine, cysteine, and similar amino acids. J Biol Chem. 1967;242(22):5237-46.

95. Scalise M, Pochini L, Pingitore P, Hedfalk K, Indiveri C. Cysteine is not a substrate but a specific modulator of human ASCT2 (SLC1A5) transporter. FEBS Lett. 2015;589(23):3617-23.

96. Broer A, Wagner C, Lang F, Broer S. Neutral amino acid transporter ASCT2 displays substrate-induced Na+ exchange and a substrate-gated anion conductance. Biochem J. 2000;346 Pt 3:705-10.

97. Zerangue N, Kavanaugh MP. ASCT-1 is a neutral amino acid exchanger with chloride channel activity. J Biol Chem. 1996;271(45):27991-4.

98. Scopelliti AJ, Heinzelmann G, Kuyucak S, Ryan RM, Vandenberg RJ. Na+ interactions with the neutral amino acid transporter ASCT1. J Biol Chem. 2014;289(25):17468-79.

99. Owe SG, Marcaggi P, Attwell D. The ionic stoichiometry of the GLAST glutamate transporter in salamander retinal glia. J Physiol. 2006;577(Pt 2):591-9.

100. Zerangue N, Kavanaugh MP. Flux coupling in a neuronal glutamate transporter. Nature. 1996;383(6601):634-7.

101. Levy LM, Warr O, Attwell D. Stoichiometry of the glial glutamate transporter GLT-1 expressed inducibly in a Chinese hamster ovary cell line selected for low endogenous Na+-dependent glutamate uptake. J Neurosci. 1998;18(23):9620-8.

102. Grewer C, Grabsch E. New inhibitors for the neutral amino acid transporter ASCT2 reveal its Na+-dependent anion leak. J Physiol. 2004;557(Pt 3):747-59.

103. Wadiche JI, Amara SG, Kavanaugh MP. Ion fluxes associated with excitatory amino acid transport. Neuron. 1995;15(3):721-8.

104. Billups B, Rossi D, Attwell D. Anion conductance behavior of the glutamate uptake carrier in salamander retinal glial cells. J Neurosci. 1996;16(21):6722-31.

105. Vandenberg RJ, Arriza JL, Amara SG, Kavanaugh MP. Constitutive ion fluxes and substrate binding domains of human glutamate transporters. J Biol Chem. 1995;270(30):17668-71.

106. Ryan RM, Vandenberg RJ. A channel in a transporter. Clin Exp Pharmacol Physiol. 2005;32(1-2):1-6.

107. Gameiro A, Braams S, Rauen T, Grewer C. The discovery of slowness: low-capacity transport and slow anion channel gating by the glutamate transporter EAAT5. Biophys J. 2011;100(11):2623-32.

108. Veruki ML, Morkve SH, Hartveit E. Activation of a presynaptic glutamate transporter regulates synaptic transmission through electrical signaling. Nat Neurosci. 2006;9(11):1388-96.

109. Wadiche JI, Arriza JL, Amara SG, Kavanaugh MP. Kinetics of a human glutamate transporter. Neuron. 1995;14(5):1019-27.

110. Wadiche JI, Kavanaugh MP. Macroscopic and microscopic properties of a cloned glutamate transporter/chloride channel. J Neurosci. 1998;18(19):7650-61.

111. Bergles DE, Tzingounis AV, Jahr CE. Comparison of coupled and uncoupled currents during glutamate uptake by GLT-1 transporters. J Neurosci. 2002;22(23):10153-62.

112. Grewer C, Watzke N, Wiessner M, Rauen T. Glutamate translocation of the neuronal glutamate transporter EAAC1 occurs within milliseconds. Proc Natl Acad Sci U S A. 2000;97(17):9706-11.

113. Tzingounis AV, Wadiche JI. Glutamate transporters: confining runaway excitation by shaping synaptic transmission. Nat Rev Neurosci. 2007;8(12):935-47.

114. Gendreau S, Voswinkel S, Torres-Salazar D, Lang N, Heidtmann H, Detro-Dassen S, et al. A trimeric quaternary structure is conserved in bacterial and human glutamate transporters. J Biol Chem. 2004;279(38):39505-12.

115. Leary GP, Holley DC, Stone EF, Lyda BR, Kalachev LV, Kavanaugh MP. The central cavity in trimeric glutamate transporters restricts ligand diffusion. Proc Natl Acad Sci U S A. 2011;108(36):14980-5.

116. Lolkema JS, Slotboom DJ. The major amino acid transporter superfamily has a similar core structure as Na+-galactose and Na+-leucine transporters. Mol Membr Biol. 2008;25(6-7):567-70.

117. Slotboom DJ, Konings WN, Lolkema JS. Structural features of the glutamate transporter family. Microbiol Mol Biol Rev. 1999;63(2):293-307.

118. Slotboom DJ, Lolkema JS, Konings WN. Membrane topology of the C-terminal half of the neuronal, glial, and bacterial glutamate transporter family. J Biol Chem. 1996;271(49):31317-21.

119. Grunewald M, Bendahan A, Kanner BI. Biotinylation of single cysteine mutants of the glutamate transporter GLT-1 from rat brain reveals its unusual topology. Neuron. 1998;21(3):623-32.

120. Grewer C, Balani P, Weidenfeller C, Bartusel T, Tao Z, Rauen T. Individual subunits of the glutamate transporter EAAC1 homotrimer function independently of each other. Biochemistry. 2005;44(35):11913-23.

121. Koch HP, Brown RL, Larsson HP. The glutamate-activated anion conductance in excitatory amino acid transporters is gated independently by the individual subunits. J Neurosci. 2007;27(11):2943-7.

122. Leary GP, Stone EF, Holley DC, Kavanaugh MP. The glutamate and chloride permeation pathways are colocalized in individual neuronal glutamate transporter subunits. J Neurosci. 2007;27(11):2938-42.

123. Brocke L, Bendahan A, Grunewald M, Kanner BI. Proximity of two oppositely oriented reentrant loops in the glutamate transporter GLT-1 identified by paired cysteine mutagenesis. J Biol Chem. 2002;277(6):3985-92.

124. Grunewald M, Menaker D, Kanner BI. Cysteine-scanning mutagenesis reveals a conformationally sensitive reentrant pore-loop in the glutamate transporter GLT-1. J Biol Chem. 2002;277(29):26074-80.

125. Grunewald M, Kanner BI. The accessibility of a novel reentrant loop of the glutamate transporter GLT-1 is restricted by its substrate. J Biol Chem. 2000;275(13):9684-9.

126. Seal RP, Leighton BH, Amara SG. A model for the topology of excitatory amino acid transporters determined by the extracellular accessibility of substituted cysteines. Neuron. 2000;25(3):695-706.

127. Slotboom DJ, Sobczak I, Konings WN, Lolkema JS. A conserved serine-rich stretch in the glutamate transporter family forms a substrate-sensitive reentrant loop. Proc Natl Acad Sci U S A. 1999;96(25):14282-7.

128. Seal RP, Amara SG. A reentrant loop domain in the glutamate carrier EAAT1 participates in substrate binding and translocation. Neuron. 1998;21(6):1487-98.

129. Slotboom DJ, Konings WN, Lolkema JS. Cysteine-scanning mutagenesis reveals a highly amphipathic, pore-lining membrane-spanning helix in the glutamate transporter GltT. J Biol Chem. 2001;276(14):10775-81.

130. Watzke N, Bamberg E, Grewer C. Early intermediates in the transport cycle of the neuronal excitatory amino acid carrier EAAC1. J Gen Physiol. 2001;117(6):547-62.

131. Koch HP, Hubbard JM, Larsson HP. Voltage-independent sodium-binding events reported by the 4B-4C loop in the human glutamate transporter excitatory amino acid transporter 3. J Biol Chem. 2007;282(34):24547-53.

132. Zhang Z, Tao Z, Gameiro A, Barcelona S, Braams S, Rauen T, et al. Transport direction determines the kinetics of substrate transport by the glutamate transporter EAAC1. Proc Natl Acad Sci U S A. 2007;104(46):18025-30.

133. Tao Z, Zhang Z, Grewer C. Neutralization of the aspartic acid residue Asp-367, but not Asp-454, inhibits binding of Na+ to the glutamate-free form and cycling of the glutamate transporter EAAC1. J Biol Chem. 2006;281(15):10263-72.

134. Borre L, Kanner BI. Coupled, but not uncoupled, fluxes in a neuronal glutamate transporter can be activated by lithium ions. J Biol Chem. 2001;276(44):40396-401.

135. Larsson HP, Wang X, Lev B, Baconguis I, Caplan DA, Vyleta NP, et al. Evidence for a third sodium-binding site in glutamate transporters suggests an ion/substrate coupling model. Proc Natl Acad Sci U S A. 2010;107(31):13912-7.

136. Tao Z, Grewer C. Cooperation of the conserved aspartate 439 and bound amino acid substrate is important for high-affinity Na+ binding to the glutamate transporter EAAC1. J Gen Physiol. 2007;129(4):331-44.

137. Rosental N, Gameiro A, Grewer C, Kanner BI. A conserved aspartate residue located at the extracellular end of the binding pocket controls cation interactions in brain glutamate transporters. J Biol Chem. 2011;286(48):41381-90.

138. Rosental N, Bendahan A, Kanner BI. Multiple consequences of mutating two conserved beta-bridge forming residues in the translocation cycle of a neuronal glutamate transporter. J Biol Chem. 2006;281(38):27905-15.

139. Kavanaugh MP, Bendahan A, Zerangue N, Zhang Y, Kanner BI. Mutation of an amino acid residue influencing potassium coupling in the glutamate transporter GLT-1 induces obligate exchange. J Biol Chem. 1997;272(3):1703-8.

140. Zhang Y, Bendahan A, Zarbiv R, Kavanaugh MP, Kanner BI. Molecular determinant of ion selectivity of a (Na+ + K+)-coupled rat brain glutamate transporter. Proc Natl Acad Sci U S A. 1998;95(2):751-5.

141. Ryan RM, Kortt NC, Sirivanta T, Vandenberg RJ. The position of an arginine residue influences substrate affinity and K+ coupling in the human glutamate transporter, EAAT1. J Neurochem. 2010;114(2):565-75.

142. Borre L, Kanner BI. Arginine 445 controls the coupling between glutamate and cations in the neuronal transporter EAAC-1. J Biol Chem. 2004;279(4):2513-9.

143. Seal RP, Shigeri Y, Eliasof S, Leighton BH, Amara SG. Sulfhydryl modification of V449C in the glutamate transporter EAAT1 abolishes substrate transport but not the substrate-gated anion conductance. Proc Natl Acad Sci U S A. 2001;98(26):15324-9.

144. Watzke N, Rauen T, Bamberg E, Grewer C. On the mechanism of proton transport by the neuronal excitatory amino acid carrier 1. J Gen Physiol. 2000;116(5):609-22.

145. Grewer C, Watzke N, Rauen T, Bicho A. Is the glutamate residue Glu-373 the proton acceptor of the excitatory amino acid carrier 1? J Biol Chem. 2003;278(4):2585-92.

146. Bendahan A, Armon A, Madani N, Kavanaugh MP, Kanner BI. Arginine 447 plays a pivotal role in substrate interactions in a neuronal glutamate transporter. J Biol Chem. 2000;275(48):37436-42.

147. Teichman S, Kanner BI. Aspartate-444 is essential for productive substrate interactions in a neuronal glutamate transporter. J Gen Physiol. 2007;129(6):527-39.

148. Teichman S, Qu S, Kanner BI. Conserved asparagine residue located in binding pocket controls cation selectivity and substrate interactions in neuronal glutamate transporter. J Biol Chem. 2012;287(21):17198-205.

149. Yernool D, Boudker O, Jin Y, Gouaux E. Structure of a glutamate transporter homologue from Pyrococcus horikoshii. Nature. 2004;431(7010):811-8.

150. Boudker O, Ryan RM, Yernool D, Shimamoto K, Gouaux E. Coupling substrate and ion binding to extracellular gate of a sodium-dependent aspartate transporter. Nature. 2007;445(7126):387-93.

151. Ryan RM, Compton EL, Mindell JA. Functional characterization of a Na+-dependent aspartate transporter from Pyrococcus horikoshii. J Biol Chem. 2009;284(26):17540-8.

152. Groeneveld M, Slotboom DJ. Na(+):aspartate coupling stoichiometry in the glutamate transporter homologue Glt(Ph). Biochemistry. 2010;49(17):3511-3.

153. Scopelliti AJ, Font J, Vandenberg RJ, Boudker O, Ryan RM. Structural characterisation reveals insights into substrate recognition by the glutamine transporter ASCT2/SLC1A5. Nat Commun. 2018;9(1):38.

154. Verdon G, Oh S, Serio RN, Boudker O. Coupled ion binding and structural transitions along the transport cycle of glutamate transporters. Elife. 2014;3:e02283.

155. Focke PJ, Annen AW, Valiyaveetil FI. Engineering the glutamate transporter homologue GltPh using protein semisynthesis. Biochemistry. 2015;54(8):1694-702.

156. Jardetzky O. Simple allosteric model for membrane pumps. Nature. 1966;211(5052):969-70.

157. Drew D, Boudker O. Shared Molecular Mechanisms of Membrane Transporters. Annu Rev Biochem. 2016;85:543-72.

158. Reyes N, Ginter C, Boudker O. Transport mechanism of a bacterial homologue of glutamate transporters. Nature. 2009;462(7275):880-5.

159. Lee C, Kang HJ, von Ballmoos C, Newstead S, Uzdavinys P, Dotson DL, et al. A two-domain elevator mechanism for sodium/proton antiport. Nature. 2013;501(7468):573-7.

160. Mulligan C, Fenollar-Ferrer C, Fitzgerald GA, Vergara-Jaque A, Kaufmann D, Li Y, et al. The bacterial dicarboxylate transporter VcINDY uses a two-domain elevator-type mechanism. Nat Struct Mol Biol. 2016;23(3):256-63.

161. Lolkema JS, Slotboom DJ. Structure and elevator mechanism of the Na(+)-citrate transporter CitS. Curr Opin Struct Biol. 2017;45:1-9.

162. Cao Y, Jin X, Levin EJ, Huang H, Zong Y, Quick M, et al. Crystal structure of a phosphorylation-coupled saccharide transporter. Nature. 2011;473(7345):50-4.

163. Verdon G, Boudker O. Crystal structure of an asymmetric trimer of a bacterial glutamate transporter homolog. Nat Struct Mol Biol. 2012;19(3):355-7.

164. Guskov A, Jensen S, Faustino I, Marrink SJ, Slotboom DJ. Coupled binding mechanism of three sodium ions and aspartate in the glutamate transporter homologue GltTk. Nat Commun. 2016;7:13420.

165. Jensen S, Guskov A, Rempel S, Hanelt I, Slotboom DJ. Crystal structure of a substrate-free aspartate transporter. Nat Struct Mol Biol. 2013;20(10):1224-6.

166. Teichman S, Qu S, Kanner BI. The equivalent of a thallium binding residue from an archeal homolog controls cation interactions in brain glutamate transporters. Proc Natl Acad Sci U S A. 2009;106(34):14297-302.

167. Mwaura J, Tao Z, James H, Albers T, Schwartz A, Grewer C. Protonation state of a conserved acidic amino acid involved in Na(+) binding to the glutamate transporter EAAC1. ACS Chem Neurosci. 2012;3(12):1073-83.

168. Silverstein N, Sliman A, Stockner T, Kanner BI. Both reentrant loops of the sodium-coupled glutamate transporters contain molecular determinants of cation selectivity. J Biol Chem. 2018;293(37):14200-9.

169. Bastug T, Heinzelmann G, Kuyucak S, Salim M, Vandenberg RJ, Ryan RM. Position of the third Na+ site in the aspartate transporter GltPh and the human glutamate transporter, EAAT1. PLoS One. 2012;7(3):e33058.

170. Shrivastava IH, Jiang J, Amara SG, Bahar I. Time-resolved mechanism of extracellular gate opening and substrate binding in a glutamate transporter. J Biol Chem. 2008;283(42):28680-90.

171. Heinzelmann G, Kuyucak S. Molecular dynamics simulations of the mammalian glutamate transporter EAAT3. PLoS One. 2014;9(3):e92089.

172. Kortzak D, Alleva C, Weyand I, Ewers D, Zimmermann MI, Franzen A, et al. Allosteric gate modulation confers K(+) coupling in glutamate transporters. EMBO J. 2019;38(19):e101468.

173. Notredame C, Higgins DG, Heringa J. T-Coffee: A novel method for fast and accurate multiple sequence alignment. J Mol Biol. 2000;302(1):205-17.

174. Shachnai L, Shimamoto K, Kanner BI. Sulfhydryl modification of cysteine mutants of a neuronal glutamate transporter reveals an inverse relationship between sodium dependent conformational changes and the glutamate-gated anion conductance. Neuropharmacology. 2005;49(6):862-71.

175. Ryan RM, Mitrovic AD, Vandenberg RJ. The chloride permeation pathway of a glutamate transporter and its proximity to the glutamate translocation pathway. J Biol Chem. 2004;279(20):20742-51.

176. Cater RJ, Vandenberg RJ, Ryan RM. Tuning the ion selectivity of glutamate transporter-associated uncoupled conductances. J Gen Physiol. 2016;148(1):13-24.

177. Ryan RM, Mindell JA. The uncoupled chloride conductance of a bacterial glutamate transporter homolog. Nat Struct Mol Biol. 2007;14(5):365-71.

178. Chen I, Pant S, Wu Q, Cater RJ, Sobti M, Vandenberg RJ, et al. Glutamate transporters have a chloride channel with two hydrophobic gates. Nature. 2021;591(7849):327-31.

179. Kolen B, Kortzak D, Franzen A, Fahlke C. An amino-terminal point mutation increases EAAT2 anion currents without affecting glutamate transport rates. J Biol Chem. 2020;295(44):14936-47.

180. Cheng MH, Torres-Salazar D, Gonzalez-Suarez AD, Amara SG, Bahar I. Substrate transport and anion permeation proceed through distinct pathways in glutamate transporters. Elife. 2017;6.

181. Erkens GB, Hanelt I, Goudsmits JM, Slotboom DJ, van Oijen AM. Unsynchronised subunit motion in single trimeric sodium-coupled aspartate transporters. Nature. 2013;502(7469):119-23.

182. Akyuz N, Altman RB, Blanchard SC, Boudker O. Transport dynamics in a glutamate transporter homologue. Nature. 2013;502(7469):114-8.

183. Georgieva ER, Borbat PP, Ginter C, Freed JH, Boudker O. Conformational ensemble of the sodium-coupled aspartate transporter. Nat Struct Mol Biol. 2013;20(2):215-21.

184. Hanelt I, Wunnicke D, Bordignon E, Steinhoff HJ, Slotboom DJ. Conformational heterogeneity of the aspartate transporter Glt(Ph). Nat Struct Mol Biol. 2013;20(2):210-4.

185. Ruan Y, Miyagi A, Wang X, Chami M, Boudker O, Scheuring S. Direct visualization of glutamate transporter elevator mechanism by high-speed AFM. Proc Natl Acad Sci U S A. 2017;114(7):1584-8.

186. Ciftci D, Huysmans GHM, Wang X, He C, Terry D, Zhou Z, et al. Single-molecule transport kinetics of a glutamate transporter homolog shows static disorder. Sci Adv. 2020;6(22):eaaz1949.

187. Huysmans GHM, Ciftci D, Wang X, Blanchard SC, Boudker O. The high-energy transition state of the glutamate transporter homologue GltPh. EMBO J. 2021;40(1):e105415.

188. Matin TR, Heath GR, Huysmans GHM, Boudker O, Scheuring S. Millisecond dynamics of an unlabeled amino acid transporter. Nat Commun. 2020;11(1):5016.

189. Zhou W, Fiorin G, Anselmi C, Karimi-Varzaneh HA, Poblete H, Forrest LR, et al. Large-scale state-dependent membrane remodeling by a transporter protein. Elife. 2019;8.

190. Arkhipova V, Guskov A, Slotboom DJ. Structural ensemble of a glutamate transporter homologue in lipid nanodisc environment. Nat Commun. 2020;11(1):998.

191. Wang X, Boudker O. Large domain movements through the lipid bilayer mediate substrate release and inhibition of glutamate transporters. Elife. 2020;9.

192. McIlwain BC, Vandenberg RJ, Ryan RM. Transport rates of a glutamate transporter homologue are influenced by the lipid bilayer. J Biol Chem. 2015;290(15):9780-8.

193. Canul-Tec JC, Assal R, Cirri E, Legrand P, Brier S, Chamot-Rooke J, et al. Structure and allosteric inhibition of excitatory amino acid transporter 1. Nature. 2017;544(7651):446-51.

194. Garaeva AA, Guskov A, Slotboom DJ, Paulino C. A one-gate elevator mechanism for the human neutral amino acid transporter ASCT2. Nat Commun. 2019;10(1):3427.

195. Yu X, Plotnikova O, Bonin PD, Subashi TA, McLellan TJ, Dumlao D, et al. Cryo-EM structures of the human glutamine transporter SLC1A5 (ASCT2) in the outward-facing conformation. Elife. 2019;8.

196. Garaeva AA, Oostergetel GT, Gati C, Guskov A, Paulino C, Slotboom DJ. Cryo-EM structure of the human neutral amino acid transporter ASCT2. Nat Struct Mol Biol. 2018;25(6):515-21.

197. Qiu B, Matthies D, Fortea E, Yu Z, Boudker O. Cryo-EM structures of excitatory amino acid transporter 3 visualize coupled substrate, sodium, and proton binding and transport. Sci Adv. 2021;7(10).

198. Qu S, Kanner BI. Substrates and non-transportable analogues induce structural rearrangements at the extracellular entrance of the glial glutamate transporter GLT-1/EAAT2. J Biol Chem. 2008;283(39):26391-400.

199. Zhang Y, Kanner BI. Two serine residues of the glutamate transporter GLT-1 are crucial for coupling the fluxes of sodium and the neurotransmitter. Proc Natl Acad Sci U S A. 1999;96(4):1710-5.

200. Leighton BH, Seal RP, Watts SD, Skyba MO, Amara SG. Structural rearrangements at the translocation pore of the human glutamate transporter, EAAT1. J Biol Chem. 2006;281(40):29788-96.

201. Zomot E, Bahar I. Intracellular gating in an inward-facing state of aspartate transporter Glt(Ph) is regulated by the movements of the helical hairpin HP2. J Biol Chem. 2013;288(12):8231-7.

202. Reyes N, Oh S, Boudker O. Binding thermodynamics of a glutamate transporter homolog. Nat Struct Mol Biol. 2013;20(5):634-40.

203. Alleva C, Kovalev K, Astashkin R, Berndt MI, Baeken C, Balandin T, et al. Na(+)-dependent gate dynamics and electrostatic attraction ensure substrate coupling in glutamate transporters. Sci Adv. 2020;6(47).

204. Compton EL, Taylor EM, Mindell JA. The 3-4 loop of an archaeal glutamate transporter homolog experiences ligand-induced structural changes and is essential for transport. Proc Natl Acad Sci U S A. 2010;107(29):12840-5.

205. Mulligan C, Mindell JA. Mechanism of transport modulation by an extracellular loop in an archaeal excitatory amino acid transporter (EAAT) homolog. J Biol Chem. 2013;288(49):35266-76.

206. Stolzenberg S, Khelashvili G, Weinstein H. Structural intermediates in a model of the substrate translocation path of the bacterial glutamate transporter homologue GltPh. J Phys Chem B. 2012;116(18):5372-83.

207. Wang J, Qu S. Conformationally Sensitive Proximity Between the TM3-4 Loop and Hairpin Loop 2 of the Glutamate Transporter EAAT2 Revealed by Paired-Cysteine Mutagenesis. ACS Chem Neurosci. 2021;12(1):163-75.

208. Focke PJ, Moenne-Loccoz P, Larsson HP. Opposite movement of the external gate of a glutamate transporter homolog upon binding cotransported sodium compared with substrate. J Neurosci. 2011;31(16):6255-62.

209. Riederer EA, Valiyaveetil FI. Investigation of the allosteric coupling mechanism in a glutamate transporter homolog via unnatural amino acid mutagenesis. Proc Natl Acad Sci U S A. 2019;116(32):15939-46.

210. Hanelt I, Jensen S, Wunnicke D, Slotboom DJ. Low Affinity and Slow Na+ Binding Precedes High Affinity Aspartate Binding in the Secondary-active Transporter GltPh. J Biol Chem. 2015;290(26):15962-72.

211. Ewers D, Becher T, Machtens JP, Weyand I, Fahlke C. Induced fit substrate binding to an archeal glutamate transporter homologue. Proc Natl Acad Sci U S A. 2013;110(30):12486-91.

212. Gu Y, Shrivastava IH, Amara SG, Bahar I. Molecular simulations elucidate the substrate translocation pathway in a glutamate transporter. Proc Natl Acad Sci U S A. 2009;106(8):2589-94.

213. DeChancie J, Shrivastava IH, Bahar I. The mechanism of substrate release by the aspartate transporter GltPh: insights from simulations. Mol Biosyst. 2011;7(3):832-42.

214. Venkatesan S, Saha K, Sohail A, Sandtner W, Freissmuth M, Ecker GF, et al. Refinement of the Central Steps of Substrate Transport by the Aspartate Transporter GltPh: Elucidating the Role of the Na2 Sodium Binding Site. PLoS Comput Biol. 2015;11(10):e1004551.

215. Setiadi J, Kuyucak S. Free-Energy Simulations Resolve the Low-Affinity Na(+)-High-Affinity Asp Binding Paradox in GltPh. Biophys J. 2019;117(4):780-9.

216. Heinzelmann G, Bastug T, Kuyucak S. Mechanism and energetics of ligand release in the aspartate transporter GltPh. J Phys Chem B. 2013;117(18):5486-96.

217. Heinzelmann G, Bastug T, Kuyucak S. Free energy simulations of ligand binding to the aspartate transporter Glt(Ph). Biophys J. 2011;101(10):2380-8.

218. Forrest LR, Kramer R, Ziegler C. The structural basis of secondary active transport mechanisms. Biochim Biophys Acta. 2011;1807(2):167-88.

219. Jiang J, Amara SG. New views of glutamate transporter structure and function: advances and challenges. Neuropharmacology. 2011;60(1):172-81.

220. Auger C, Attwell D. Fast removal of synaptic glutamate by postsynaptic transporters. Neuron. 2000;28(2):547-58.

221. Huang Z, Tajkhorshid E. Dynamics of the extracellular gate and ion-substrate coupling in the glutamate transporter. Biophys J. 2008;95(5):2292-300.

222. Huang Z, Tajkhorshid E. Identification of the third Na+ site and the sequence of extracellular binding events in the glutamate transporter. Biophys J. 2010;99(5):1416-25.

223. Chatterjee A, Sun SB, Furman JL, Xiao H, Schultz PG. A versatile platform for single- and multiple-unnatural amino acid mutagenesis in Escherichia coli. Biochemistry. 2013;52(10):1828-37.

224. Ryu Y, Schultz PG. Efficient incorporation of unnatural amino acids into proteins in Escherichia coli. Nat Methods. 2006;3(4):263-5.

225. Miyake-Stoner SJ, Miller AM, Hammill JT, Peeler JC, Hess KR, Mehl RA, et al. Probing protein folding using site-specifically encoded unnatural amino acids as FRET donors with tryptophan. Biochemistry. 2009;48(25):5953-62.

226. Lolkema JS, Slotboom DJ. The Hill analysis and co-ion-driven transporter kinetics. J Gen Physiol. 2015;145(6):565-74.

227. Kuriyan J, Boyana, K., and Wemmer, D. The Molecules of Life: Physical and Cehmical Principles. New York, NY: Garland Science; 2013.

228. Vogt AD, Di Cera E. Conformational selection or induced fit? A critical appraisal of the kinetic mechanism. Biochemistry. 2012;51(30):5894-902.

229. Smart OS, Neduvelil JG, Wang X, Wallace BA, Sansom MS. HOLE: a program for the analysis of the pore dimensions of ion channel structural models. J Mol Graph. 1996;14(6):354-60, 76.

230. Van Arnam EB, Blythe EE, Lester HA, Dougherty DA. An unusual pattern of ligand-receptor interactions for the alpha7 nicotinic acetylcholine receptor, with implications for the binding of varenicline. Mol Pharmacol. 2013;84(2):201-7.

231. Oh S, Boudker O. Kinetic mechanism of coupled binding in sodium-aspartate symporter GltPh. Elife. 2018;7.

232. Young DD, Young TS, Jahnz M, Ahmad I, Spraggon G, Schultz PG. An evolved aminoacyl-tRNA synthetase with atypical polysubstrate specificity. Biochemistry. 2011;50(11):1894-900.

233. Lakowicz JR. Principles of fluorescence spectroscopy. New York, NY Kluwer Academic/Plenum Publishers; 1999.

234. Harpaz Y, Gerstein M, Chothia C. Volume changes on protein folding. Structure. 1994;2(7):641-9.

235. Boudker O, Oh S. Isothermal titration calorimetry of ion-coupled membrane transporters. Methods. 2015;76:171-82.

236. Bungard CI, McGivan JD. Glutamine availability up-regulates expression of the amino acid transporter protein ASCT2 in HepG2 cells and stimulates the ASCT2 promoter. Biochem J. 2004;382(Pt 1):27-32.

237. Chang JM, Di Tommaso P, Taly JF, Notredame C. Accurate multiple sequence alignment of transmembrane proteins with PSI-Coffee. BMC Bioinformatics. 2012;13 Suppl 4:S1.

238. Silverstein N, Ewers D, Forrest LR, Fahlke C, Kanner BI. Molecular Determinants of Substrate Specificity in Sodium-coupled Glutamate Transporters. J Biol Chem. 2015;290(48):28988-96.

239. Forrest LR. Structural Symmetry in Membrane Proteins. Annu Rev Biophys. 2015;44:311-37.

240. Veenhoff LM, Heuberger EH, Poolman B. Quaternary structure and function of transport proteins. Trends Biochem Sci. 2002;27(5):242-9.

241. Yang Y, Yan Y, Sigworth FJ. How does the W434F mutation block current in Shaker potassium channels? J Gen Physiol. 1997;109(6):779-89.

242. Gordon SE, Zagotta WN. Subunit interactions in coordination of Ni2+ in cyclic nucleotide-gated channels. Proc Natl Acad Sci U S A. 1995;92(22):10222-6.

243. Lim NK, Lam AK, Dutzler R. Independent activation of ion conduction pores in the double-barreled calcium-activated chloride channel TMEM16A. J Gen Physiol. 2016;148(5):375-92.

244. Raghuraman H, Cordero-Morales JF, Jogini V, Pan AC, Kollewe A, Roux B, et al. Mechanism of Cd2+ coordination during slow inactivation in potassium channels. Structure. 2012;20(8):1332-42.

245. Last NB, Kolmakova-Partensky L, Shane T, Miller C. Mechanistic signs of double-barreled structure in a fluoride ion channel. Elife. 2016;5.

246. Wang S, Vafabakhsh R, Borschel WF, Ha T, Nichols CG. Structural dynamics of potassium-channel gating revealed by single-molecule FRET. Nat Struct Mol Biol. 2016;23(1):31-6.

247. Becker M, Maximov S, Becker M, Meyer U, Wittmann A, Kramer R. Analysis of putative protomer crosstalk in the trimeric transporter BetP: The heterotrimer approach. Biochim Biophys Acta. 2014;1837(6):888-98.

248. Lu W, Du J, Goehring A, Gouaux E. Cryo-EM structures of the triheteromeric NMDA receptor and its allosteric modulation. Science. 2017;355(6331).

249. Neumann J, Klein N, Otzen DE, Schneider D. Folding energetics and oligomerization of polytopic alpha-helical transmembrane proteins. Arch Biochem Biophys. 2014;564:281-96.

250. Popot JL. Folding membrane proteins in vitro: a table and some comments. Arch Biochem Biophys. 2014;564:314-26.

251. Akyuz N, Georgieva ER, Zhou Z, Stolzenberg S, Cuendet MA, Khelashvili G, et al. Transport domain unlocking sets the uptake rate of an aspartate transporter. Nature. 2015;518(7537):68-73.

252. Koch HP, Larsson HP. Small-scale molecular motions accomplish glutamate uptake in human glutamate transporters. J Neurosci. 2005;25(7):1730-6.

253. Fafarman AT, Borbat PP, Freed JH, Kirshenbaum K. Characterizing the structure and dynamics of folded oligomers: Pulsed ESR studies of peptoid helices. Chem Commun (Camb). 2007(4):377-9.

254. Borbat PP, Freed JH. Pulse Dipolar ELectron Spin Resonance: Distance Measurements. In: Timmel CR, Harmer JR, editors. Structural Information from Spin-Labels and Intrinsic Paramagnetic Centers in the Biosciences. 152. Berlin: Springer-Verlag; 2014. p. 1-82.

255. Jeschke G. DEER distance measurements on proteins. Annu Rev Phys Chem. 2012;63:419-46.

256. Borbat PP, Freed JH. Measuring distances by pulsed dipolar ESR spectroscopy: spin-labeled histidine kinases. Methods Enzymol. 2007;423:52-116.

257. Georgieva ER, Ramlall TF, Borbat PP, Freed JH, Eliezer D. Membrane-bound alpha-synuclein forms an extended helix: long-distance pulsed ESR measurements using vesicles, bicelles, and rodlike micelles. J Am Chem Soc. 2008;130(39):12856-7.

258. Schmidt T, Walti MA, Baber JL, Hustedt EJ, Clore GM. Long Distance Measurements up to 160 A in the GroEL Tetradecamer Using Q-Band DEER EPR Spectroscopy. Angew Chem Int Ed Engl. 2016;55(51):15905-9.

259. Dastvan R, Fischer AW, Mishra S, Meiler J, McHaourab HS. Protonation-dependent conformational dynamics of the multidrug transporter EmrE. Proc Natl Acad Sci U S A. 2016;113(5):1220-5.

260. Khantwal CM, Abraham SJ, Han W, Jiang T, Chavan TS, Cheng RC, et al. Revealing an outward-facing open conformational state in a CLC Cl(-)/H(+) exchange transporter. Elife. 2016;5.

261. Borbat PP, Surendhran K, Bortolus M, Zou P, Freed JH, McHaourab HS. Conformational motion of the ABC transporter MsbA induced by ATP hydrolysis. PLoS Biol. 2007;5(10):e271.

262. Endeward B, Butterwick JA, MacKinnon R, Prisner TF. Pulsed electron-electron double-resonance determination of spin-label distances and orientations on the tetrameric potassium ion channel KcsA. J Am Chem Soc. 2009;131(42):15246-50.

263. Dalmas O, Hyde HC, Hulse RE, Perozo E. Symmetry-constrained analysis of pulsed double electron-electron resonance (DEER) spectroscopy reveals the dynamic nature of the KcsA activation gate. J Am Chem Soc. 2012;134(39):16360-9.

264. Jeschke G, Sajid M, Schulte M, Godt A. Three-spin correlations in double electron-electron resonance. Phys Chem Chem Phys. 2009;11(31):6580-91.

265. Jaehme M, Michel H. Evaluation of cell-free protein synthesis for the crystallization of membrane proteins--a case study on a member of the glutamate transporter family from Staphylothermus marinus. FEBS J. 2013;280(4):1112-25.

266. Mancusso R, Gregorio GG, Liu Q, Wang DN. Structure and mechanism of a bacterial sodium-dependent dicarboxylate transporter. Nature. 2012;491(7425):622-6.

267. Dutzler R, Campbell EB, Cadene M, Chait BT, MacKinnon R. X-ray structure of a ClC chloride channel at 3.0 A reveals the molecular basis of anion selectivity. Nature. 2002;415(6869):287-94.

268. Accardi A, Miller C. Secondary active transport mediated by a prokaryotic homologue of ClC Cl- channels. Nature. 2004;427(6977):803-7.

269. Chadda R, Krishnamani V, Mersch K, Wong J, Brimberry M, Chadda A, et al. The dimerization equilibrium of a ClC Cl(-)/H(+) antiporter in lipid bilayers. Elife. 2016;5.

270. Devaraneni PK, Devereaux JJ, Valiyaveetil FI. In vitro folding of KvAP, a voltage-gated K+ channel. Biochemistry. 2011;50(48):10442-50.

271. Weiss JN. The Hill equation revisited: uses and misuses. FASEB J. 1997;11(11):835-41.

272. Ge L, Perez C, Waclawska I, Ziegler C, Muller DJ. Locating an extracellular K+-dependent interaction site that modulates betaine-binding of the Na+-coupled betaine symporter BetP. Proc Natl Acad Sci U S A. 2011;108(43):E890-8.

273. Chen YJ, Pornillos O, Lieu S, Ma C, Chen AP, Chang G. X-ray structure of EmrE supports dual topology model. Proc Natl Acad Sci U S A. 2007;104(48):18999-9004.

274. Latorraca NR, Fastman NM, Venkatakrishnan AJ, Frommer WB, Dror RO, Feng L. Mechanism of Substrate Translocation in an Alternating Access Transporter. Cell. 2017;169(1):96-107 e12.

275. Joo C, Balci H, Ishitsuka Y, Buranachai C, Ha T. Advances in single-molecule fluorescence methods for molecular biology. Annu Rev Biochem. 2008;77:51-76.

276. McHaourab HS, Steed PR, Kazmier K. Toward the fourth dimension of membrane protein structure: insight into dynamics from spin-labeling EPR spectroscopy. Structure. 2011;19(11):1549-61.

277. Zou P, Bortolus M, McHaourab HS. Conformational cycle of the ABC transporter MsbA in liposomes: detailed analysis using double electron-electron resonance spectroscopy. J Mol Biol. 2009;393(3):586-97.

278. Harris NJ, Booth PJ. Folding and stability of membrane transport proteins in vitro. Biochim Biophys Acta. 2012;1818(4):1055-66.

279. Robertson JL, Kolmakova-Partensky L, Miller C. Design, function and structure of a monomeric ClC transporter. Nature. 2010;468(7325):844-7.

280. Gupta K, Donlan JAC, Hopper JTS, Uzdavinys P, Landreh M, Struwe WB, et al. The role of interfacial lipids in stabilizing membrane protein oligomers. Nature. 2017;541(7637):421-4.

281. Munro JB, Altman RB, O'Connor N, Blanchard SC. Identification of two distinct hybrid state intermediates on the ribosome. Mol Cell. 2007;25(4):505-17.

282. Dave R, Terry DS, Munro JB, Blanchard SC. Mitigating unwanted photophysical processes for improved single-molecule fluorescence imaging. Biophys J. 2009;96(6):2371-81.

283. Juette MF, Terry DS, Wasserman MR, Altman RB, Zhou Z, Zhao H, et al. Single-molecule imaging of non-equilibrium molecular ensembles on the millisecond timescale. Nat Methods. 2016;13(4):341-4.

284. Borbat PP, Crepeau RH, Freed JH. Multifrequency two-dimensional Fourier transform ESR: an X/Ku-band spectrometer. J Magn Reson. 1997;127(2):155-67.

285. Georgieva ER, Borbat PP, Norman HD, Freed JH. Mechanism of influenza A M2 transmembrane domain assembly in lipid membranes. Sci Rep. 2015;5:11757.

286. Jeschke G. Distance measurements in the nanometer range by pulse EPR. Chemphyschem. 2002;3(11):927-32.

287. Chiang YW, Borbat PP, Freed JH. The determination of pair distance distributions by pulsed ESR using Tikhonov regularization. J Magn Reson. 2005;172(2):279-95.

288. Chiang YW, Borbat PP, Freed JH. Maximum entropy: a complement to Tikhonov regularization for determination of pair distance distributions by pulsed ESR. J Magn Reson. 2005;177(2):184-96.

289. Accardi A, Kolmakova-Partensky L, Williams C, Miller C. Ionic currents mediated by a prokaryotic homologue of CLC Cl- channels. J Gen Physiol. 2004;123(2):109-19.

290. Walden M, Accardi A, Wu F, Xu C, Williams C, Miller C. Uncoupling and turnover in a Cl-/H+ exchange transporter. J Gen Physiol. 2007;129(4):317-29.

291. Scopelliti AJ, Ryan RM, Vandenberg RJ. Molecular determinants for functional differences between alanine-serine-cysteine transporter 1 and other glutamate transporter family members. J Biol Chem. 2013;288(12):8250-7.

292. Mansoor SE, Dewitt MA, Farrens DL. Distance mapping in proteins using fluorescence spectroscopy: the tryptophan-induced quenching (TrIQ) method. Biochemistry. 2010;49(45):9722-31.

293. Hilaire MR, Ahmed IA, Lin CW, Jo H, DeGrado WF, Gai F. Blue fluorescent amino acid for biological spectroscopy and microscopy. Proc Natl Acad Sci U S A. 2017;114(23):6005-9.

294. Hirschi M, Johnson ZL, Lee SY. Visualizing multistep elevator-like transitions of a nucleoside transporter. Nature. 2017;545(7652):66-70.